UNIVERSITY OF NAPLES "FEDERICO II"

DEPARTMENT OF PHARMACY

Ph.D. THESIS

IN

"PHARMACEUTICAL SCIENCE"

Phytochemical and synthetic studies on bioactive secondary metabolites from Apiaceae plants growing in Mediterranean and Middle-East regions

Supervisor:
Prof. Daniela Rigano

Coordinator:
Prof. Maria Valeria D'Auria

Candidate:
Dr. Carmina Sirignano

XXXI cycle
2015/2018

Look up at the stars and not down at your feet. Try to make sense of what you see, and wonder about what makes the universe exist. Be curious.

(Stephen Hawking)

Table of contents

Abstract

Natural products represent a remarkable source of lead molecules for drug discovery, given their impressive structural diversity and their still unexplored potential. Considering that more than 90% of the world's biodiversity still waits to be investigated, Nature continues to be a gold mine of new chemotypes and pharmacophores. Thus, taking into account all the potential sources, including plants, fungi, bacteria, and marine environment, approximately one-third of all New Molecular Entities (NMEs) approved by Food and Drug Administration (FDA) derives from natural products. In this context, the research work reported in this Ph.D. thesis has been focused on the phytochemical investigation of plants belonging to the Iranian and Northern African flora, in order to discover and rationalize their pharmacological potential. In particular, the first part of my work has been devoted to the characterization of the polyacetylene fraction of *Echinophora platyloba*, which pointed out a new interesting TRPA1 modulating activity of C_{14} polyacetylenes isolated from this Iranian endemic plant. Subsequently, the bio-guided fractionation of the apolar extract obtained from *Daucus virgatus*, a Tunisian endemic plant, led to the isolation of angeloylated germacranolides showing a promising *Plasmodium* transmission blocking activity. Moreover, the complete phytochemical characterization of *D. virgatus* apolar extract has resulted in the isolation of additional antiproliferative secondary metabolites. Part of my Ph.D. project has been spent at University College of Dublin (UCD), to design and initiate a synthetic strategy for the preparation of daucovirgolide G, the angeloylated germacranolide that showed the most promising anti-malarial activity, among all those isolated from *D. virgatus*. The total synthesis of daucovirgolide G, which is still in progress, will have as final goal the preparation of the active compound and of several analogues to be pharmacologically evaluated.

The results obtained during my Ph.D. have been reported in nine papers already published or ready for publication.

Publications of the candidate during the Ph.D. period

1. Chianese, G., Yu, H. B., Yang, F., Sirignano, C., Luciano, P., Han, B. N., & Taglialatela-Scafati, O. (**2016**). PPAR modulating polyketides from a Chinese *Plakortis simplex* and clues on the origin of their chemodiversity. *The Journal of organic chemistry*, *81*(12), 5135-5143.

2. Formisano, C., Sanna, C., Ballero, M., Chianese, G., Sirignano, C., Rigano, D., & Taglialatela-Scafati, O. (**2017**). Anti-inflammatory sesquiterpene lactones from *Onopordum illyricum* L. (Asteraceae), an Italian medicinal plant. *Fitoterapia*, *116*, 61-65.

3. Formisano, C., Sirignano, C., Rigano, D., Chianese, G., Zengin, G., Seo, E. J., & Taglialatela-Scafati, O. (**2017**). Antiproliferative activity against leukemia cells of sesquiterpene lactones from the Turkish endemic plant *Centaurea drabifolia* subsp. *detonsa*. *Fitoterapia*, 120, 98-102.

4. Del Prete, D., Taglialatela-Scafati, O., Minassi, A., Sirignano, C., Cruz, C., Bellido, M. L., & Appendino, G. (**2017**). Electrophilic triterpenoid enones: a comparative thiol-trapping and bioactivity study. *Journal of natural products*, *80*(8), 2276-2283.

5. Rigano, D., Sirignano, C., & Taglialatela-Scafati, O. (**2017**). The potential of natural products for targeting PPARα. *Acta Pharmaceutica Sinica B*, *7*(4), 427-438.

6. Snene, A., [#] Sirignano, C., [#] Rigano, D., Formisano, C., El Mokni, R., Ercolano, G., & Taglialatela-Scafati, O. (**2017**). Antiproliferative metabolites from the Northern African endemic plant *Daucus virgatus* (Apiaceae). *Phytochemistry*, *143*, 194-198.

7. Sirignano, C., [#] Snene, A., [#] Rigano, D., Tapanelli, S., Formisano, C., Luciano, P., & Taglialatela-Scafati, O. (**2017**). Angeloylated Germacranolides from *Daucus virgatus* and Their *Plasmodium*

Transmission Blocking Activity. *Journal of natural products*, *80*(10), 2787-2794.

8. Chianese, G., [#] Sirignano, C., [#] Shokoohinia, Y., Mohammadi, Z., Bazvandi, L., Jafari, F., & Rigano, D. (**2018**). TRPA1 Modulating C14 Polyacetylenes from the Iranian Endemic Plant *Echinophora platyloba*. *Molecules*, *23*(7), 1750.

9. Formisano, C., Rigano, D., Lopatriello, A., Sirignano, C., Arnoldi, L., Sardone, N., & Taglialatela-Scafati, O. Detailed phytochemical characterization of Bergamot by UPLC-DAD-MS and LC-NMR Analyses. Submitted

[#] These Authors contributed equally

CHAPTER 1

NATURAL PRODUCTS: A NEVER-ENDING INSPIRATION FOR DRUG DISCOVERY

Natural products can be defined as secondary metabolites produced by natural sources, with the aim of ensuring an evolutionary advantage to the organisms that produce them. Indeed, unlike the primary metabolites (nucleic acids, proteins, fats, and carbohydrates), natural products are not necessary for survival, but they play an important role in defending terrestrial and marine organisms from predators or external threats, and in the interaction between species. Biological processes involved in the formation of secondary metabolites are essentially three: glycolysis, Krebs cycle, and photosynthesis; these metabolic reactions are responsible for the synthesis of intermediates, such as shikimic acid, acetyl coenzyme A (acetyl-CoA), mevalonic acid and 1-deoxyxylulose-5-phosphate, which provide a potentially unlimited number of natural products. In fact, due to different reasons, like environmental changes, chemicals, viruses etc., it can be seen that the secondary metabolism varies depending on the specific organism or species. Hence the extraordinary structural variability associated to natural compounds.[1]

Historically, many diseases have been treated utilizing natural remedies; over centuries, natural products have retained their relevance in the drug discovery process, even overcoming the slight downturn determined by the development of combinatorial chemistry and high-throughput screening (HTS). Thus, if we do not simply consider the number of natural products which effectively become final drugs, but also the number of new chemical entities (NCEs) inspired by the "Nature's treasure trove of small molecules", it seems to be clear that this field of research continues to be of remarkable impact. Suffice to say that in a 30-year period, of 175 small molecules approved as new drugs with anticancer activity by FDA, or similar organizations, almost 50% is composed of natural products or compounds arising from their scaffolds.[2] Besides, a huge sense of optimism has been brought to the worldwide research in the natural products field, by the award in 2015 of the Nobel Prize in Physiology or Medicine to William C. Campbell and Satoshi Omura, for the discovery of the microbial natural products avermectins,[3] active against

onchocerciasis and lymphatic filariasis, and to Youyou Tu, for the discovery of artemisinin, an antimalarial natural product isolated from *Artemisia annua* L.[4] This milestone provides a remarkable illustration of the value reached by the natural products-based drug discovery and opens the way to new challenging achievements in this field.[5]

1.1 Plants as a source of natural products

Since the dawn of time, mankind has been assisted by Nature to gain useful remedies to treat all kinds of illness. There is a huge wealth of knowledge on the use of medicinal plants that is possible to find in the traditional medicine from all over the world. Taking advantage of the known information handed down over time about the healing properties of some plant species, a specific line of research has led to the isolation of several new natural products with a broad variety of pharmacological properties. The study of medicinal plants used in traditional medicine, focusing on the active metabolites responsible for the pharmacological effect, is termed ethnopharmacology, and this kind of scientific approach has resulted in the discovery of many well-known pharmaceuticals. One of the better examples is galanthamine,[6] an alkaloid derived from *Galanthus* and *Leucojum* species (Amaryllidaceae), plants used for centuries in Eastern Europe as a remedy for neurological conditions. Currently, galanthamine is used as anti-Alzheimer's drug and it represents a successful illustration of an ethnopharmacology-driven development of a drug starting from a natural source. Another interesting compound is represented by prostratin,[7] a 12-deoxyphorbol ester isolated from *Homalanthus nutans* (G. Forst.) Guill. (Euphorbiaceae), a small rainforest tree utilised by Samoan healers to cure hepatitis (**Fig. 1.1**). Prostratin is a candidate lead for treating AIDS and clinical trials are currently underway.

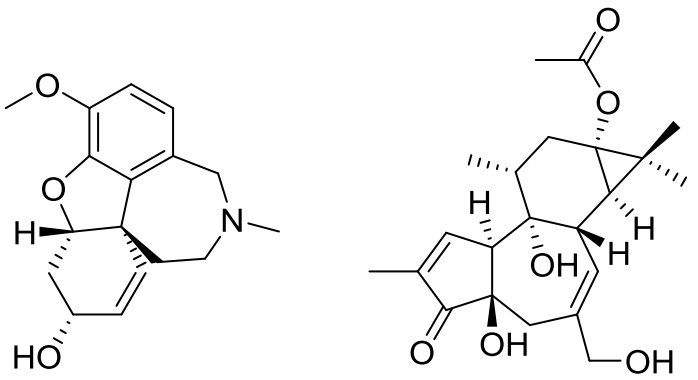

Figure 1.1 Structures of galanthamine and prostratin

These two drugs are reported to give an example of the most recent application of the ethnopharmacology to the modern drug discovery. When there is a lack of information about the pharmacological use of a plant in the traditional medicine of a specific area, natural extracts can be screened using functional biological assays; after selecting the most promising fractions, it is possible to purify and identify natural compounds responsible for the activity. Following simple instructions for the biological screening of extracts, an enhanced efficacy of the assay is obtained. For example, a prefractionation of the crude extract deriving from the plant, using normal phase or reverse phase chromatography, is undoubtedly necessary. Fractionation would provide less-complex samples, certainly more suitable for the sensitive biological text.[8]

In conclusion, utilizing different kinds of approaches, the research of new natural leads from plants is endless; all the extracts which were screened for a specific pharmacological activity, have to be considered as "uninvestigated" with respect to other pharmacological properties. Therefore, the continuing success of plant-derived drug discovery proves that, with the correct tools, it is still possible to gain the best results from the world of natural products.[9]

1.2 The role of synthetic chemistry in the natural products field

The Achille's heel of a natural products-based drug discovery is often represented by the limited amount of promising secondary metabolites present in the natural sources, thus making it difficult to perform additional biological studies or to

explore in detail the structure-activity relationship (SAR) of new natural leads. In this context, synthetic chemistry provides a useful tool to ensure sufficient quantities of compounds, which would be used in the drug development process. It should be mentioned that the structural diversity of natural products offers the opportunity to develop new synthetic strategies and methodologies in order to achieve advanced levels of knowledge in organic chemistry, explaining the reason why synthetic chemists have long been fascinated and inspired by natural compounds. Another important goal reached by applying synthetic chemistry to natural products' field is to confirm the structures of isolated compounds, in some cases leading to the assignment of absolute configuration.

There are several strategies adopted by organic chemists for the efficient synthesis of chemical entities' libraries employed for pharmacological screening: Diversity Oriented Synthesis (DOS), Function Oriented Synthesis (FOS) and Target Oriented Synthesis (TOS).[10]

DOS is based on the development of libraries constituted of structurally complex and diverse small molecules, differing in stereochemistry and skeletal arrays. Screening of such compounds can provide key informations about the identification of therapeutic protein targets, along with a reasonable number of hits set to be optimized. If the mechanism of action of a natural compound is known, an interesting strategy is represented by FOS, which is focused on the function of the molecule rather than its structure; applying this method it is possible to develop analogs with a simplified structure by only including the activity-determining structural features.[11]

Lastly, Target Oriented Synthesis (TOS) allows chemists to prepare bioactive compounds using a retrosynthetic analysis; thus, starting from a structurally complex target, is possible to find a simple and small molecule that can be utilized to start the synthesis.

The combination of the mentioned synthetic methodologies, along with the kaleidoscopic chemical structures created by Nature, has provided the possibility to bridge the gap between research in the natural products' field and drug discovery. This concept is demonstrated by two recently approved drugs: trabectedin and ingenol mebutate; due to their lower abundance in the natural source, it would be impossible to reach the clinical phase, without the involvement of a proper synthetic strategy.

Trabectedin (**Fig. 1.2**),[12] isolated from the Caribbean tunicate *Ecteinascidia turbinate*, was synthesized by PharmaMar, starting from cyanosafracin B, a natural product readily available using fermentation technology.

Figure 1.2 Trabectedin isolated from *Ecteinascidia turbinate*

The synthetic approach was inspired by the total synthesis of trabectedin designed by Corey in 1996. This molecule has been approved since 2007 for the treatment of advanced soft tissue sarcoma, under the name Yondelis®, and then in 2009 for the treatment of ovarian cancer. Currently, 21 open studies concerning Phase I to Phase III are present.[13]

Another powerful example, that explains the key role of the total synthesis in drug discovery, is represented by ingenol mebutate (**Fig. 1.3**), a macrocyclic diterpene ester isolated from *Euphorbia peplus* L., a species belonging to Euphorbiaceae family, mostly distributed in Europe and traditionally used to treat skin diseases. In 2012, a gel containing ingenol mebutate (Picato®, Leo Pharma A/S, Ballerup, Denmark) was approved by FDA and the European Medicines Agency (EMA) for the treatment of actinic keratosis, and a clinical research addressed to the application to other cancer types is still ongoing.[14] The active compound can be recovered from the natural source as 1 mg per kilogram of plant material, suggesting that this option cannot be invoked. Given the complexities to design a suitable for large-scale synthesis of ingenol mebutate, the initial process included the isolation of unesterified diterpene ingenol from the closely related plant, *Euphorbia lathryis* L., using the liquid–liquid isolation procedure described by Appendino *et al.*[15] Then,

chemists of LEO Pharma were able to prepare the desired active product employing a three-step process, starting from natural ingenol. Recently, the Baran group designed synthetic routes in order to obtain the active compound and some analogues; in this way, it may be possible to explore new pharmacological targets. For example, modifications of the angelate ester moiety seem to produce new promising drug candidates, that could be employed in highly active antiretroviral therapy (HAART) against HIV.[16]

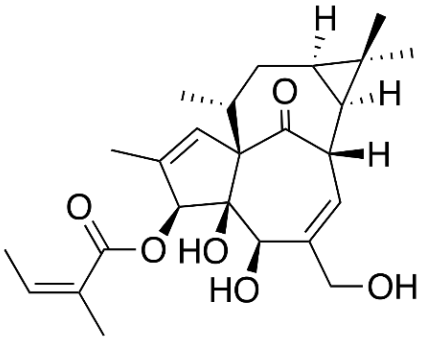

Figure 1.3 Structure of ingenol mebutate

For many years, chemists have focused their attention on the development of synthetic strategies "to build" the complex structures of natural products; the achievements in this challenging field during the last century have been astonishing. In addition to its fascinating beauty, total synthesis provides an important opportunity to better understand biological processes and to develop new pharmaceutically promising molecules. Synthetic chemists have increasingly realized that they could integrate their synthetic efforts with biological studies to provide more helpful total synthesis.

References

1. Croteau, R., Kutchan, T. M., & Lewis, N. G. (**2000**). Natural products (secondary metabolites). *Biochemistry and molecular biology of plants*, *24*, 1250-1319.

2. Butler, M. S., Robertson, A. A., & Cooper, M. A. (**2014**). Natural product and natural product derived drugs in clinical trials. *Nat. Prod. Rep.*, *31*(11), 1612-1661.

3. Campbell, W. C. (**1993**). Ivermectin, an antiparasitic agent. *Med. Res. Rev.*, *13*(1), 61-79.

4. Tu, Y. (**2011**). The discovery of artemisinin (qinghaosu) and gifts from Chinese medicine. *Nat. Med.*, *17*(10), 1217.

5. Shen, B. (**2015**). A new golden age of natural products drug discovery. *Cell*, *163*(6), 1297-1300.

6. S. G., Attar, U. A., Yadav, P. B., & Lekhak, M. M. (**2018**). Antioxidant, anti-diabetic, acetylcholinesterase inhibitory potential and estimation of alkaloids (lycorine and galanthamine) from *Crinum* species: An important source of anticancer and anti-Alzheimer drug. *Ind. Crops Prod.*, *125*, 168-177.

7. Chen, D., Wang, H., Aweya, J. J., Chen, Y., Chen, M., Wu, X., & Liu, M. (**2016**). HMBA enhances prostratin-induced activation of latent HIV-1 *via* suppressing the expression of negative feedback regulator A20/TNFAIP3 in NF-κB signaling. *Biomed Res. Int.*, *2016*.

8. Rishton, G. M. (**2008**). Natural products as a robust source of new drugs and drug leads: past successes and present-day issues. *Am. J. Cardiol.*, *101*(10), S43-S49.

9. Potterat, O., & Hamburger, M. (**2008**). Drug discovery and development with plant-derived compounds. *Natural Compounds as Drugs* Volume I (pp. 45-118). Birkhäuser Basel.

10. Galloway, W. R., Isidro-Llobet, A., & Spring, D. R. (**2010**). Diversity-oriented synthesis as a tool for the discovery of novel biologically active small molecules. *Nat. Commun.*, *1*, 80.

11. Wender, P. A., Verma, V. A., Paxton, T. J., & Pillow, T. H. (**2007**). Function-oriented synthesis, step economy, and drug design. *Acc. Chem. Res.*, *41*(1), 40-49.

12. Radjasa, O. K., Vaske, Y. M., Navarro, G., Vervoort, H. C., Tenney, K., Linington, R. G., & Crews, P. (**2011**). Highlights of marine invertebrate-derived biosynthetic products: Their biomedical potential and possible production by microbial associants. *Bioorg. Med. Chem.*, *19*(22), 6658-6674.

13. Molinski, T. F., Dalisay, D. S., Lievens, S. L., & Saludes, J. P. (**2009**). Drug development from marine natural products. *Nat. Rev. Drug Discov.*, *8*(1), 69.

14. Vasas, A., Rédei, D., Csupor, D., Molnár, J., & Hohmann, J. (**2012**). Diterpenes from European *Euphorbia* species serving as prototypes for natural-product-based drug discovery. *Eur. J. Org. Chem.*, *2012*(27), 5115-5130.

15. Appendino, G. (**2014**). *Omnia praeclara rara*. The quest for ingenol heats up. *Angew. Chem. Int. Ed.*, *53*(4), 927-929.

16. Appendino, G. (**2016**). Ingenane diterpenoids. *Prog. Chem. Org. Nat. Prod. 102* (1-90). Springer, Cham.

CHAPTER 2

TECHNIQUES AND METHODS EMPLOYED IN THIS STUDY

The scientific research in the field of natural products requires different steps; first of all, there are a number of procedures that is possible to employ, in order to achieve the isolation and purification of compounds from a natural source. Thus, the application of spectrometric and spectroscopic techniques ensures the structural determination of new natural molecules; finally, the assignment of relative and absolute configuration is carried out through the analysis of information deriving from NMR data, computational approaches, or with the derivatization of the natural product with chiral derivatizing agents (CDA).

2.1 Isolation procedures

The isolation of natural products represents a crucial step because, depending on the amount of the available biological material, it is necessary to employ various analytical and preparative chromatographic methods, in order to reach the best conditions to obtain the optimal separation and isolation of new natural molecules.
First, the biological material is extracted with an organic solvent, such as methanol. Then, the crude extract is partitioned between solvent with different polarity. In some cases, a modified Kupchan's method[1] can be used as follows:

- The methanol extract is dissolved in a mixture of 10% H_2O/MeOH and partitioned against *n*-hexane.
- The water content (% v/v) in the MeOH extract is adjusted to 30% and partitioned against $CHCl_3$.
- MeOH is removed from the aqueous phase by evaporation, and then the aqueous phase is extracted with *n*-BuOH.

Applying this method, four extracts (*n*-hexane, $CHCl_3$, *n*-BuOH and H_2O extracts), containing molecules with increasing polarity, can be obtained. Having reached this point, crude extracts are further fractioned, applying sequential chromatographic procedures, which involve methods with a high loading capacity and not expensive

stationary phases during the first step of separation. Subsequent purifications require techniques which demand smaller samples (HPLC, for example).

MPLC (Medium Pressure Liquid chromatography) is one of the various preparative chromatography techniques, based on the use of a medium pressure to facilitate the transition of the liquid mobile phase through the stationary phase, which consists of a normal or reverse solid phase (usually silica gel resin). MPLC is widely used in the pharmaceutical, food, and chemical industries and many applications are possible in natural product isolation. The pressure normally used is about 5-40 bar, and can be loaded a sample weighing generally 100 mg-100 g.[2]

HPLC (High Performance or High-Pressure Liquid Chromatography), represents a helpful technique used in the last step of the purification process, to afford pure compounds in high yields. The stationary phase may consist of normal or reverse phase silica gel, depending on the physicochemical properties of the sample to purify. Additionally, it is possible to employ chromatographic columns equipped with a chiral stationary phase, in order to perform enantiomeric separations.[3]

After achieving the isolation of a new natural product, the next step envisages the characterization of its structure and the subsequent submission of the molecule to pharmacological assays. In our group this crucial part of the work is mainly carried out using NMR spectroscopy and mass spectrometry, taking advantage of the equipment available at the CSIAS center of the Department of Pharmacy.

2.2 Mass spectrometry

Mass spectrometry represents a useful analytical tool, used in particular in the organic chemistry field, which allows determining the elementary formula of unknown compounds, measuring their molecular masses. A molecule, to be analyzed, must be ionized and then separated on the basis of its mass/charge (*m/z*) ratio; once accelerated by an electric field, charged molecules can be detected by an analyzer, which separates different ions on the basis of their (*m/z*) ratio. Results of the analysis are displayed as spectra of the relative abundance of ions as a function of the *m/z*. The mass spectrometer can be divided into three core parts: *ionization source*, *analyzer*, and *detector*.[4] A large part of compounds

described in the following chapters has been analyzed by *Electrospray Ionization* (ESI) mass spectrometry through an *Orbitrap* system.

Electrospray ionization (**Fig. 2.1**) has played a key role in the development of mass spectrometry, due to its utilization as a soft ionization source for analysis of biomolecules. ESI can efficiently be coupled with HPLC, for example, to easily perform MS analysis of complex mixtures. The molecule of interest is usually dissolved in water mixed with organic solvents (methanol or acetonitrile), and the solvent containing the analyte is dispersed by electrospray into fine droplets. The particles formed with the help of electrospray, through a heated capillary carrying a potential difference, are subjected to further solvent evaporation, until the point that they "explode", forming many smaller and stabilized droplets.[5]

Due to the potential difference of the capillary, each droplet of the spray carries positive or negative charges, causing protonation or deprotonation of the analytes, which become ions. The ions displayed by mass spectrometry are ions created by the addition of a hydrogen cation, and denoted as $[\mathbf{M}+\mathrm{H}]^{+}$, or of another cation, for example, sodium, $[\mathbf{M}+\mathrm{Na}]^{+}$; the removal of a hydrogen nucleus, can create $[\mathbf{M}-\mathrm{H}]^{-}$ anion. Multiply charged ions, $[\mathbf{M}+n\mathrm{H}]^{n+}$ can be also observed.[6]

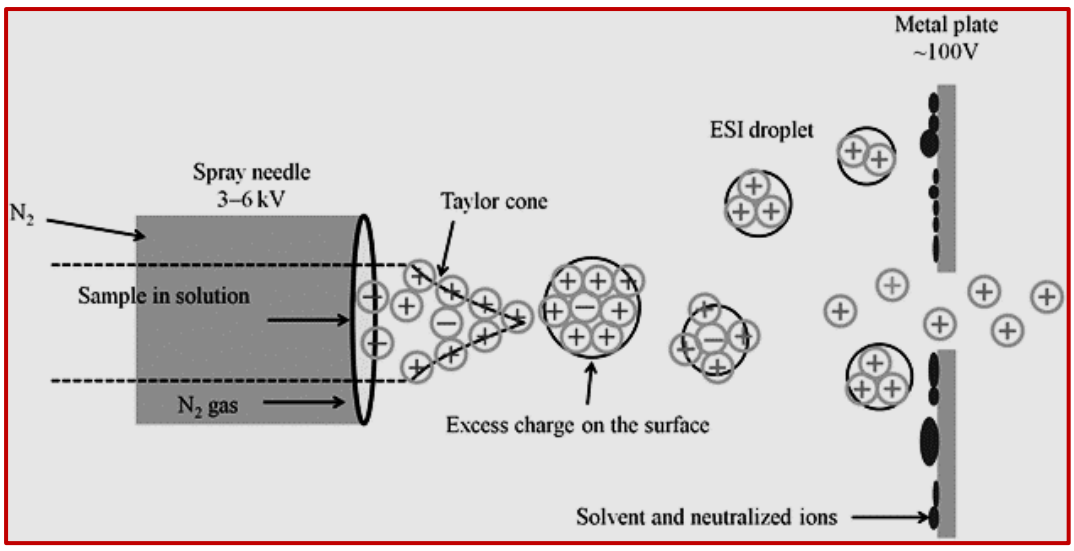

Figure 2.1 ESI mass spectrometry

Nitrogen is often used as carrier gas in order to help the liquid nebulization and the evaporation of solvent presents in the droplets.

High-resolution mass spectrometry (HRMS) is an excellent technique, which ensures the determination of accurate masses of analyzed ions; the instrumental systems comprise Fourier-transform ion cyclotron resonance (FT-ICR), time-of-flight (TOF), and Orbitrap mass spectrometry (**Fig. 2.2**).

Orbitrap mass spectrometry takes its name from the analyzer system, which utilizes orbital trapping of ions that in an electrostatic field rotate around the central electrode, oscillating along it. The frequency of the oscillations is not the result of the ion speed and it is inversely proportional to the square root of the (*m/z*). The ions oscillations are transformed by Fourier transformation to give individual signals with high resolving power (up to 200,000), and high-accuracy mass determination (1-2 ppm). In 2003, Hardman and Makarov reported the Orbital mass spectrometry coupled with an electrospray ionization source.[7]

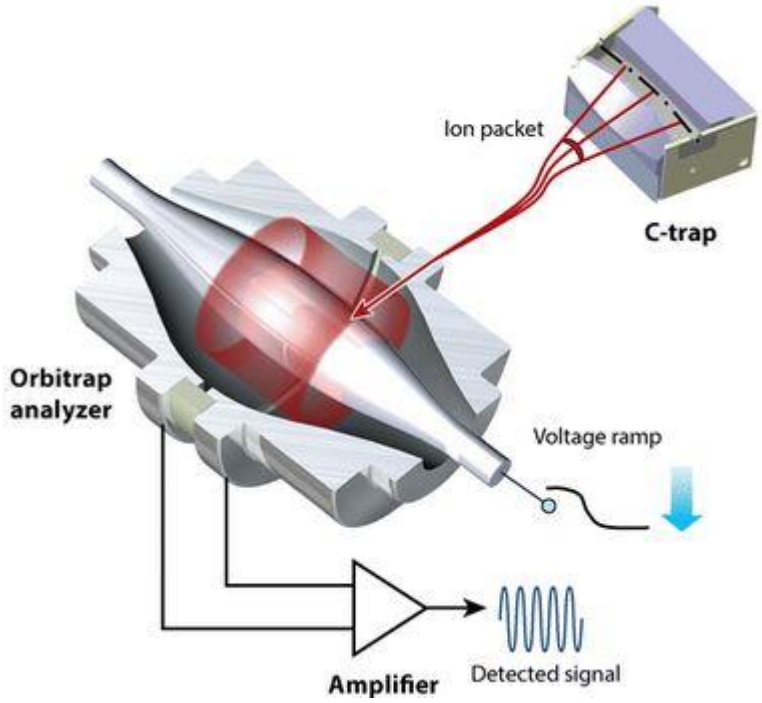

Figure 2.2 Orbitrap system

2.3 Nuclear Magnetic Resonance

Nuclear Magnetic Resonance (NMR) spectroscopy is a powerful analytical tool used to determine the structure of the isolated secondary metabolites in a non-destructive way. The nuclei of many elemental isotopes are characterized by

a specific number of spin (**I**). A spinning charge can generate a magnetic field, creating a spin-magnet with a magnetic moment (**μ**) proportional to the spin. Applying an external magnetic field ($\mathbf{B_0}$), it is possible to create different spin states of a nucleus, depending on the value of I (this number is equal to 2I+1) with different energy; this difference depends on the applied magnetic field strength. Nuclei with I=0 are known as "NMR inactive", because they are not equipped with the nuclear spin property, essential to allow an NMR analysis. Hydrogen (^{1}H), carbon (^{13}C), fluorine (^{19}F) and phosphorus (^{31}P) represent nuclei possessing I=1/2, that means they can be analyzed using NMR. If nuclei with I≠0 are placed in a magnetic field, they will assume a possible number of different orientations that will correspond to specific energy levels; this number depends on the value of I, in particular, it is equal to 2I+1.

When an external magnetic field is applied to nuclei with I= ½, they can assume two possible orientations, α parallel (I = ½), corresponding to the lower level of energy, or β antiparallel (I = - ½), corresponding to the higher level. The difference of energy is equal to:

$$\Delta E = \gamma B_0$$

γ represents the gyromagnetic ratio, that is specific for certain nuclei. The protons are distributed between the two levels (α and β), with an excess of protons population in the α state, with its lower energy.[8]

When an energy is applied (a radio frequency pulse), the nuclei undertake transitions from lower to higher energy levels; once the radiofrequency is switched off, is possible to observe the Free Induction Decay (FID), which is converted in the frequency domain, applying the Fourier Transform (FT).

To carry out my research work, 1D and 2D NMR experiments have been widely used for structural elucidation of new natural compounds.

COSY (COrrelation SpectroscopY) is a homonuclear chemical shift correlation experiment, based on the transfer polarization between spins that are directly J-coupled. It is useful to establish the connectivity of a molecule by determining which protons are spin-spin coupled.

HSQC (Heteronuclear Single Quantum Correlation) experiment is a heteronuclear correlation technique, in which only one-bond proton-carbon couplings ($^{1}J_{CH}$) are

revealed. Through the HSQC experiment is possible to correlate the chemical shift of a proton with the chemical shift of the directly bonded carbon.

HMBC (Heteronuclear Multiple Bond Correlation) is a heteronuclear correlation experiment able to detect correlations between protons and carbons separated by two, three and, in the case of conjugated systems, four bonds; cross peaks between protons and carbons directly bonded are suppressed. This experiment is essential to obtain the connection of the fragments revealed through COSY and HSQC experiments, in order to unambiguously define the structure of the new natural products.[9]

2.4 Determination of stereochemistry

The determination of the absolute and relative configuration of a new natural compound is a crucial phase in the structure elucidation process, given the close relationship between the spatial arrangement of atoms in a molecule and the biological activity.

Many natural products possess one or more chiral centers; a useful tool to establish their relative configuration is based on the analysis of NMR experiments, in particular through the evaluation of coupling constants (*J*), chemical shifts (δ), and NOE effects.

2.4.1 Determination of relative configuration

The proton chemical shifts of two diastereomers are different because they have diverse chemical milieu. The Karplus equation correlates ^{3}J coupling constants and dihedral torsion angles

$$^{3}J = A\cos\theta^{2} + B\cos\theta + C$$

where ^{3}J coupling constant indicates the correlation between two vicinal hydrogen atoms, θ is the dihedral angle, and A, B, and C are empiric parameters based on the substituents involved. The value of the coupling constant is the smallest when the torsion angle is close to 90° and largest when the angles are between 0° and 180°.

Using the Karplus equation is possible to have some preliminary informations about the relative atomic spatial arrangement of a molecule.

NOESY (Nuclear Overhauser Enhancement SpectroscopY) is a useful NMR-based method to assign the relative configuration of stereogenic centers; the NOE effect can be detected after irradiation on a specific NMR signal, during the acquisition of the spectra: as a result, the relaxation times of all the protons close to the irradiated center (distance < 2.5 A°) change, including even those protons not belonging to the same spin system. In fact, the NOE effect occurs through space, not through chemical bonds; thus, atoms that are in proximity to each other can give NOE.

ROESY (Rotating-frame Overhauser SpectroscopY) experiment is based on a chemical shift homonuclear correlation, as well as NOESY, which can detect ROE (Rotating-frame Overhauser Effect). This method is used for molecules with a molecular weight around 1000 daltons, for which the NOE is too weak to be observed.[10]

2.4.1.1 Murata's Method

Murata *et al.*[11] have reported a method for the assignment of relative configuration of acyclic compounds based on the combined use of homonuclear proton-proton coupling constants $^{3}J_{H\text{-}H}$, heteronuclear proton-carbon coupling constants $^{2,3}J_{H\text{-}C}$ and NOE data. This model is basically applied to acyclic molecules presenting stereogenic carbons bearing hydroxyl, alkoxy or methyl substituents. Every chiral molecule containing streochemical centers can be ideally divided in two carbon fragments. This simplification allows to determine, for each single fragment, the predominant rotamer with the exact configuration, among all the possible staggered conformers by using a *J*-based NMR approach, see **Scheme 2.1**. It is possible to compare every single couple of vicinal asymmetric carbons to those belonging to a 2,3-disubstituted butane system, which could have two relative diastereomeric configurations, named syn (or threo) and anti (or erythro). Each of these two configurations can be arranged in three staggered rotamers, for a total of six possible conformers, as shown in **Scheme 2.1** (A1, A2, A3, B1, B2, B3). Every single rotamer shows its own homonuclear and heteronuclear coupling constant pattern; thus, $^{3}J_{H\text{-}H}$ and $^{2,3}J_{C\text{-}H}$ lead to unambiguously identify four of the six rotamers,

namely A1, A3, B1, B3. The two rotamers A2 and B2, characterized by an anti position of the two vicinal protons, can be distinguished on the basis of NOE (or ROE) data, because they show the same coupling constant pattern.

The first step to determine the relative configuration of two vicinal methines involves the evaluation of homonuclear proton-proton coupling constant of the C2 fragment of interest. Small $^{3}J_{H\text{-}H}$ (0-4 Hz) indicate a gauche arrangement of H2 and H3 protons. In this case the relative configuration can be obtained from the heteronuclear coupling constants values. These $^{2,3}J_{C\text{-}H}$ values, indeed, allow to establish the arrangement (*gauche* or *anti*) of H2 and H3, leading to choose the correct gauche rotamer among A1, A3 (*threo*), B1 and B3 (*erythro*). Large $^{3}J_{H\text{-}H}$ values (8-12 Hz) indicate an anti disposition of the protons. Nevertheless, the $^{2,3}J_{C\text{-}H}$ values are the same for both rotamers A2 (*threo*) and B2 (*erythro*) (**Scheme 2.1**). In this case it is necessary to perform NOE experiments.

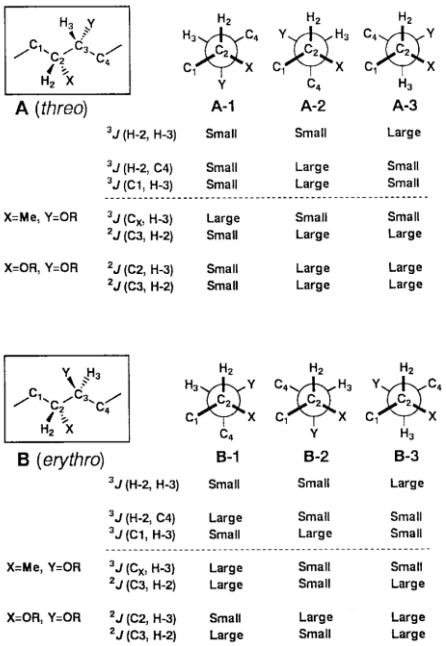

Scheme 2.1 Identification of the single conformer with the correct configuration through the combined use of measured $^{3}J_{H\text{-}H}$ and $^{2,3}J_{C\text{-}H}$ values.

2.4.2 Determination of absolute configuration

2.4.2.1 Marfey's Method

The most widely used method to determinate the absolute stereochemistry of ribosomial amino acids is the Marfey's method. This method consists of the derivatization of amino acid residues, obtained by complete acid hydrolysis of peptide, with a chiral agent FDAA (1-fluoro-2,4-dinitrophenyl-L-alaninamide, **Fig. 2.3**), and then the comparison of retention times of these derivates from parent peptide with the retention time of appropriate standards D and L through HPLC.
This method is enough easy for ribosomial amino acids, commercially available, and consist of four phases:
a) hydrolysis of parent peptide with HCl 6 N;
b) derivatization of the hydrolyzed mixture with L-FDAA;
c) derivatization of both standards, D and L, with L-FDAA. It is possible to derivatize L-amino acid with D-FDAA, if the D-standard isn't commercially available or is too expensive.
d) analysis through HPLC of retention times.[12]

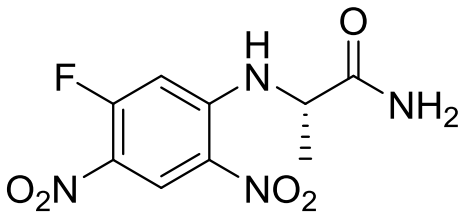

Figure 2.3 Structure of L-FDAA

2.4.2.2 Mosher's Method

Mosher's method represents a valuable procedure to assign the correct absolute configuration to a chiral substrate by using NMR. It is based on the formation of a covalent bond between an unknown enantiomer and a chiral derivatizing agent (CDA); for our purposes α-methoxy-α-trifluoromethylphenylacetic acid (MTPA) has been used as a CDA.

The first step of the method consists in derivatizing the molecule, which possesses the unknown absolute configuration, with the two enantiomers of the MTPA separately, and comparing the NMR spectra of the two resulting diastereoisomers. The aryl ring present in the MTPA structure, causes different values of chemical shifts for the two substituents L_1 and L_2 present in the two MTPA derivatives (**Fig. 2.4**), giving clear information about their spatial position.[13]

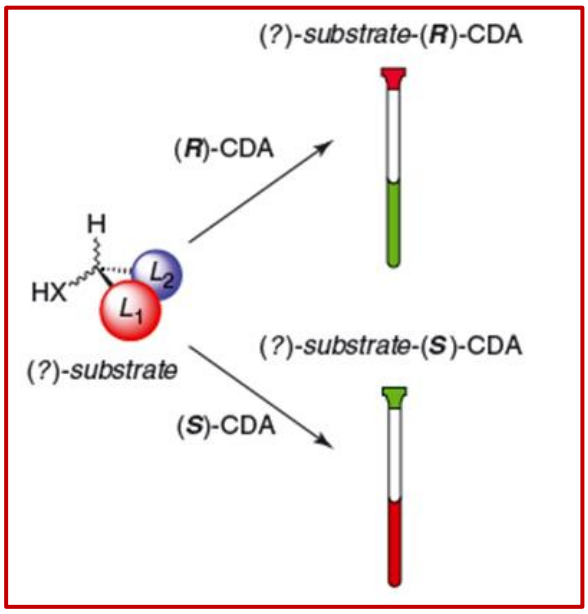

Figure 2.4 Derivatization of the substrate with CDA

After the subtraction of the chemical shift values for the two substituents L_1 and L_2 of the (*R*)-MTPA derivative minus the values of the (S)-MTPA derivative, it is possible to create a tetrahedral model in which the substituent with the negative difference is placed in the front position, while the substituent with the positive difference is placed in the back position around the stereogenic carbon (**Fig. 2.5**).

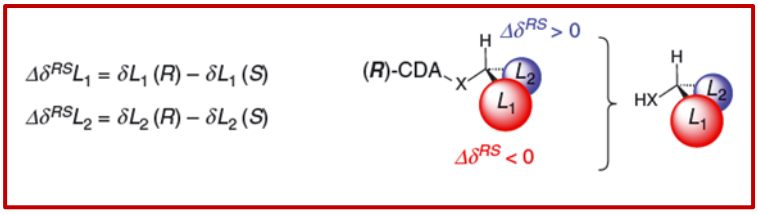

Figure 2.5 Assignment of configuration

2.4.2.3 Electronic circular dichroism

When a molecule presents a chromophore in its structure, electronic circular dichroism (ECD) can be a successful method to determine the absolute configuration of the compound. Usually, the range used by UV-vis spectropolarimeters is between 170–800 nm. An electronic transition can be associated to a positive or a negative ECD band, which is called a Cotton effect.

ECD is a sensitive method that can be used with minute amounts of material. The interpretation of the obtained results is often carried out by a comparison between the experimentally obtained and computationally calculated ECD spectra (**Fig. 2.6**).

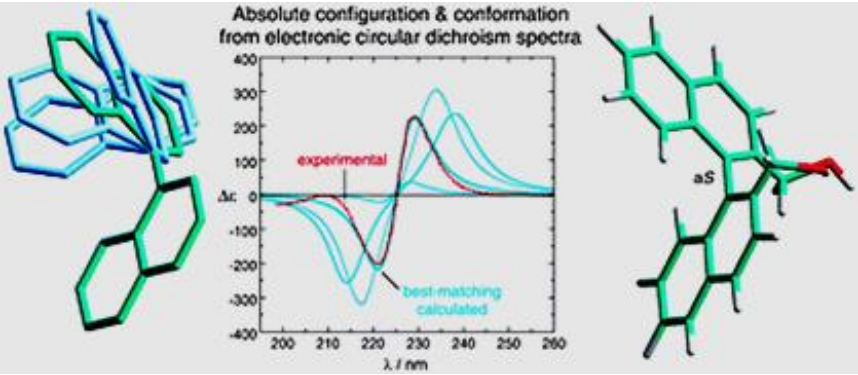

Figure 2.6 ECD spectrum

The first step of an ECD calculation is characterized by the conformational analysis of the molecule to obtain the relative energy evaluation of the possible conformers, while the second step provides the UV/ECD TDDFT (time-dependent density functional theory) calculation of each conformers. The UV/ECD spectra of the conformers are Boltzmann averaged, and then the calculated UV/ECD spectra of the isomers are performed. At this point, by comparison of the calculated ECD spectra with the experimental ECD of the natural product, the assignment of the absolute stereochemistry can be carried out.[14]

2.5 General Experimental Section for this PhD thesis

Optical rotations ($CHCl_3$) were measured at 589 nm on a JASCO P2000 polarimeter. UV spectra were acquired on a Tecan Italia spectrophotometer and on an EL 311s automated microplate reader (Bio-Tek Instruments). ECD spectra were registered on a JASCO J-710 instrument. ^{1}H (500 MHz) and ^{13}C (125 MHz) NMR spectra were measured on a Varian INOVA NMR spectrometer. Chemical shifts are referenced to the residual solvent signal ($CDCl_3$: δ_H 7.26, δ_C 77.0). Homonuclear ^{1}H connectivities were determined by COSY experiments; one-bond heteronuclear $^{1}H–^{13}C$ connectivities by the HSQC experiment; and two- and three-bond $^{1}H–^{13}C$ connectivities by gradient-HMBC experiments optimized for a $^{2,3}J$ value of 8 Hz. Through-space ^{1}H connectivities were obtained using a ROESY experiment with a mixing time of 500 ms. Low- and high-resolution ESIMS were performed on an LTQ OrbitrapXL (Thermo Scientific) mass spectrometer. Medium-pressure liquid chromatography was performed on a Büchi (Switzerland) apparatus using a silica gel (7−230 mesh) column; separations were monitored by TLC on Merck 60 F_{254} (0.25 mm) plates and were visualized by UV inspection and/or staining with 5% H_2SO_4 in ethanol and heating. HPLC was conducted on a Knauer apparatus equipped with a refractive index detector. Luna (normal phase, SI60, 250 × 4 mm) (Phenomenex) columns were used, with 0.7 mL/min as flow rate.

References

1. Kupchan, S. M., Britton, R. W., Ziegler, M. F., & Sigel, C. W. (**1973**). Bruceantin, a new potent antileukemic simaroubolide from *Brucea antidysenterica*. *J. Org. Chem.*, 38(1), 178-179.

2. Stecher, G., Huck, C. W., Stöggl, W. M., Guggenbichler, W., Bakry, R., & Bonn, G. K. (**2002**). High performance separation technologies and spectroscopic tools for plant extract characterization in phytomics. *Phytochem. Rev.*, *1*(3), 413-426.

3. Kelm, M. A., Johnson, J. C., Robbins, R. J., Hammerstone, J. F., & Schmitz, H. H. (**2006**). High-performance liquid chromatography separation and purification of cacao (*Theobroma cacao* L.) procyanidins according to degree of polymerization using a diol stationary phase. *J. Agric. Food Chem.*, *54*(5), 1571-1576.

4. Hillenkamp, F., Karas, M., Beavis, R. C., & Chait, B. T. (**1991**). Matrix-assisted laser desorption/ionization mass spectrometry of biopolymers. *Anal. Chem.*, *63*(24), 1193A-1203A.

5. Evans, A. M., DeHaven, C. D., Barrett, T., Mitchell, M., & Milgram, E. (**2009**). Integrated, nontargeted ultrahigh performance liquid chromatography/electrospray ionization tandem mass spectrometry platform for the identification and relative quantification of the small-molecule complement of biological systems. *Anal. Chem.*, *81*(16), 6656-6667.

6. Kebarle, P., & Tang, L. (**1993**). From ions in solution to ions in the gas phase-the mechanism of electrospray mass spectrometry. *Anal. Chem.*, *65*(22), 972A-986A.

7. Makarov, A., Denisov, E., Kholomeev, A., Balschun, W., Lange, O., Strupat, K., & Horning, S. (**2006**). Performance evaluation of a hybrid linear ion trap/orbitrap mass spectrometer. *Anal. Chem.*, *78*(7), 2113-2120.

8. Dias, D. A., Jones, O. A., Beale, D. J., Boughton, B. A., Benheim, D., Kouremenos, K. A., & Wishart, D. S. (**2016**). Current and future perspectives on the structural identification of small molecules in biological systems. *Metabolites*, *6*(4), 46.

9. Summers, M. F., Marzilli, L. G., & Bax, A. (**1986**). Complete proton and carbon-13 assignments of coenzyme B12 through the use of new two-dimensional NMR experiments. *J. Am. Chem. Soc.*, *108*(15), 4285-4294.

10. Altona, C., Ippel, J. H., Hoekzema, A. J. W., Erkelens, C., Groesbeek, M., & Donders, L. A. (**1989**). Relationship between proton-proton NMR coupling constants and substituent electronegativities. V—Empirical substituent constants deduced from ethanes and propanes. *Magn. Reson. Chem.*, *27*(6), 564-576.

11. Matsumori, N., Kaneno, D., Murata, M., Nakamura, H., & Tachibana, K. (**1999**). Stereochemical determination of acyclic structures based on carbon− proton spin-coupling constants. A method of configuration analysis for natural products. *J. Org. Chem.*, *64*(3), 866-876.

12. Fujii, K., Ikai, Y., Mayumi, T., Oka, H., Suzuki, M., & Harada, K. I. (**1997**). A nonempirical method using LC/MS for determination of the absolute configuration of constituent amino acids in a peptide: elucidation of limitations of Marfey's method and of its separation mechanism. *Anal. Chem.*, *69*(16), 3346-3352.

13. Seco, J. M., Quiñoá, E., & Riguera, R. (**2012**). Assignment of the absolute configuration of polyfunctional compounds by NMR using chiral derivatizing agents. *Chem. Rev.*, *112*(8), 4603-4641.

14. Di Bari, L., & Pescitelli, G. (**2010**). Electronic circular dichroism. *Computational Spectroscopy: Methods, Experiments and Applications*, 241-277.

CHAPTER 3:

TRPA1 MODULATING C_{14} POLYACETYLENES FROM THE IRANIAN ENDEMIC PLANT *ECHINOPHORA PLATYLOBA*

The first part of my Ph.D. thesis has been focused on the phytochemical investigation of the polyacetylene fraction obtained from *Echinophora platyloba* DC, an Iranian endemic plant belonging to the family Apiaceae, thank to a collaboration with Kermanshah University of Medical Sciences (Iran). The isolated compounds, characterized by the very rare α- pyrone moiety almost completely unprecedented in the structure of natural polyacetylenes, were evaluated for their modulation of six thermo-TRP channels. The results obtained have led to disclose a selective activity on TRPA1, an ion channel involved in the mediation of neuropathic and inflammatory pain.

3.1 The Apiaceae family

The Apiaceae (or Umbelliferae) family, one of the biggest families of flowering plants, includes 3780 species in more than 400 genera. It is worldwide distributed, mainly in the mild climate of northern regions, and a significant number of its members are endemic to Mediterranean area. Plants of the Apiaceae family are generally characterized by aromatic nature, alternate leaves, small flowers arranged in simple or compound umbel, and indehiscent fruits. As reported by a large number of studies found in the literature, these plants have been historically used in traditional medicine to treat gastrointestinal and neurological diseases, respiratory ailments, along with cardiac and urinary disorders. The broad variety of pharmacological activities displayed by the Apiaceae is due to their richness in secondary metabolites, such as polyacetylenes, terpenes, steroids, flavonoids, and coumarins, detected as its main constituents.[1] Nowadays a significant number of Apiaceae family's plants are used for seasoning, staining and as fragrance in the cosmetics industry. Several species represent a remarkable source of essential oils characterized by the presence of more than 800 different components belonging to diverse chemical classes with a great pharmaceutical interest.

The most representative and cultivated members of this family are: caraway (*Carum carvi* L.), cumin (*Cuminum cyminum* L.), parsley (*Petroselinum crispum* L.), coriander (*Coriandrum sativum* L.), fennel (*Foeniculum vulgare* Mill.), anise (*Pimpinella anisum* L.), dill (*Anethum graveolens* L.), and carrot (*Daucus carota* L.) (**Fig. 3.1**).[2]

Figure 3.1 Illustrative picture containing the most representative members of Apiaceae family

Coriander has been traditionally used as remedy to treat different ailments, such as digestive disorders, respiratory and urinary systems diseases, considering that it has diuretic, carminative, diaphoretic and stimulant activities; besides, coriander seeds are a spice widely used in the Mediterranean area. Interestingly, as proved by *in vivo* studies, coriander showed to possess the capacity to enhance the activity of enzymes that have a key role in the digestive process, both of pancreatic and intestinal origin. In Ayurvedic literature, the regular use of a coriander seed decoction was reported to have an effective hypolipidemic potential. Moreover, in Moroccan and Palestinian pharmacopeia the use of coriander as a traditional diuretic or to treat urinary

infections has been reported. In traditional Iranian medicine, coriander has a long history of medicinal use for preventing convulsions, anxiety and insomnia.[3]

Cuminum cyminum L., is one of the oldest and economically important plant species, widely cultivated in Asia, Africa and Europe. Cumin seeds have retained their importance as culinary spices, and they have been used in folklore therapy in different geographical areas, to treat various health disorders and ailments, such as toothaches, epilepsy, dyspepsia, and jaundice. These pharmacological activities have generally been attributed to the rich content of active natural compounds, such as terpenes, phenols, and flavonoids.[4-5]

Foeniculum vulgare, commonly known as fennel, is a medicinal and aromatic plant traditionally used as carminative, lactogogue, diuretic, and also to treat respiratory and gastrointestinal disorders. Phenols, phenolic glycosides and volatile metabolites, such as *trans*-anethole, fenchone, and estragole have been reported as the major secondary metabolites present in this species. Several in vitro and in vivo pharmacological studies have demonstrated the ability of *F. vulgare* to exhibit antifungal, antibacterial, antithrombotic and hepatoprotective activities, rationalizing several of its traditional uses.[6]

Pimpinella is a genus comprising almost 150 species distributed in Europe, Asia and Africa; among the *Pimpinella* species, *P. anisum* is the most widespread member, which has long been used as a folk remedy against respiratory and gastrointestinal disorders. Seeds are determined as the most commonly used part of these plants. According to several pharmacological studies, *Pimpinella* species exhibited various pharmacological activities such as antimicrobial, anti-diabetic, anti-inflammatory, neuroprotective, and antiviral.[7]

3.1.1 *Echinophora* genus

Echinophora is a genus of the Apiaceae family (tribe Echinophoreae) widely distributed in the Mediterranean regions, from Spain to the Balkans, and the Middle East. These herbs are characterized by spiny leaves and yellow flowers, indeed their Latin name derives from echino = spine, phora = leaf, and their prefer to grow especially in sandy coastal areas. Due to the pleasant aromatic taste, some *Echinophora* species have found use as seasoning in the preparation of food or as a

flavoring agent for soups, meats, and dairy products.[8] Fresh or dried herbs are also employed in the traditional medicine, not only for the well-known antimicrobial and antifungal activities, but also to treat gastric ulcers.[9-10] Although a direct correlation between claimed biological activity and secondary metabolite content is still lacking, the *Echinophora* genus has been the object of intense phytochemical investigations that have disclosed the presence of saponins, flavonoids[11] and polyacetylenes.[12] Among the about 20 *Echinophora* species described to date, only *E. cinerea* (Boiss.) Hedge et Lamond and *E. platyloba* DC are endemic to Iran (**Fig. 3.2**).

Figure 3.2 *Echinophora platyloba* DC

The Irano-Anatolian region, covering an area of about 899,773 km^2, represents one of the three biodiversity hotspots present in the Middle East, which comprise different kinds of ecosystems, including deserts, oases, forests and savannas. The Irano-Anatolian area is a World Heritage Site, appreciated for its great biodiversity, with about 6000 plant species. In particular, Iran massively contribute to this richness because, given the innumerable natural habitats present in the region, it is characterized by many unique plants and centers of local endemism. More than 8000 plant species are recognized throughout the country, of which about 2000 are endemic.[13] Due to the remarkable source of diversity that occurs in the Iranian flora and in the frame of our research project aimed at discovering the medicinal potential of Iranian endemic plants, the aerial parts of *E. platyloba* DC, for which only fragmentary phytochemical characterization was available in the literature, were investigated.

E. platyloba is a perennial aromatic plant, called "Khousharizeh" or "Tigh Touragh" in Persian, and commonly used as an edible vegetable.[14] The aerial parts and essential oils of the plant are also used by local people as anti-mold agent to preserve the quality of food and as folk remedy for several ailments, especially for its antispasmodic, diuretic, and antimicrobial activities.[15-16] In the present chapter, I describe the isolation of polyacetylene derivatives (**1**–**3**) from *E. platyloba*, which includes the new secondary metabolite echinophorin D (**1**), along with coriolic acid (**4**) (**Fig. 3.3**). The isolated polyacetylenes were evaluated for their interaction with the transient receptor potential (TRP) channels of ankyrin type-1 (TRPA1), cation channels widely expressed in the oral and nasal cavity, which play an important role in the perception of nociceptive and inflammatory pain.

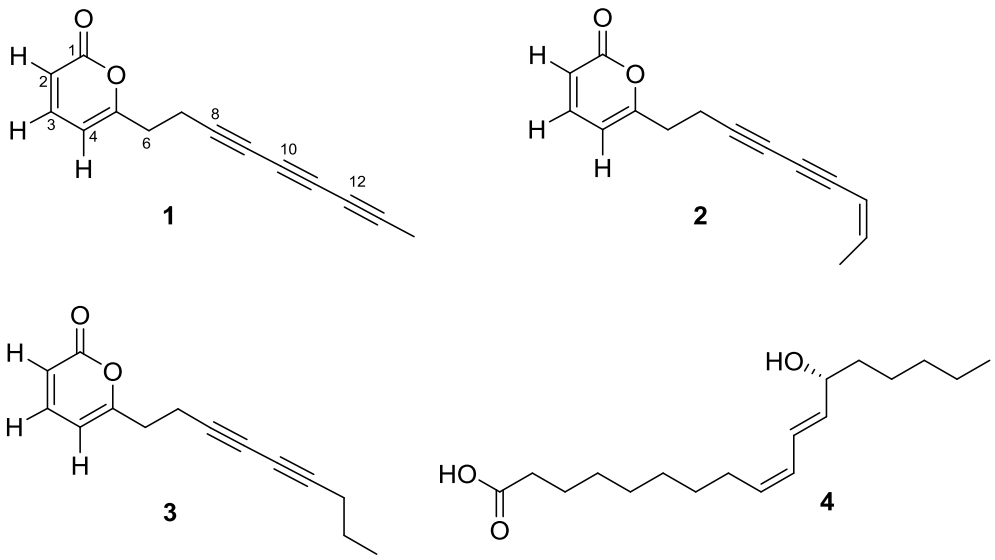

Figure 3.3 The chemical structures of **1**–**4**, isolated from *E. platyloba.*

3.2 Polyacetylenes from Apiaceae family and their biosynthesis

Polyacetylenes are a class of molecules characterized by the presence of two or more carbon–carbon triple bonds in their structure. These compounds have been isolated from different natural sources, such as plants, marine organisms, fungi etc., proving to possess a wide range of pharmacological activities. Focusing on plants, polyacetylenes are common secondary metabolites that is possible to find in many food plants, especially among those belonging to the Apiaceae family. The most widespread polyacetylenes found in these plants are of the falcarinol-type, like falcarinol (**5**), falcarindiol-3-acetate (**6**), falcarindiol (**7**), and falcarinone (**8**) (**Fig. 3.4**), that are the main compounds responsible for the bitter off-taste of carrots; in addition, these compounds showed cytotoxicity against leukemia and myeloma cell lines.[17]

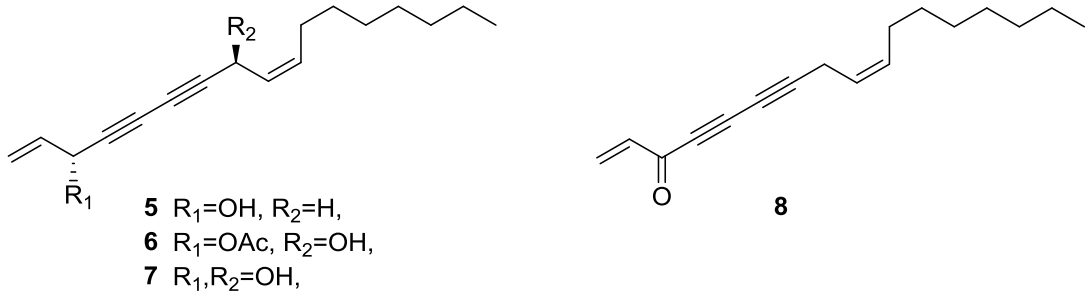

5 R_1=OH, R_2=H,
6 R_1=OAc, R_2=OH,
7 R_1,R_2=OH,

8

Figure 3.4 Falcarinol-type polyacetylenes

From the essential oil of *Selinum tenuifolium* Wall., an aromatic plant native of the Himalayan region, several C_9-polyynes were isolated (**9-11**);[18] interestingly, these structures, bearing a ketone function or a hydroxyl group, were known as synthetic compounds, but they have never been reported as natural products (**Fig. 3.5**).
Other falcarindiol derivatives, such as notoethers (**12-13**) and notoincisol A (**14**), were isolated from *Notopterygium incisium* Ting, a plant used in Chinese traditional medicine to treat inflammatory diseases such as rheumatoid arthritis; moreover, these natural products showed also a promising agonistic activity for PPARγ activation.[19]
The C_{34}-tetraynic aldehyde aciphyll (**15**) obtained from *Aciphylla scott-thomsonii* Cockayne & Allan, a plant widespread in New Zealand, showed antifungal activity.[20]

Furthermore, polyacetylenic β-D-glucopyranosyl glycosides (**16-17**) were obtained from the aerial parts of *Mediasia macrophylla* (Regel ex Schmalh.) Pimenov, a medicinal plant traditionally used in Uzbekistan for its anti-inflammatory properties and as natural preservative.[21]

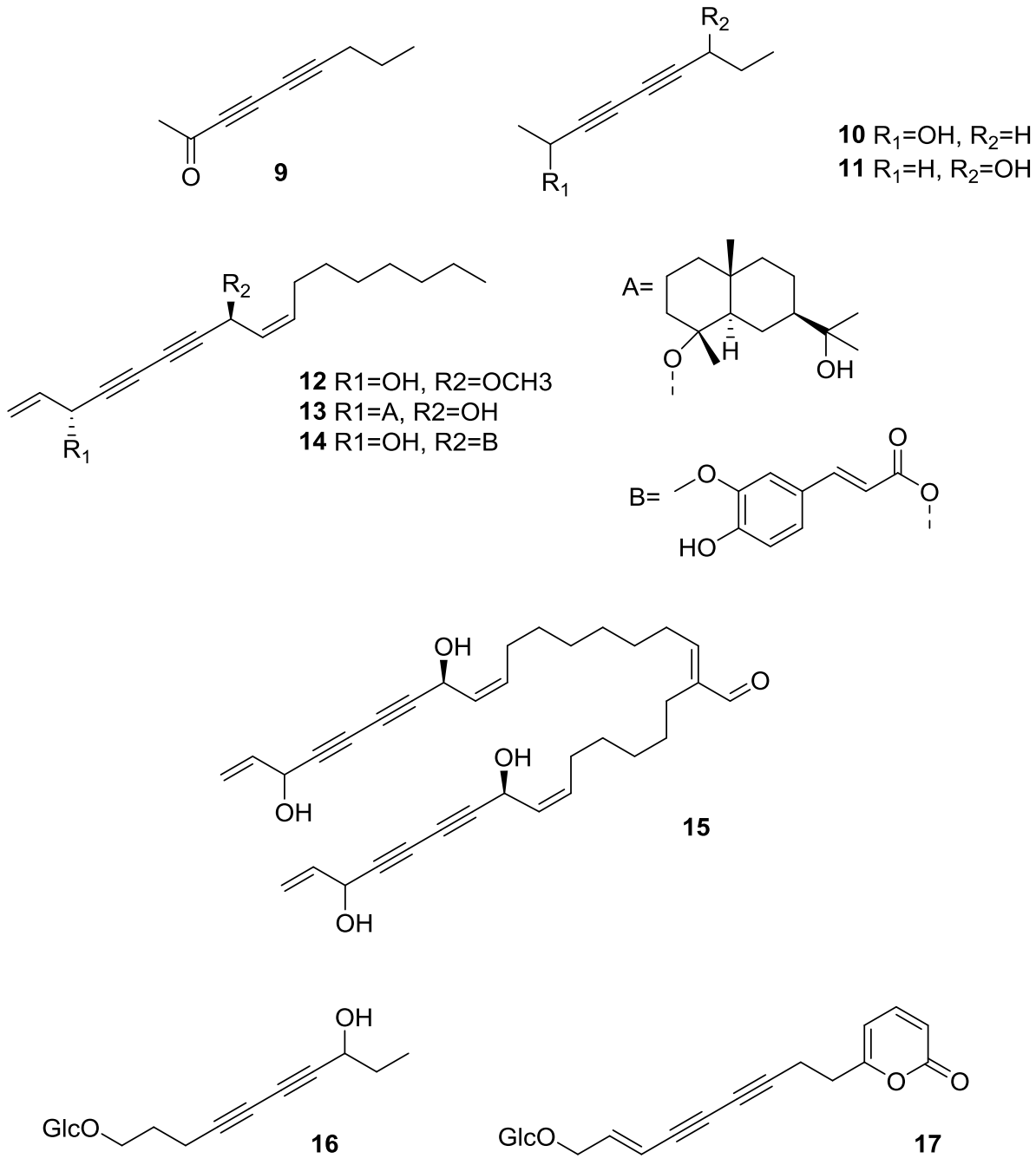

Figure 3.5 Selected polyacetylenes from the Apiaceae family

It is important to underline that one of the isolated compounds (**17**) is the first natural polyacetylenic product characterized by the presence of an α-pyrone moiety. The same uncommon feature has been recently found in *Echinophora cinerea* and *E. platyloba*, the plant described in this chapter.

Given the pharmacological potential of Apiaceae polyacetylenes, biosynthetic pathway leading to their formation in the natural source has been studied in detail. As outlined in **Scheme 3.1**, the starting building blocks for polyacetylenes production is represented by saturated fatty acids, produced by the head-to-tail addition of malonyl entities to a growing acyl chain. At this stage, two different hypothesis that explain the key step of a preexisting double bond oxidation to the triple one, have been proposed; the first one proposes desaturation through an iron-catalyzed dehydrogenation with molecular oxygen; the second hypothesis is based on the elimination reaction of an activated enol carboxylate intermediate. The two biosynthetic routes can provide three different intermediates, such as crepenynic, stearolic and tariric acids; these monoacetylenic intermediates are the substrates for several possible reactions, leading to the great chemical diversity of natural polyynes. In the Apiaceae family, the crepenynate pathway is predominant.

Crepenynic acid results from oleic and linoleic acids; after modification of chain length and unsaturation reactions, additional alkyne moieties, usually conjugated, are introduced in the initial skeleton. Hence, several reactions are performed in order to generate polyynes decorated with hydroxyl, ketone and epoxide groups; hydroxyl function can be further derivatized to give esters or glycosylated compounds. As regards C_{17} polyacetylenes, or more generally polyacetylenes with an odd number of carbon atoms in their structure, they are formed by decarboxylation.[17,22]

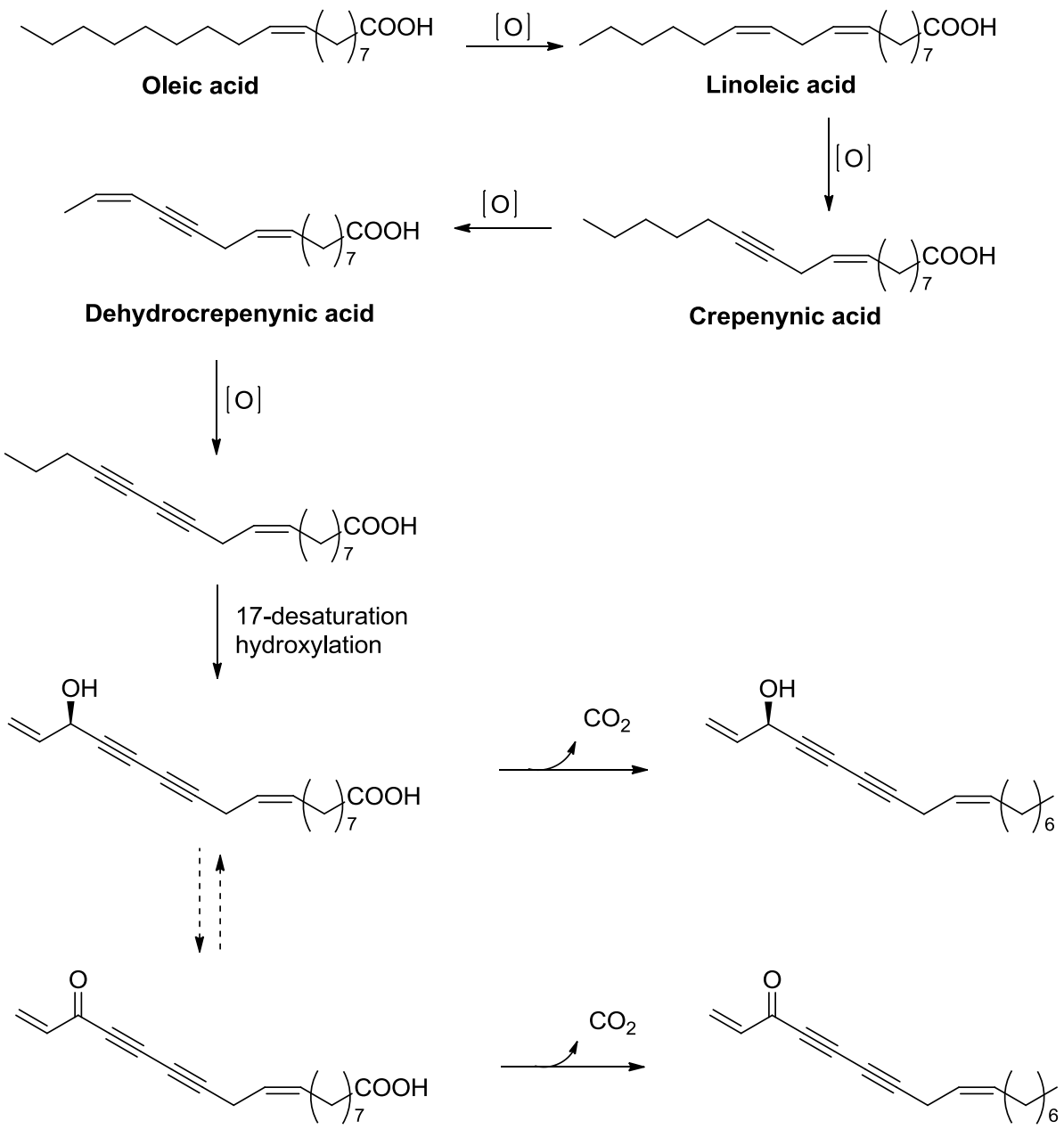

Scheme 3.1 Biosynthesis of polyacetylenes in the Apiaceae family

3.3 Polycetylenes from *Echinophora platyloba*

Aerial parts of *E. platyloba* were collected in the area of Marivan, Iran, and were dried and extracted sequentially with *n*-hexane, dichloromethane and acetone. Repeated purifications of the dichlorometane fraction by column chromatography and HPLC led to the isolation of pure compounds **1-4**. The structures of the known

echinophorins B (**2**) and A (**3**) were secured by comparison of their spectroscopic data with those available in the literature.[23] The acetone fraction was found to contain the non-polyacetylene oxylipin coriolic acid (**4**):[24] to our knowledge, this is the first report of coriolic acid from a plant of the Apiaceae family.

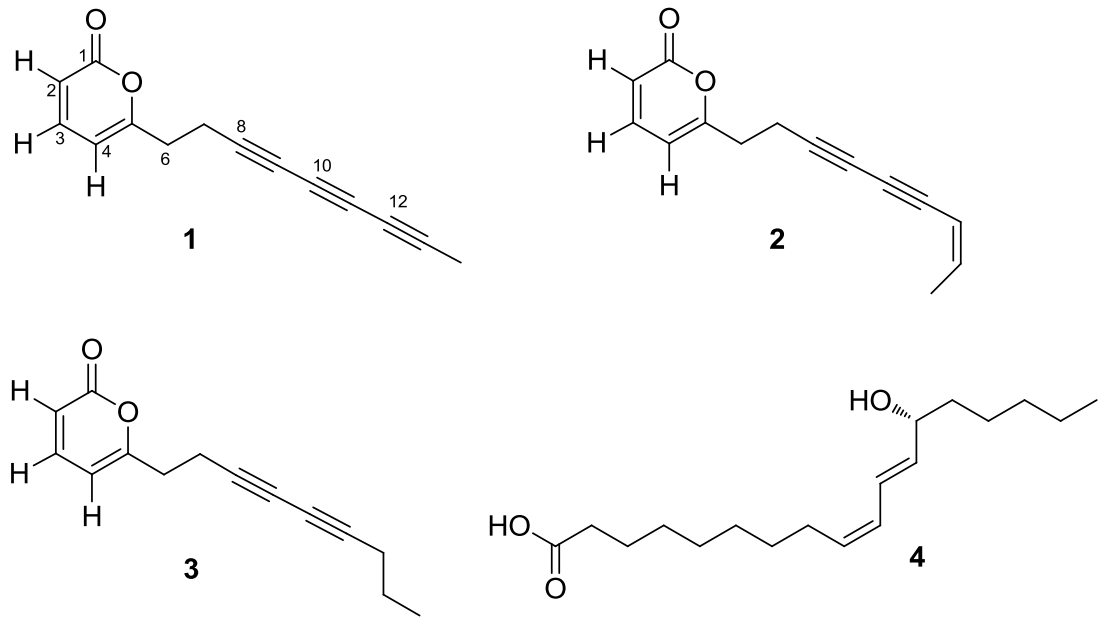

Echinophorin D (**1**) was isolated as a brown oil with molecular formula $C_{14}H_{10}O_2$, as deduced on the basis of HR-ESIMS data. The ^{1}H NMR spectrum of **1** (**Table 3.1**) was very simple, showing two doublets at δ_H 6.20 (J = 9.2 Hz) and 6.07 (J = 6.8 Hz), and a double doublet at 7.28 (J = 9.2 and 6.8 Hz), two coupled methylenes between δ_H 2.65 and 2.75 and a methyl singlet resonating at δ_H 1.95. All these proton resonances were associated to those of the directly attached carbon atoms by means of the 2D NMR HSQC spectrum, thus disclosing the marked high-field resonance of the methyl carbon (δ_C 4.5). In agreement with the molecular formula, the ^{13}C NMR spectrum of **1** showed the resonances of eight non-protonated carbons, two of which were coincident at δ_C 75.6. The α-pyrone ring was defined on the basis of the HMBC correlations H-2/C-1, H-3/C-5 and H-7/C-5 and on the basis of the comparison of H/C resonances with NMR data of echinophorins A and B.[23] The assignment of the carbon resonances of the three conjugated triple bonds was achieved through inspection of the HMBC spectrum. In particular, the $^2J_{C\text{-}H}$ and $^3J_{C\text{-}H}$ correlations of Me-14 (δ_H 1.95) to C-12 (δ_C 64.7) and C-13 (δ_C 75.6) and of H_2-7 (δ_H 2.68) with C-8 (δ_C 75.6) and C-9 (δ_C 67.3) led to the assignment of resonances for two of the three

triple bonds. Since weak peaks for longer correlations (namely $^4J_{C\text{-}H}$) can be observed for proton-deficient molecules embedding extensively conjugated systems, we could complete the assignment of the carbon resonances of the acetylenic system taking advantage of the HMBC cross-peaks from Me-14 to C-11 (δ_C 61.5) and H_2-7 to C-10 (δ_C 59.2). Thus, the structure of **1** was unambiguously determined as the first polyacetylenic compound to include an α-pyrone system and three conjugated triple bonds.

Table 3.1 ^{1}H and ^{13}C NMR data of Echinophorin D (**1**) [a]

Pos.	δ_H, mult., *J* in Hz	δ_C, mult.
1	-	162.2, C
2	6.20, d, *J* = 9.2 Hz	114.2, CH
3	7.28, dd, *J* = 9.2, 6.8 Hz	143.4, CH
4	6.07, d, *J* = 6.8 Hz	103.7, CH
5	-	162.9, C
6	2.71, m	32.4, CH_2
7	2.67, m	17.4, CH_2
8	-	75.6, C
9	-	67.3, C
10	-	59.2, C
11	-	61.5, C
12	-	64.7, C
13	-	75.6, C
14	1.95, s	4.5, CH_3

[a] Spectra registered in $CDCl_3$

3.4 Activity on transient receptor potential ion channels

Transient receptor potential (TRP) ion channels represent one of the most important class of calcium-permeable channels, first discovered in mutant *Drosophila* that, when exposed to intense light, showed transient calcium influx into photoreceptor cells; this is the explanation why the mutant gene was defined as

'transient receptor potential'. TRP channels, with their six *trans*-membrane (TM) domains, comprise a large family of channel proteins, expressed in vertebrates and invertebrates, subdivided into six subfamilies: TRPV (vanilloid), TRPC (canonical), TRPM (melastatin), TRPML (mucolipin), TRPP (polycystin), and TRPA (ankyrin), differing in their primary amino acid sequences. [25]

TRP channels not only play a key role in physiological processes, such as signal transmission, but they can be defined as cellular sensors involved in nociception, thermosensation, and taste perception. Many diseases are related to dysfunction of these channels, including chronic pain, diabetes, obesity, chronic obstructive pulmonary disease, cancer etc. Notably, TRP channels are important targets for several natural products with therapeutic potential.[26] For instance, capsaicin or menthol are able to activate the heat-sensitive TRPV1 and the cold-sensitive TRPM8 channels, referring to them as not only temperature sensors but also chemosensory channels. Moreover, TRPV1 mediates excitation and subsequent desensitization to a naturally occurring compound called resiniferatoxin, found in *Euphorbia resinifera* and representing a more potent analog of capsaicin; resiniferatoxin is currently undergoing clinical trials to achieve permanent analgesia in the event of intractable cancer pain. Furthermore, TRPC6 is related in mediating the mood-improving effect of hyperforin, the main compound present in plants of the *Hypericum* genus. In summary, there are clear experimental and clinical data to define TRP channels as appealing drug targets, and several compounds targeting these channels are undergoing clinical trials, demonstrating that the discovery and development on new leads in this field is of great significance.[27]

The Transient Receptor Potential Ankyrin 1 (TRPA1) is a channel characterized by the presence of 17 ankyrin-repeats and a calcium binding site in its N-terminus, along with a zinc binding site in the C-terminus (**Fig. 3.6**). It can be defined as a pain sensor, because it is mainly expressed in sensory neurons (where it is coexpressed with TRPV1), but recent works outlined that functional TRPA1 is also present in non-neuronal tissues such as heart, lung, small intestine, and pancreas. Many studies carried out using TRPA1 knock-out mice and specific antagonists, have related the function of TRPA1 to the regulation of temperature perception, inflammation, and pain.[28] It is activated by many irritant natural products, including allyl isothiocyanate, cinnamaldehyde and allicin, contained in mustard oil, cinnamon and garlic respectively, or by environmental irritants, such as acrolein or formalin. TRPA1 is

also activated by the non-pungent capsaicin analogue, capsiate, and by the non-psychotropic cannabinoid, cannabichromene. This is remarkable because cannabichromene is considered to play a critical role in the anti-inflammatory and analgesic activity of cannabis extracts. In general, reactive chemicals activate TRPA1 by inducing covalent modification of cysteines in the N-terminus. To date, only two TRPA1 antagonists designed to treat chronic and acute surgical pain have reached clinical stage of development.

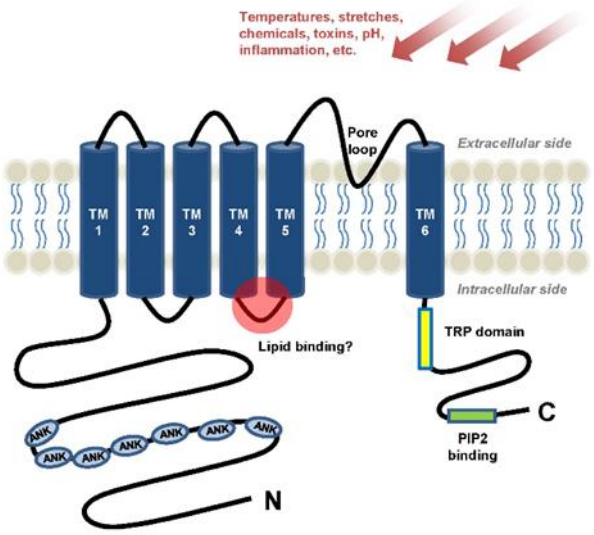

Figure 3.6 TRPA1 channel

The activation of TRPA1 at nerve terminals results in membrane depolarization, mainly due to Na^+ influx, and induces a local calcium influx through the channel which further releases neuropeptides such as calcitonin gene-related peptide (CGRP), substance P, or neurokinin A, from large dense-core vesicles *via* Ca^{2+}-dependent exocytosis. The presence of neuropeptides causes a further amplification of nociception, recruitment of immune cells, vasodilatation and neurogenic inflammation. Accordingly, TRPA1 has been functionally linked to a number of chronic pain conditions associated with inflammation, including arthritic and cancer pain.[29] From these informations it is possible to conclude that new TRP modulators are needed as viable candidates for drug discovery, and in this frame, natural product ligands are still intensely investigated as leads for TRP channels deorphanization. Natural products have a long history as TRP ligands, and many TRP channels are

activated/antagonized by secondary metabolites; for instance, it has been recently reported by our group the identification of some TRPA1 ligands from natural sources, e.g., curcumin[30] and leucettamols,[31] and two-headed sphingoid-like compounds. In the frame of this research project, the three polyacetylenic compounds from *E. platyloba* **1-3** have been evaluated by Dr. Luciano De Petrocellis (CNR, Pozzuoli, Italy) against six thermo-TRP channels (TRPA1, TRPV1, TRPV2, TRPV3, TRPV4, TRPM8) of great biomedical relevance. Coriolic acid (**4**) was not evaluated due to the small amount available. While the overall activity on the remaining TRPs was negligible, we found that the three compounds were able to modulate TRPA1 (detailed results are reported in **Table 3.2**). Using a fluorimetric test, we observed that rat TRPA1-HEK293 cells exhibited an increase in intracellular $[Ca^{2+}]_i$ upon application of **1**–**3**. All compounds showed a discrete potency in the range 20–30 μM with echinophorin D, bearing three conjugated triple bonds, being the less potent compound of the series, and the two analogues showing two triple bonds exhibited an activity of almost the same magnitude. The activity of the compounds was normalised to the maximum intracellular Ca^{2+} elevation generated by application of allylisothiocyanate (AITC) 100 μM. Echinophorins A (**3**) and B (**2**) were able to reach about 80% of the maximal response of AITC, while the less active echinophorin D (**1**) reached only about 52%.

Table 3.2 Activity of compounds **1-3** on calcium influx in HEK293 cells transfected with rTRPA1

Compounds	**Efficacy**	**Potency EC_{50} μM**	**IC_{50} inh TRPA1 μM (AITC 100 μM)**
Echinophorin D (**1**)	51.7±1.3	30.9±2.8	87.0±1.5
Echinophorin B (**2**)	82.0±2.8	25.0±3.0	37.2±0.8
Echinophorin A (**3**)	81.0±3.3	20.3±3.2	45.7±3.5

[a] % AITC (Allylisothiocyanate) at 100 μM, used as a control

Although the results obtained in this investigation are preliminary, since they derive from a very limited panel of natural products, they appear nevertheless interesting

for a couple of reasons. Firstly, to the best of our knowledge, this is the first report describing the modulation of TRP channels by polycetylenic compounds. Secondly, what is also remarkable is the selectivity of echinophorins toward TRPA1, an endpoint of relevance for treatment of inflammation and pain. Several polyacetylenic compounds have shown anti-inflammatory effects, mainly related to inhibition of NF-kB or to the modulation of prostaglandin catabolism.[32] Our results suggest that modulation of TRPA1 could be another anti-inflammatory mechanism of polyacetylenes worthy of being explored.

3.5 Experimental section

3.5.1 Plant material, extraction and isolation

The aerial parts of *E. platyloba* were collected in May 2010 on Mount Abidar, Marivan, Iran. The species was identified by Dr. Sayed Mohammad Masoumi, Razi University, and compared to the herbarium sample No. RUH585, Hamedan Herbarium, Iran. Aerial parts of *E. platyloba* (dry weight, 456 g) were extracted subsequently with *n*-hexane, dichloromethane and acetone using Soxhlet apparatus, 4 h for each. The hexane phase (4.85 g) was composed mainly of fats and fatty acids and was no further investigated. The dichloromethane extract (4.98 g) was dissolved in MeOH (60 mL) and stored at -20 °C for 2 days. Afterwards, it was filtered chilled and the filtrate was fractionated by gravity column on RP18 stationary phase, using a solvent gradient from MeOH/H_2O 1:1 to MeOH to obtain six fractions. The fraction eluted with MeOH/H_2O 7:3 (62.0 mg) contained polyacetylenes, by ^{13}C NMR of the crude fraction, and was therefore separated by HPLC (*n*-hexane/EtOAc 1:1, flow rate 0.7 mL/min) to afford pure echinophorin B (**2**, 5.1 mg), echinophorin A (**3**, 1.3 mg) and echinophorin D (**1**, 24.3 mg). The acetone extract (4.75 g) was fractionated by gravity column on silica gel using a gradient of heptane/EtOAc of increasing polarity (from heptane/EtOAc 9:1 to 1:1) to get eight fractions. The fraction eluted with heptane/EtOAc 7:3 (150 mg) was purified by HPLC (*n*-hexane/EtOAc 7:3, flow rate 0.8 mL/min) to yield coriolic acid (**4**, 0.8 mg).

3.5.2 Spectroscopic data for the isolated compound

Echinophorin D (1): Brown oil. ^{1}H NMR (500 MHz): Table 1; ^{13}C NMR (125 MHz): Table 1. ESI-MS (positive ions): m/z 233 $[M + Na]^{+}$; HRESI-MS: found m/z 233.0583, $C_{14}H_{10}O_2Na$ requires 233.0578.

3.5.3 Thermo TRPs Receptor Assays

HEK-293 cells stably over-expressing recombinant rat TRPA1, TRPM8, TRPV2-4, TRPM8 or human TRPV1 were selected by Geneticin 600 µg mL^{-1}, grown on 100-mm diameter Petri dishes as monolayers in minimum essential medium supplemented with non-essential amino acids, 10% fetal bovine serum, and 2 mM glutamine, and maintained under 5% CO_2 at 37 °C. Stable expression of each channel was checked by quantitative real time-PCR. The effect of the substances on intracellular Ca^{2+} concentration $[Ca^{2+}]_i$ was determined using Fluo-4, a selective intracellular fluorescent probe for Ca^{2+}. Toward this aim, on the day of the experiment, cells over-expressing the TRP channels were loaded for 1 h in the dark at room temperature with the methyl ester Fluo4-AM (4 µM in DMSO containing 0.02% Pluronic F-127, Invitrogen, Carlsbad, CA, USA) in minimum essential medium without fetal bovine serum. After the loading, cells were washed twice in Tyrode's buffer (145 mM NaCl, 2.5 mM KCl, 1.5 mM $CaCl_2$, 1.2 mM $MgCl_2$, 10 mM D-glucose, and 10 mM HEPES, pH 7.4), re-suspended in Tyrode's buffer, and transferred (about 100,000 cells) to the quartz cuvette of the spectrofluorimeter (Perkin-Elmer LS50B; PerkinElmer Life and Analytical Sciences, Waltham, MA, USA) under continuous stirring. $[Ca^{2+}]_i$ was determined before and after the addition of various concentrations of test compounds by measuring cell fluorescence at 25 °C (λ_{EX} = 488 nm, λ_{EM} = 516 nm). Curve fitting (sigmoidal dose-response variable slope) and parameter estimation were performed with GraphPad Prism® (GraphPad Software Inc., San Diego, CA, USA). Potency was expressed as the concentration of test substances exerting a half-maximal agonist effect (i.e., half-maximal increases in $[Ca^{2+}]_i$ (EC_{50}), calculated by using GraphPad®. The efficacy of the agonists was first determined by normalizing their effect to the maximum Ca^{2+} influx effect on $[Ca^{2+}]_i$ observed with application of 4 µM ionomycin (Sigma, St. Louis, MO, USA). The increases in fluorescence in wild-type HEK293 cells (i.e., not transfected with

any construct) were used as baseline and subtracted from the values obtained from transfected cells. The effects of TRPA1 agonists are expressed as a percentage of the effect obtained with 100 μM allyl isothiocyanate (AITC). Antagonist/desensitizing behavior was evaluated for TRPA1 by adding the test compounds in the quartz cuvette 5 min before stimulation of cells with the agonist AITC (100 μM). Data are expressed as the concentration exerting a half maximal inhibition of agonist-induced $[Ca^{2+}]_i$ elevation (IC_{50}), which was calculated again using GraphPad Prism® software. The effect on $[Ca^{2+}]_i$ exerted by agonist alone was taken as 100%. Dose-response curves were fitted by a sigmoidal regression with variable slope. All determinations were at least performed in triplicate. Statistical analysis of the data was performed by analysis of variance at each point using ANOVA followed by Bonferroni's test.

References

1. Sayed-Ahmad, B., Talou, T., Saad, Z., Hijazi, A., & Merah, O. (**2017**). The Apiaceae: Ethnomedicinal family as source for industrial uses. *Ind. Crops Prod.*, *109*, 661-671.

2. Holub, M., & Budeˇsˇínský, M. (**1986**). Sesquiterpene lactones of the Umbelliferae. *Phytochemistry*, *25*(9), 2015-2026.

3. Laribi, B., Kouki, K., M'Hamdi, M., & Bettaieb, T. (**2015**). Coriander (*Coriandrum sativum* L.) and its bioactive constituents. *Fitoterapia*, *103*, 9-26.

4. Ebada, M. E. (**2017**). Cuminaldehyde: A potential drug candidate. *J. Pharmacol. Clin. Res.*, *2*, 555585.

5. Mnif, S., & Aifa, S. (**2015**). Cumin (*Cuminum cyminum* L.) from traditional uses to potential biomedical applications. *Chem. Biodivers.*, *12*(5), 733-742.

6. Rather, M. A., Dar, B. A., Sofi, S. N., Bhat, B. A., & Qurishi, M. A. (**2016**). *Foeniculum vulgare*: a comprehensive review of its traditional use, phytochemistry, pharmacology, and safety. *Arabian Journal of Chemistry*, *9*, S1574-S1583.

7. Tepe, A. S., & Tepe, B. (**2015**). Traditional use, biological activity potential and toxicity of *Pimpinella* species. *Ind. Crops Prod.*, *69*, 153-166.

8. Hosseini, Z., Lorigooini, Z., Rafieian-Kopaei, M., Shirmardi, H. A., & Solati, K. (**2017**). A review of botany and pharmacological effect and chemical composition of *Echinophora* species growing in Iran. *Pharmacognosy Res.*, *9*(4), 305.

9. Mirghazanfari, S. M., Hosseinzadeh, L., Shokoohinia, Y., Aslany, M., & Kamali-Nejad, M. (**2012**). Acute and subchronic toxicological evaluation of *Echinophora platyloba* DC (Apiaceae) total extract in Wistar rats. *Clinics*, *67*(5), 497-502.

10. Gokbulut, I., Bilenler, T., & Karabulut, I. (**2013**). Determination of chemical composition, total phenolic, antimicrobial, and antioxidant activities of *Echinophora tenuifolia* essential oil. *Int. J. Food Prop.*, *16*(7), 1442-1451.

11. Shokoohinia, Y., Rashidi, M., Hosseinzadeh, L., Jelodarian, Z. (**2015**). Quercetin-3-O-β-D-glucopyranoside, a dietary flavonoid, protects PC12 cells from H_2O_2-induced cytotoxicity through inhibition of reactive oxygen species. *Food Chem.*, 167, 162–167.

12. Khazai, V., Piri, K.H., Nazeri, S., Karamian, R., Zamani, N. (**2011**). Free radical scavenging activity and phenolic and flavonoid contents of *Echinophora platyloba* DC. *Asian J. Med. Pharm. Res.*, 1, 9–11.

13. Kiani, M., Mohammadi, S., Babaei, A., Sefidkon, F., Naghavi, M. R., Ranjbar, M., & Potter, D. (**2017**). Iran supports a great share of biodiversity and floristic endemism for *Fritillaria* spp. (Liliaceae) A Review. *Plant Divers*.

14. Moghaddam, M., Taheri, P., Pirbalouti, A. G., & Mehdizadeh, L. (**2015**). Chemical composition and antifungal activity of essential oil from the seed of *Echinophora platyloba* DC. against phytopathogens fungi by two different screening methods. *LWT-Food Science and Technology*, *61*(2), 536-542.

15. Sepehri, Z., Javadian, F., Khammari, D., & Hassanshahian, M. (**2016**). Antifungal effects of the aqueous and ethanolic leaf extracts of *Echinophora platyloba* and *Rosmarinus officinalis*. *Curr. Med. Mycol.*, *2*(1), 30.

16. Shahneh, F., Baradaran, B., Majidi, J., & Babaloo, Z. (**2014**). *Echinophora platyloba* DC (Apiaceae) crude extract induces apoptosis in human prostate adenocarcinoma cells (PC 3). *Biomed. J.*, *37*(5).

17. Negri, R. (**2015**). Polyacetylenes from terrestrial plants and fungi: recent phytochemical and biological advances. *Fitoterapia*, *106*, 92-109.

18. Chauhan, R. S., Nautiyal, M. C., Tava, A., & Mella, M. (**2012**). Chemical composition of the volatile oil from the roots of *Selinum tenuifolium* Wall. *Helv. Chim. Acta*, *95*(5), 780-787.

19. Liu, X., Kunert, O., Blunder, M., Fakhrudin, N., Noha, S. M., Malainer, C., & Schuster, D. (**2014**). Polyyne hybrid compounds from *Notopterygium incisum* with peroxisome proliferator-activated receptor gamma agonistic effects. *J. Nat. Prod.*, *77*(11), 2513-2521.

20. Perry, N. B., Span, E. M., & Zidorn, C. (**2001**). Aciphyllal—a C34-polyacetylene from *Aciphylla scott-thomsonii* (Apiaceae). *Tetrahedron Lett.*, *42*(26), 4325-4328.

21. Kurimoto, S. I., Okasaka, M., Kashiwada, Y., Kodzhimatov, O. K., & Takaishi, Y. (**2010**). A C14-polyacetylenic glucoside with an α-pyrone moiety and four C10-polyacetylenic glucosides from *Mediasia macrophylla*. *Phytochemistry*, *71*(5-6), 688-692.

22. Chen, Y., Peng, S., Luo, Q., Zhang, J., Guo, Q., Zhang, Y., & Chai, X. (**2015**). Chemical and pharmacological progress on polyacetylenes isolated from the family Apiaceae. *Chem. Biodivers.*, *12*(4), 474-502.

23. Jelodarian, Z., Shokoohinia, Y., Rashidi, M., Ghiasvand, N., Hosseinzadeh, L., & Iranshahi, M. (**2017**). New polyacetylenes from *Echinophora cinerea* (Boiss.) Hedge et Lamond. *Nat. Prod. Res.*, 31(19), 2256-2263.

24. Babudri, F., Fiandanese, V., Marchese, G., & Punzi, A. (**2000**). Novel synthetic approach to (*S*)-coriolic acid. *Tetrahedron*, 56(2), 327-331.

25. Kaneko, Y., & Szallasi, A. (**2014**). Transient receptor potential (TRP) channels: a clinical perspective. *Br. J. Pharmacol.*, *171*(10), 2474-2507.

26. Uchida, K., Sun, W., Yamazaki, J., & Tominaga, M. (**2018**). Role of thermo-sensitive Transient Receptor Potential Channels in brown adipose tissue. *Biol. Pharm. Bull.*, *41*(8), 1135-1144.

27. Galindo, T., Reyna, J., & Weyer, A. (**2018**). Evidence for Transient Receptor Potential (TRP) channel contribution to arthritis pain and pathogenesis. *Pharmaceuticals*, *11*(4), 105.

28. Viana, F. (**2016**). TRPA1 channels: molecular sentinels of cellular stress and tissue damage. *J. Physiol.*, *594*(15), 4151-4169.

29. Kadkova, A., Synytsya, V., Krusek, J., Zímová, L., & Vlachová, V. (**2017**). Molecular basis of TRPA1 regulation in nociceptive neurons. A review. *Physiol. Res.*, *66*(3).

30. Avonto, C., Taglialatela-Scafati, O., Pollastro, F., Minassi, A., Di Marzo, V., De Petrocellis, L., & Appendino, G. (**2011**). An NMR spectroscopic method to identify and classify thiol-trapping agents: revival of Michael acceptors for drug discovery? *Angew. Chem.*, *123*(2), 487-491.

31. Chianese, G., Fattorusso, E., Putra, M. Y., Calcinai, B., Bavestrello, G., Moriello, A. S., & Taglialatela-Scafati, O. (**2012**). Leucettamols, bifunctionalized marine sphingoids, act as modulators of TRPA1 and TRPM8 channels. *Mar. Drugs*, 10(11), 2435-2447.

32. Fujimoto, Y., Sakuma, S., Komatsu, S., Sato, D., Nishida, H., Xiao, Y. Q., & Fujita, T. (**1998**). Inhibition of 15-hydroxyprostaglandin dehydrogenase activity in rabbit gastric antral mucosa by panaxynol isolated from oriental medicines. *J. Pharm. Pharmacol.*, *50*(9), 1075-1078.

CHAPTER 4:

PLASMODIUM TRANSMISSION BLOCKING AND ANTIPROLIFERATIVE METABOLITES FROM *DAUCUS VIRGATUS*, A TUNISIAN ENDEMIC PLANT

The main part of my Ph.D. thesis involved the phytochemical investigation of the apolar extract obtained from a Tunisian endemic plant, *Daucus virgatus*, belonging to the Apiaceae family. Among the 80 species of *Daucus* genus, eleven species and seven subspecies are widespread in Tunisia, and they have been used in the traditional Tunisian medicine for their diuretic properties or as a remedy for the treatment of cutaneous infections.

Daucus virgatus (Poir.) Maire, syn. *Caucalis virgata* Poir., *Ctenodaucus virgatus* (Poir.) Pomel, grows as an herbaceous annual or biennial species. It has slender, erect, decumbent and rigid stems of 30-70 cm; umbels are short and pedunculated with small pink or white colored flowers (**Fig. 4.1**).[1]

After an initial screening of a library of plant extracts obtained from organisms belonging to the Tunisian flora, we selected *Daucus virgatus* for further investigation. The bio-guided analysis of the CH_2Cl_2 extract of *D. virgatus* revealed the presence of some fractions that showed a preliminary *Plasmodium* transmission-blocking activity, which deserved further investigation in order to obtain the structural elucidation of secondary metabolites responsible for the pharmacological results. Following these leads, eight new angeloylated germacranolides have been isolated from the antimalarial fractions.

Furthermore, the complete phytochemical characterization of the extract was performed, because interestingly, no data appear to be available in the literature about the composition of *D. virgatus*. Thus, considering the contribution of my research group to the biological and chemical profile of medicinal plants growing in Tunisia, the study of the chemical composition of this endemic plant seemed to be an appealing project.[2-4] Hence, the additional isolated compounds, belonging to different families of molecules, were evaluated for their antiproliferative activity. The entire project has been carried out in collaboration with University of Monastir (Tunisia) for the plants' collection, with University of Camerino (Italy) for the determination of the antimalarial pharmacological potential, and with University of Naples "Federico II" for the evaluation of the antiproliferative activity.

Figure 4.1 *Daucus virgatus* collected in the North of Tunisia

4.1 *Daucus* genus

The genus *Daucus* includes more than 80 accepted species, distributed mostly in Europe, North Africa, West Asia and only few in North America and Australia. The phytochemistry of the genus has been well studied, leading to determine the composition of several extracts of its members.[1] Thus, the presence of flavonoids, polyacetylenes, terpenes and coumarins (**Fig. 4.2**) was detected and reported in studies mainly focused on various subspecies of *Daucus carota*, along with less common *Daucus* species, such as *Daucus syrticus* Murb, *Daucus reboudii* Coss., *Daucus glaber* Forsk., and *Daucus gingidium* L.

The best-known member of the genus is certainly *Daucus carota* L., whose fruits are called "nanheshi" in China, and traditionally used for their diuretic, antibacterial, anthelmintic, antifungal and cytotoxic properties. Carrot has been spread in the Northern Mediterranean regions by the Arab invaders, and they also introduced several cultivars, such as yellow, purple, and red carrot. The color of the root is an indication of the nature of compounds present in different species; for example, red and yellow carrots mainly contain lutein and lycopene, while orange carrots are characterized by the presence of α- and β-carotene. Black carrots present large amounts of flavonoids, such as luteolin, quercetin, myricetin, kaempferol, and

chlorogenic acid, along with several anthocyanins, which have been shown a protective role against cancer, diabetes, and oxidative stress.[5]

The Apiaceae family is rich in polyacetylene derivatives (See Chapter 3). In particular, the most abundant compound present in *Daucus* species is falcarindiol, followed by falcarinol, and falcarindiol-3-acetate. As shown by recent in vitro and in vivo studies, aliphatic C_{17}-polyacetylenes of the falcarinol-type found in *Daucus* genus, exerted an interesting cytotoxic and chemopreventive activity; falcarinol, panaxydol, and panaxytriol, for example, were reported to possess high cytotoxic activity against leukemia (L-1210), mouse melanoma (B-16), mouse fibroblast-derived tumor (L-929), and human gastric adenocarcinoma (MK-1) cells.[6] Moreover, falcarinol has proved to be an antagonist of the cannabinoid CB1 receptor.[7]

Monoterpenes are predominantly present in essential oils obtained from different *Daucus* species, with limonene, sabinene, and geraniol as three major products, along with α-thujene, α- and β-pinene, β-myrcene, and α-phellandrene.[8]

Daucane-type sesquiterpenes, along with eudesmane and guaiane-type secondary metabolites, have been found in *Daucus* genus, and they have been shown mainly antibacterial and antiproliferative activities.[9-10]

Coumarins, lactones of o-hydroxycinnamic acid, represent a broad class of allelochemicals, which are largely spread in almost all the higher plants. The presence of coumarins in the plant kingdom proves their important ecological role both in plant protection and in the communication with the external environment. The most important coumarins found in *Daucus* species are bergapten, isopimpinellin, and xanthotoxin, which are reported to have antibacterial and antifungal activities, along with immunosuppressive and anti-inflammatory properties.[11]

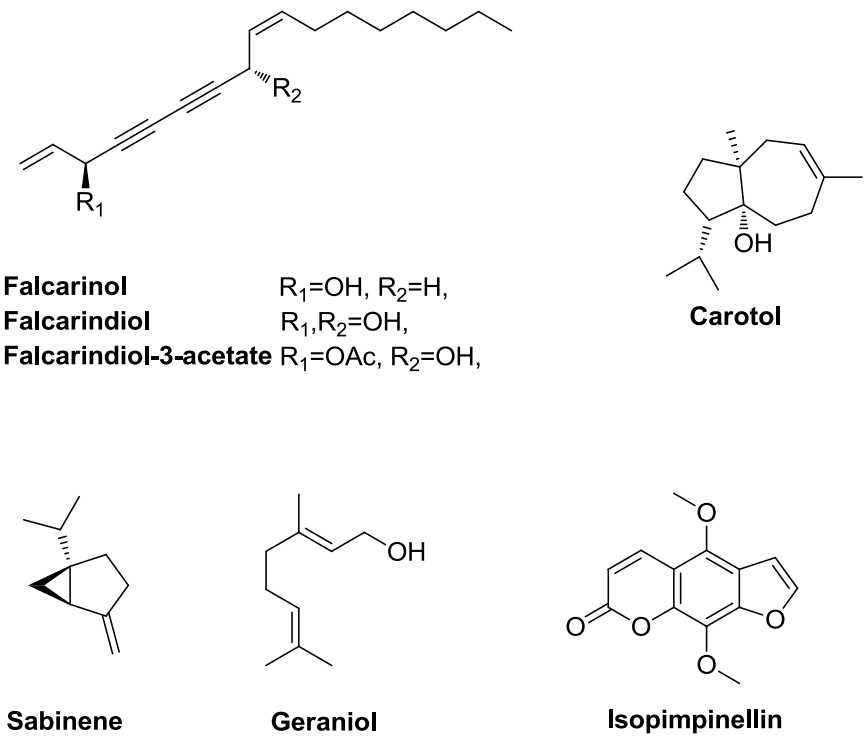

Figure 4.2 Secondary metabolites from *Daucus* genus

4.2 Malaria: a still alarming global burden

Malaria is an infectious disease transmitted by the bite of an infected female *Anopheles* mosquito and caused by several species of protozoan of the *Plasmodium* genus, four of which infect humans: *Plasmodium falciparum*, *Plasmodium. vivax, Plasmodium malariae and Plasmodium ovale*. It is endemic in more than 100 developing countries and it continues to be one of the most alarming public health problems, especially in sub- Saharan Africa, in terms of global mortality and morbidity. The World Health Organization (WHO) estimated over 400 000 deaths and 212 million new infection cases in 2015, mainly among children under the age of five and pregnant women.[12]

The *Plasmodium* life cycle (**Fig. 4.3**) begins after the release of the protozoan into the human's bloodstream; indeed, during a blood meal, an infected female mosquito inoculates sporozoites into the human host. Sporozoites undergo an initial replication in the liver (exo-erythrocytic schizogony), where they mature into merozoites and invade erythrocytes, causing anaemia (erythrocytic schizogony); the rupture of infected erythrocytes leads to the release into the bloodstream of cell debris

responsible for the fever spike patterns associated to the symptoms of malaria. Thus, the clinical symptoms of the disease are entirely attributable to *Plasmodium* in the erythrocytic stage; in lethal cases, after a modification of the erythrocytic cell membrane caused by a protein produced by the parasite, the red blood cells can stick to the walls of brain capillaries causing obstruction, followed by unconsciousness and, if it is not immediately treated, it can lead to death.

In some cases, merozoites can develop into male or female gametocytes, the sexual form of the parasite, which can be ingested by an *Anopheles* mosquito during a blood meal; the *Plasmodium* multiplication in the mosquito's midgut is known as sporogonic cycle. The fusion of gametocytes results in diploid cells (zygote) and leads to ookinetes. After mitotic divisions, sporozoites are formed, and they migrate to the salivary glands, making the mosquito infective to humans.[13]

Currently, the first-line treatment against malaria is represented by the Artemisinin-based Combination Therapy (ACT), in which some artemisinin derivatives (**Fig. 4.4**) are used in combination with long-acting antimalarial with different mechanisms of action, along with the diffusion of vector control measures, such as indoor residual spraying and insecticide-treated mosquito bed nets. Unfortunately, artemisinin-resistant strains of *P. falciparum* have appeared in South-East Asia and in five countries of the Greater Mekong subregion, with strong indications of rapid spread.[14]

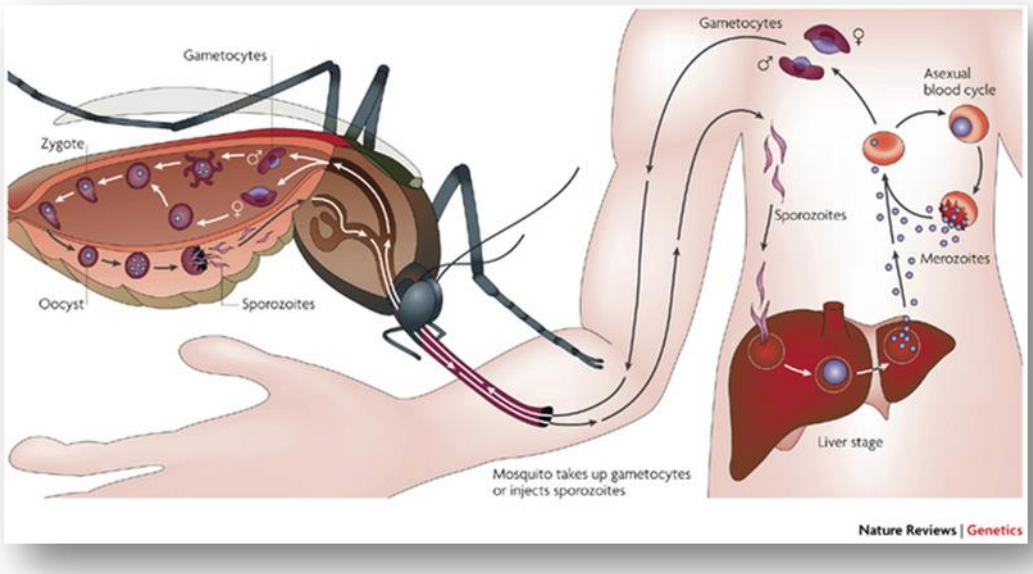

Figure 4.3 Malaria life cycle

Hence, new highly efficacious antimalarial drugs are urgently required, especially because the main drugs used to treat malaria are limited to three class of compounds, such as artemisinin analogues, quinolines and antifolates. This means that the attention of the scientific community must be focused on the malaria burden, in order to enrich the available chemotherapeutic arsenal to treat the infection, and to avoid possible resurgences of the disease, reaching the ambitious goal set by the WHO in its Global Technical Strategy for Malaria of a 90% reduction of malaria mortality within 2030.

Nowadays, the battle against malaria represents a terrible emergency, given the insurgence of insecticide-resistant vectors, drug resistance, and lack of an effective vaccine; it is therefore important to realize that a single intervention will not be enough to fulfill the WHO objective, and additional tools need to be developed and employed for malaria prevention and treatment.[15]

Thus, an integrated elimination/control strategy has a strong need to complement drugs active against the asexual blood stages of the parasite with antimalarials able to kill also the nonpathogenic *Plasmodium* stages responsible for transmission. These include gametocytes, the sexual forms of the parasite circulating for several days in the human host's bloodstream, but also the early sporogonic stages (ESS, namely, gametes, zygotes, ookinetes) developing in the *Anopheles* mosquito midgut after a gametocyte-containing blood meal. Primaquine and a few other 8-aminoquinolines are, among the drugs in use, the only ones able to target mature gametocytes in the human host. In this regard, the final aim of our research project is the design of an antimalarial combination therapy active against both the asexual and sexual stages of the parasite.[16] Hence, for pursuing this goal, the screening of natural products has already revealed to be a successful approach, especially if we consider the discovery of artemisinin as a remarkable example (See Chapter 1).

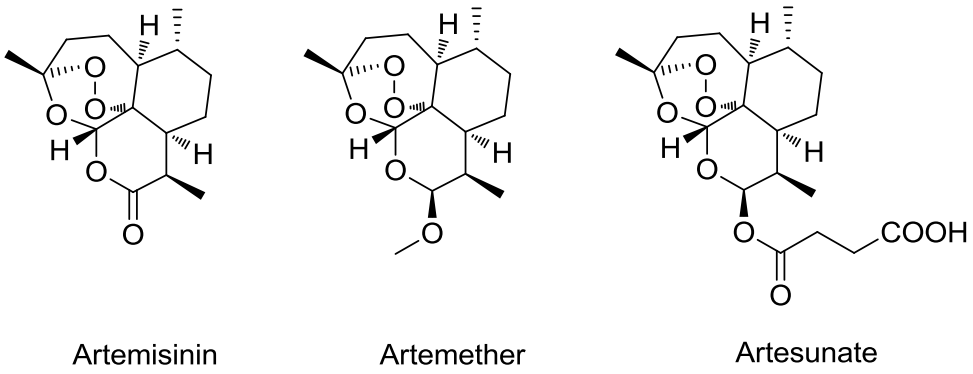

Figure 4.4 Artemisinin and its apolar (artemether) and polar (artesunate) derivatives

4.2.1 Plants traditionally used to treat malaria

Traditional herbal medicines have been used to treat malaria worldwide for centuries. The first antimalarial drug, deriving from the plant kingdom, was the alkaloid quinine, extracted from the bark of several *Cinchona* (Rubiaceae) species. Infusions of the plant bark were used to treat human malaria and in some African countries they are still largely administered. Then, years later quinine was isolated, characterized, and then used as a starting point for the synthesis of two antimalarial drugs: chloroquine and mefloquine. More recently, after the diffusion of chloroquine-resistant *P. falciparum* strains, another natural product, artemisinin (isolated from the Chinese plant *Artemisia annua*), has been successfully used to treat these difficult clinical cases.[17-18]

In the last years, there has been a great interest in the search for new natural leads that potentially could be developed as new drugs for the treatment of malaria and other infectious diseases and, in this regard, there is the possibility to draw on a huge natural heritage. Given the large number of plants traditionally used for their antimalarial activity and the recent availability of robust and reproducible screening methods for antimalarial agents, the research work aiming at the development of new drugs is still on the rise.

In addition to the historical plants mentioned above, some other species are also commonly used for malaria treatment in Africa, such as *Azadirachta indica*, *Khaya senegalensis*, and *Vernonia amygdalina*, to name a few of them.

Azadirachta indica, also known as "neem tree", is a plant still used in many African countries against fever and malaria as a decoction of the leaves, stem bark and root. NeemAzal® is a commercial extract obtained from the seeds of *Azadirachta indica*, that has shown to inhibit the *Plasmodium* development in the vector; azadirachtin A, a limonoid isolated from this plant, represent the main compound responsible for the activity. Indeed, it has been shown to significantly inhibit the formation of flagellate microgametes (one of the sexual stages of *Plasmodium*), suggesting that microgametogenesis is the final target of NeemAzal® transmission-blocking activity.[19]

All the species of the *Khaya* genus, also belonging to the Meliaceae family, are well-known for their high-quality wood, which is resistant to insect and fungal attack; they grow especially in the savannah forests, mostly in the countries of Nigeria, Senegal, Sudan, Uganda, and Zaire. In particular, stem barks decoctions of *Khaya senegalensis* and *Khaya grandifoliola*, usually planted by roadsides for shade, are extensively used as antimalarial remedies.[20]

In sub-Saharan countries, the leaves of *Vernonia amygdalina* Del. are used for the treatment and prevention of malaria, and the antiplasmodial activity of this plant, belonging to the Asteraceae family, has been proved by *in vitro* and *in vivo* studies. Different secondary metabolites responsible for the biological activity have been isolated and characterized, and among them, sesquiterpene lactones have been shown to be the most active compounds against *P. falciparum* blood stages. They include the highly oxygenated derivatives vernolide, vernodalol, vernodalinol, epivernodalol, vernodalin and vernomygdalin.[21]

In the frame of our ongoing research work, leading to the discovery of new promising natural products with *Plasmodium* transmission-blocking activity, the ethnopharmacological approach can be only a starting point, but it cannot give unequivocal indications. In fact, as mentioned in the previous paragraph, the final target of our project is the discovery of new lead compounds able to target also the non-pathogenic stage of malaria life cycle, and not only the asexual erythrocytic phase responsible for the clinical symptoms of the disease, that is normally the target of the traditional natural remedies. For this reason, the recent availability of robust and reproducible screening methods for antimalarial transmission-blocking agents inspired us to screen extracts obtained from plants of the African flora in order to select lead compounds endowed with stage-specific, transmission-blocking activity.

The bio-guided approach used in this study has been resulted in the isolation of eight new angeloylated germacranolides from the aerial parts of the endemic Tunisian plant *Daucus virgatus*, making possible to enrich the chemical weapons suited to fight the dreaded battle against malaria.

4.3 The biosynthesis of *Daucus* sesquiterpenes

Isoprenoids represent one of the biggest classes of natural products known to date. All members of this group are characterized by a five-carbon isoprene building block, that can be linked by a head-to-head or a head-to-tail condensation reaction; the introduction of different functional groups such as aldehydes, peroxides, alcohols, ketones, esters, etc., results in several linear or cyclic compounds. These include members of mono-, sesqui-, di-, and triterpene families. After modifications, the isoprene building blocks lead to the formation of isoprenoids or, as they are also called, terpenoids, which are crucial for a large number of cellular processes, comprising transcription modifications, protein degradation, photosynthesis electron transport, intracellular signaling, and defense mechanisms.[22]

Even though plant isoprenoids have been used for centuries for their pharmacological applications, flavor, and aroma, scarce information on their chemical structures and properties were available until the beginning of the 19th century. All isoprenoids are synthesized by the subsequent condensation of the five-carbon monomer isopentenyl diphosphate (IDP), formed starting from acetyl-CoA, to its isomer, dimethylallyl diphosphate (DMADP). The first intermediate that can be generated is geranyl diphosphate (GDP, C_{10}), formed by the condensation of IDP with another unit of DMADP; as outlined in **Scheme 4.1**, GDP leads to monoterpenes (C_{10}).

Reaction with an additional unit of IDP results in farnesyl diphosphate (FDP, C_{15}), the substrate for the sesquiterpenes (C_{15}), and, the subsequent elongation by addition of a C_5 moiety provides geranylgeranyl diphosphate (GGDP, C_{20}), the precursor of the diterpene family (C_{20}). The terpenoid diversity is due to the capacity of natural enzymes to synthesize multiple products from the same substrate, through a complex reaction cascade. In this way, it is possible to maximize the structural diversity of the products obtained from the natural source, using the fewest number of biosynthetic steps.[23] Sesquiterpenes are natural products found in both terrestrial and marine

environment, that have proved to possess a broad variety of promising biological activities; in this paragraph, I will focus the attention on the biosynthesis of sesquiterpene skeletons present in *Daucus* species, namely daucane-, eudesmane-, elemane- and germacranolide-type compounds. From a biosynthetic point of view, germacrane sesquiterpenes directly derive from (*E*, *E*)-farnesyl pyrophosphate (FPP), which is formed by the condensation of DMADP with two units of IDP; an enzyme, farnesyl pyrophosphate synthase, catalyzes the reaction. In turn, FPP is subjected to an ionization reaction to give a reactive transoid farnesyl carbocation, which can readily react with the C10–C11 double bond, leading to the formation of the (*E*,*E*)-germacradienyl cation (**Scheme 4.2**).

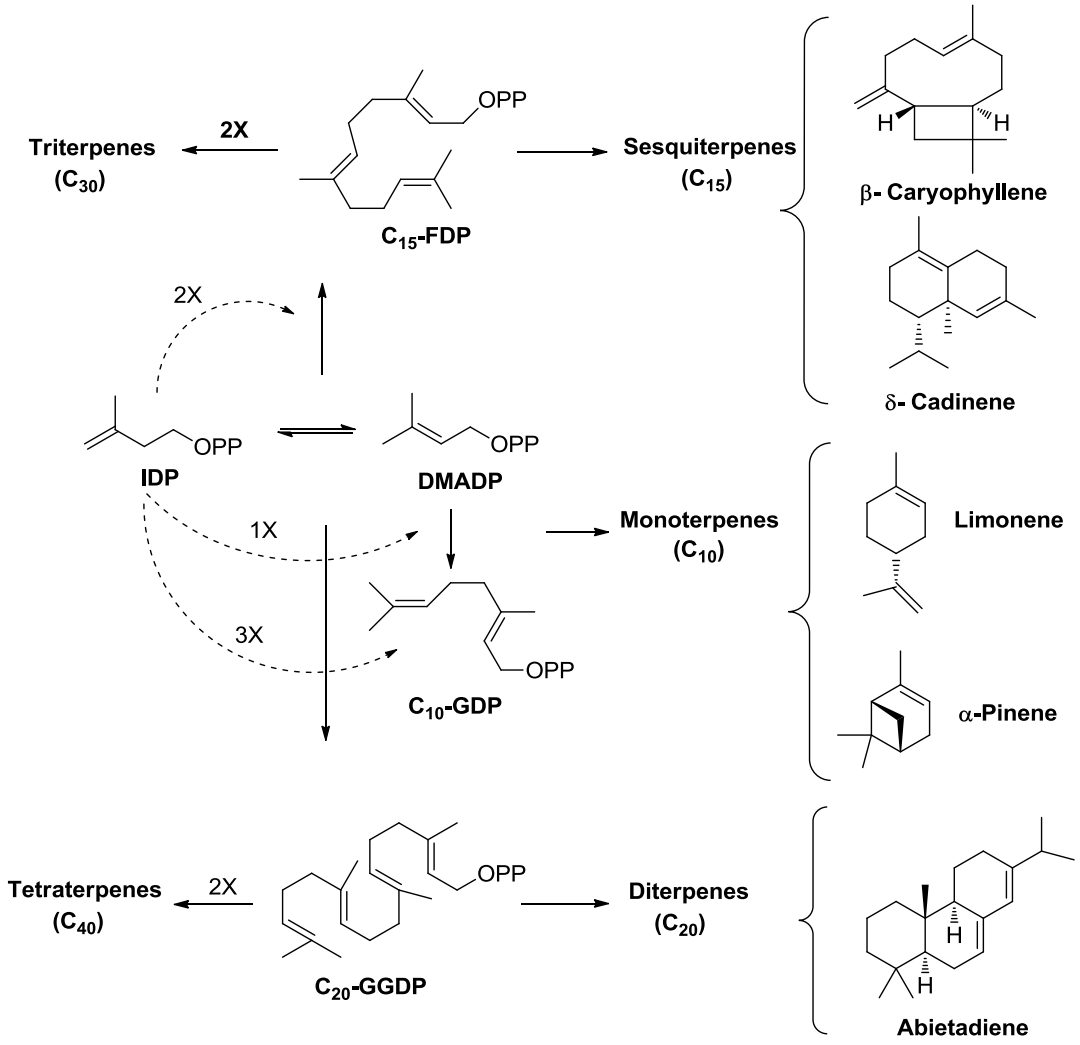

Scheme 4.1 Biosynthetic pathways of terpenoids

The cyclization step is catalyzed by an FPP cyclase and it is important to note that this reaction leads to the creation of a new stereogenic center. At this point, the resulting germacrane represents the key intermediate for the biosynthesis of eudesmane, and elemane sesquiterpenes. Otherwise, the isomerization around C2–C3 double bond can generate the cisoid nerolidyl cation, which after cyclization leads to the cycloheptenyl cation, the key intermediate in the formation of daucane sesquiterpenes.[24]

Several studies reported in the literature indicate that *Daucus* genus is characterized by the presence of sesquiterpene lactones mainly belonging to the daucane type. Remarkably, the phytochemical investigation of the apolar extract of *D. virgatus* has proved to be dominated by germacranolides and related derivatives, proving that in this species is primarily expressed the biosynthetic pathway leading to the formation of the transoid farnesyl carbocation.

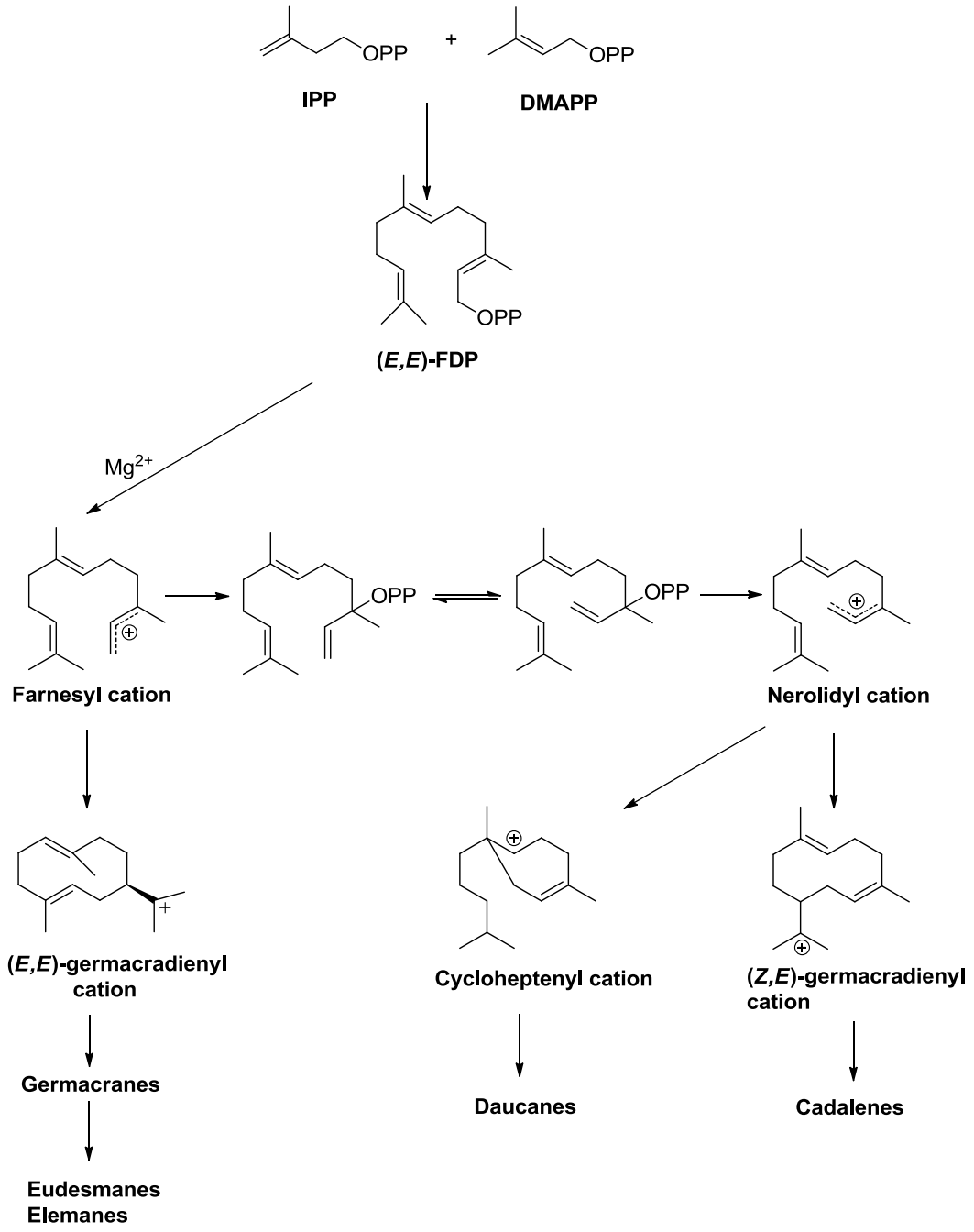

Scheme 4.2 Biosynthetic route for the sesquiterpene lactones from *D. virgatus*

With regard to the conformational behavior of the germacrane core, it is important to underline that the highest percentage of known germacranes are characterized by the flexible (*E*,*E*)-cyclodeca-l (10),4-diene ring core, but (*Z*,*Z*)-, (*Z*,*E*)-, and (*E*,*Z*)-germacranes are also present in nature (**Fig. 4.5**). The studies focused on the conformational features of germacranes, in particular, the (*E*,*E*)-germacranes, have

shown that the 10-membered ring can exist in four different conformations which can be indicated as UU, UD, DU, and DD. U (up) and D (down), indicate the orientation of the C (14) and C (15) methyl groups. These conformers are interconvertible by rotation of each double bond through the ring. The main part of the naturally occurring (*E*,*E*)-germacranolides studied, shows the UU conformation. In contrast, the DU and UD conformations seem to be typical for the melampolides and heliangolides. The occurrence of these different germacrane conformations plays an important role in the biosynthesis of other sesquiterpenes.[25]

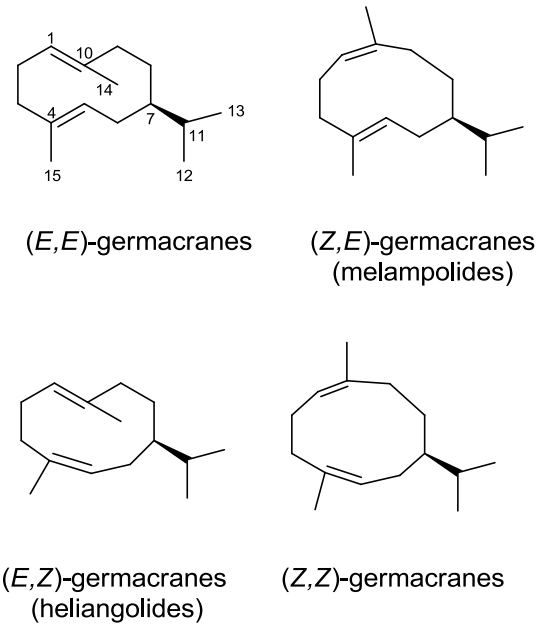

Figure 4.5 Different germacranes conformations

As an example of the biosynthetic pathway of germacranolides, and to show the mechanism for the functionalization of the isopropyl side chain, the biosynthesis of the well-known costunolide, a naturally occurring sesquiterpene lactone, will be described. This biosynthetic mechanism was proposed by de Kraker *et al*., pointing out that C15 hydrocarbon germacrene A is formed by FPP cyclization, catalyzed by germacrene A synthase (GAS); after a three-step oxidation of the methyl group at C12, by the cytochrome P450 germacrene A oxidase (GAO), the formation of germacra-1(10),4,11(13)-trien-12-oic acid is carried out. In turn, the latter is hydroxylated by (+)-costunolide synthase (COS) into an unstable intermediate that

undergoes a non-enzymatic lactonization of C6 hydroxyl and C12 carboxylic group, affording costunolide (**Scheme 4.3**).[26]

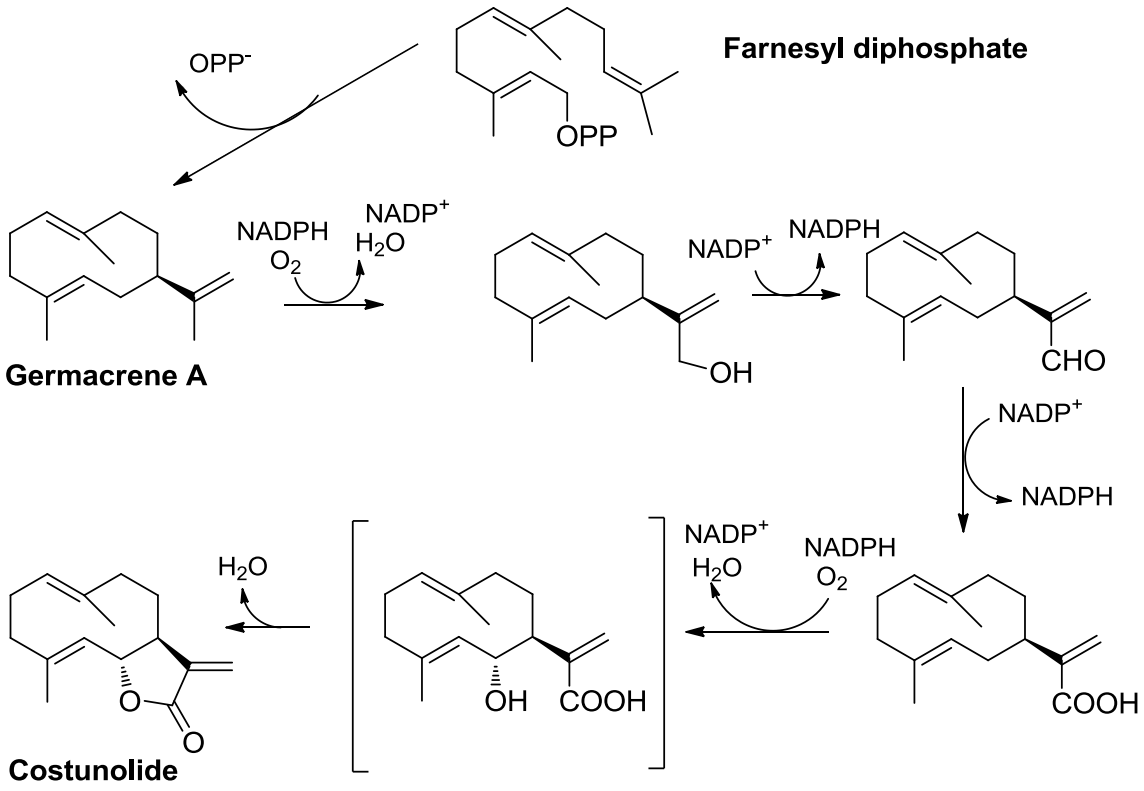

Scheme 4.3 Biosynthesis of costunolide

4.4 Isolation and structural elucidation of angeloylated germacranolides with *Plasmodium* transmission blocking activity

The aerial parts of *D. virgatus* were collected during the flowering stage in the area of Bizserta, Northwest Tunisia, dried, pulverized, and extracted by maceration in methanol. The crude methanol extract, after removal of the solvent under vacuum, was dissolved in water and defatted by partitioning with *n*-hexane and then partitioned against dichloromethane and *n*-butanol. Repeated purifications of the CH_2Cl_2 fractions, showing *Plasmodium* transmission-blocking activity, by column chromatography and HPLC, afforded daucovirgolides A−H (**1**−**8**) in the pure form (**Fig. 4.6**).

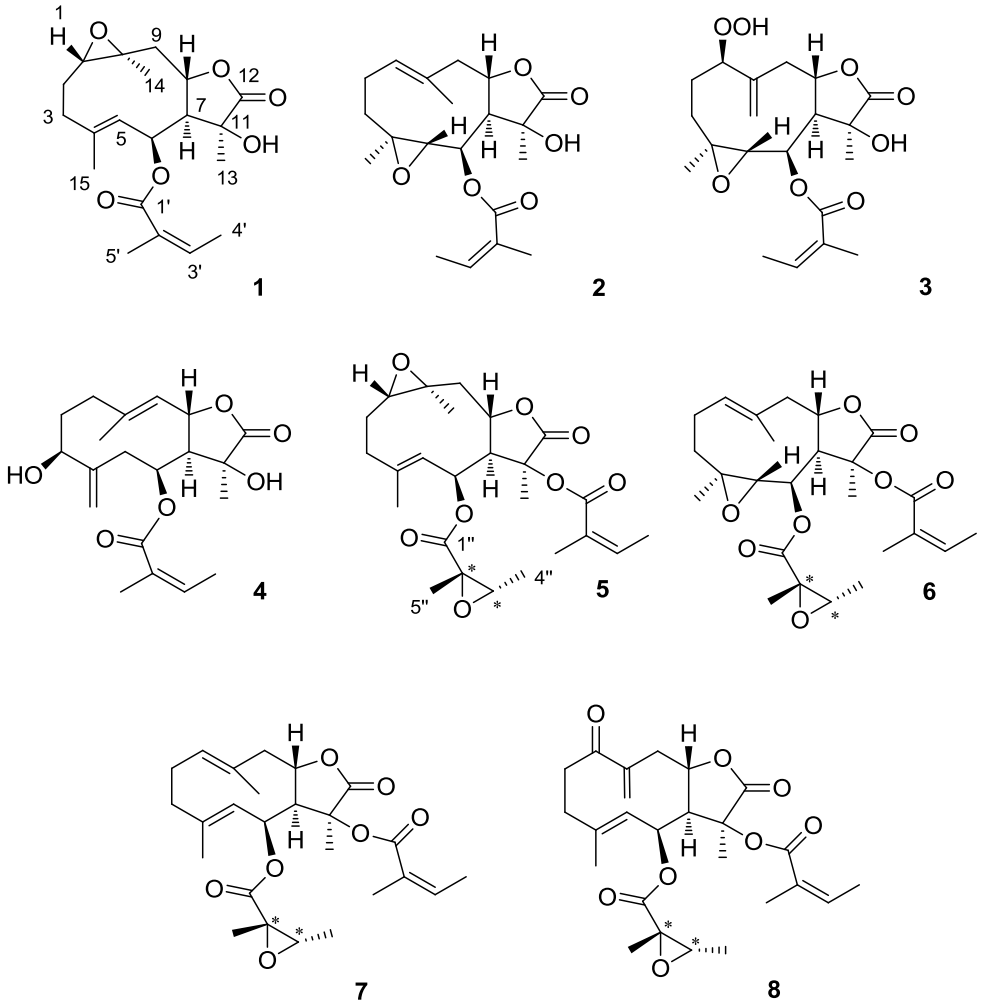

Figure 4.6 New angeloylated germacranolides from *Daucus virgatus*

The stereostructures of the isolated sesquiterpene lactones have been determined by a combination of MS, 1D and 2D NMR spectroscopy, chemical derivatization, and comparison of experimental electronic circular dichroism curves with TDDFT-predicted data. These secondary metabolites were identified as angeloylated germacranolides differing in the oxidation pattern and the acylation of the sesquiterpenoid core. Interestingly, when only an acyl group is present in the molecule, it is always an angeloyl group linked to the C-6, while if two acyl groups are present, the angeloyl group is linked to the C-11, while the other acyl group consists in an epoxy-angeloyl group linked to the C-6.

The molecular formula $C_{20}H_{28}O_6$, indicating seven unsaturation degrees, was detected for daucovirgolide A (**1**) by HRESIMS. The ^{1}H NMR spectrum of (**1)** (**Table 4.1**) showed the typical resonances of the angeloyl group (δ_H 6.11, qq, 1H; 1.99, d, 3H; 1.81, s, 3H), three resonances in the mid-field region, a series of multiplets between δ_H 2.83 and 1.43, and three relatively deshielded methyl singlets at δ_H 1.73, 1.57, and 1.36. The 2D NMR HSQC experiment (see **Table 4.2** for ^{13}C NMR assignments) indicated the presence of a trisubstituted double bond (δ_H 5.24, δ_C 126.7) and of three oxymethines (δ_H 5.79, δ_C 68.8; δ_H 4.80, δ_C 75.8; δ_H 2.83, δ_C 62.2), with the latter probably being part of an epoxide ring.

The 2D $^{1}H–^{1}H$ COSY spectrum of compound (**1)** arranged all the multiplets of the sesquiterpenoid core within two fragments (**Fig. 4.7**), the first spanning from the oxymethine H-1 to H_2-3 and the second one connecting H-5 to H_2-9 and encompassing the two remaining oxymethines (C-6 and C-8) as well as a branching at C-7. These two fragments were connected on the basis of the HMBC cross-peaks of CH_3-14 (δ_H 1.36) and CH_3-15 (δ_H 1.73) as shown in **Fig. 4.7**, resulting into the 10-membered carbocyclic ring typical of the germacrane skeleton. The third methyl group (δ_H 1.57) showed HMBC correlations with C-7, the oxygenated C-11 (δ_C 71.7), and the lactone carbonyl C-12 (δ_C 178.8).

Finally, correlations of H-8 with C-12 and of H-6 with C-1′ indicated unambiguously the lactonization and angeloylation positions on the germacrane core. The presence of an epoxide ring at C-1/ C-10 was in agreement with the molecular formula and with the H/C resonances at these positions, thus clearly defining the planar structure of daucovirgolide A (**1**)

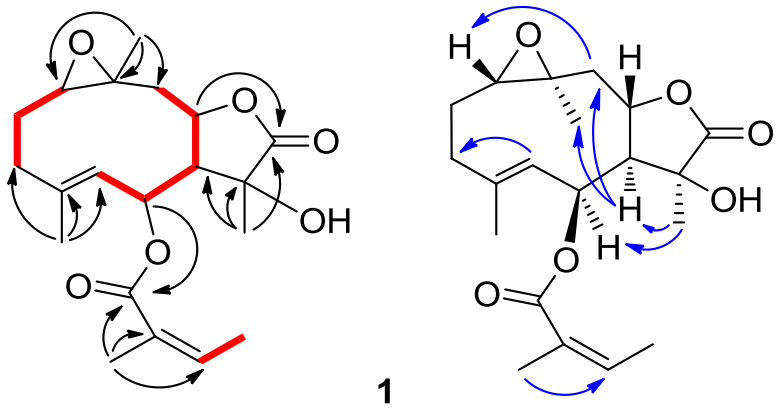

Figure 4.7 COSY (red bold line), key HMBC (black arrows), and ROESY (blue arrows) correlations detected for daucovirgolides A (**1**)

The network of ROESY correlations reported in **Fig. 4.7** was used to assign the relative configuration of the six asymmetric carbons of (**1**), resulting into a trans junction of the lactone ring. The geometries of the epoxide ring and the $\Delta^{4(5)}$ and $\Delta^{2'(5')}$ double bonds were also determined on the basis of proximities deduced from the ROESY experiment.

HRESIMS indicated that daucovirgolide B (**2**) possesses the same molecular formula of compound (**1**). Comparison of the ^{1}H NMR spectra of these two molecules showed some parallelisms, demonstrating only a small shift of resonances and, in a few cases, a change of their multiplicities. As for (**1**), the COSY spectrum of compound (**2**) showed the proton multiplets arranged in two spin systems, but clearly indicated the presence of scalar coupling between the epoxide

methine (H-5, δ_H 2.60) and the angeloylated oxymethine H-6 (δ_H 5.12), while, in turn, the sp^2 methine at δ_H 5.35 was coupled to H_2-2. Combined analysis of the HSQC and HMBC experiments confirmed that daucovirgolide B (**2**) is an isomer of (**1**), presenting inverted epoxide and double-bond positions. The HMBC fully supported this assumption, and, in addition, cross-peaks H-8/C-12 and H-6/C-1′ confirmed the placement of lactone and angeloyl groups, respectively.

Table 4.1. ^{1}H NMR Data (500 MHz) in $CDCl_3$ of selected daucovirgolides

	Daucovirgolide A (1)	**Daucovirgolide C (3)**	**Daucovirgolide D (4)**	**Daucovirgolide G (7)**
	δ_H, mult., *J* in Hz	**δ_H, mult., *J* in Hz**	**δ_H, mult., *J* in Hz**	**δ_H, mult., *J* in Hz**
1a	2.83, d, 11.0	4.53, m	2.23, m	4.98, d, 10.0
1b	-	-	2.25, m	-
1-OOH	-	7.84, s	-	-
2a	1.43, m	2.17, m	1.84, m	2.20, m
2b	2.06, m	2.17, m	2.03, m	2.41, m
3a	2.23, overlapped	2.09, m	4.28, d, 8.4	2.07, overlapped
3b	2.30, dd, 13.0, 5.2	1.22, m	-	2.21, m
5a	5.24, d, 6.3	2.83, d, 7.8	2.23, overlapped	4.80, overlapped
5b	-	-	2.44, d, 5.4	-
6	5.79, d, 6.3	5.12, d, 7.8	5.47, m	5.63, bs
7	2.41, bs	2.41, bs	3.06, t, 10.7	2.75, bs
8	4.80, bdd, 12.0, 6.0	4.94, m	5.17, d, 11.2	4.80, overlapped
9a	2.11, m	2.51, m	5.35, d, 11.2	1.88, overlapped
9b	2.22, m	3.06, dd, 13.4, 3.2		2.99, overlapped
13	1.57, s	1.59, s	1.45, s	1.84, s
14a	1.36, s	5.45, bs	1.70, s	1.73, s
14b	-	5.38, bs		-
15a	1.73, s	1.42, s	4.84, s	1.60, s
15b	-		5.14, s	-
3'	6.11, qq, 7.3, 1.1	6.11, qq, 7.3, 1.1	6.11, qq, 7.3, 1.1	6.17, qq, 7.3, 1.1
4'	1.99, d, 7.3	1.99, d, 7.3	1.98, d, 7.3	2.03, d, 7.3
5'	1.81, bs	1.84, bs	1.91, bs	1.89, bs
3''	-	-	-	2.98, q, 5.4
4''	-	-	-	1.23, d, 5.4
5''	-	-	-	1.45, s

The ROESY spectrum, besides confirming the relative arrangement at C-6, C-7, C-8, and C-11, indicated the relative configuration of the epoxide ring (from cross-peaks of CH_3-15 with H-6 and H-7).

Daucovirgolide C (**3**), $C_{20}H_{28}O_8$ by HRESIMS, was identified as an analogue of (**2**) with an oxidative modification at the $\Delta^{1(10)}$ double bond. Inspection of the ^{1}H and ^{13}C NMR spectra of (**3**), clearly indicated that the sp^2 methine signal at C-1 of (**2**) was replaced by a hydroperoxy-bearing sp^3 methine (δ_H 4.53, δ_C 85.2; −OOH δ_H 7.84), and the CH_3-14 singlet of (**2**) had been replaced by an sp^2 methylene (δ_H 5.38 and 5.45, δ_C 121.0). Detailed analysis of the 2D NMR spectra of (**3**) supported this inference and, accordingly, H/C resonances at the remaining positions were closely

comparable to analogous signals for (**2**). The ROESY spectrum of (**3**) confirmed the relative arrangement for positions C-4/C-5/C-6/C-7/C-8 and C-11 and indicated the relative configuration at C-1 (cross-peaks H- 1/H-7 and OOH-1/H-9α), thus defining the relative stereostructure of (**3**).

The ^{1}H NMR spectrum of daucovirgolide D (**4**) ($C_{20}H_{28}O_6$ by HRESIMS) clearly suggested that this compound belongs to the daucovirgolide structural series, exhibiting the presence of an angeloyl moiety, an exomethylene group (δ_H 5.14 and 4.84, both bs), and two methyl singlets at δ_H 1.45 and 1.70. Having associated all the proton signals to the directly linked carbon atoms by means of the HSQC spectrum, the proton multiplets were arranged into the two spin systems shown in **Fig. 4.8**.

The 10-membered ring of the germacranolide system was assembled on the basis of the HMBC cross-peaks of CH_3-14 and H_2-15 (**Fig. 4.8**), while HMBC correlations of H-6 and H-8 with the ester carbonyls indicated the relative placement of the angeloyl moiety and of the lactone ring, respectively. Finally, HMBC correlations of CH_3-13 with C-7, the oxygenated C-11, and the carbonyl C-12 completed the definition of the planar structure of daucovirgolide D (**4**).

The relative configuration at C-6, C-7, C-8, and C-11 of (**4**) proved to be the same as that of **1**–**3**, on the basis of the network of ROESY cross-peaks shown in **Fig. 4.8**. This configuration was connected to that at C-3 based on the marked ROESY correlation H-3/H-6, which indicated the β-orientation of the hydroxy group at C-3.

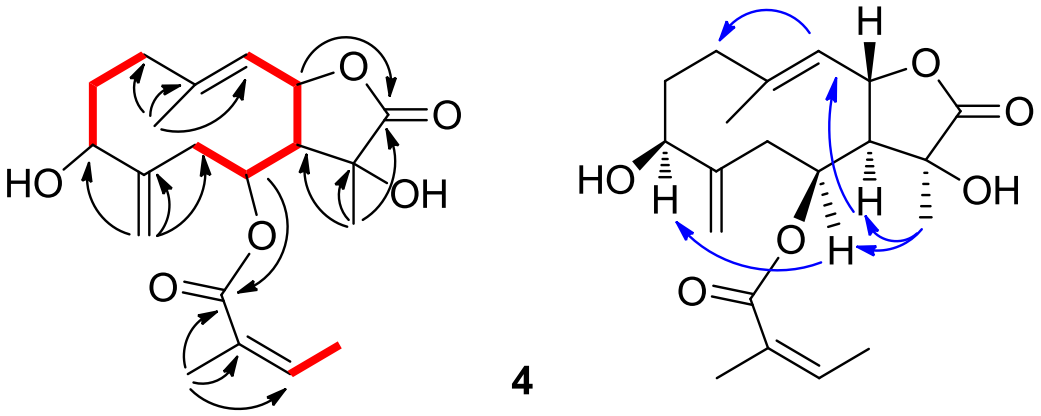

4

Figure 4.8 COSY (red bold line), key HMBC (black arrows), and ROESY (blue arrows) correlations detected for daucovirgolides D (**4**).

The structures of the remaining daucovirgolides E−H (**5**−**8**) included two different acyl groups, identified readily as angeloyl and epoxyangeloyl units on the basis of their NMR spectroscopic data (see **Tables 4.1** and **4.2**). Interestingly, the epoxyangeloyl group was attached consistently at C-6 (HMBC cross-peak H-6/C-″), while the angeloyl group was linked at C-11 in each case. The relative configuration of the epoxyangloyl group was inferred from the ROESY cross-peak between H-3″ and Me-5. It should be noted that, for all of compounds **5**−**8**, the relative configuration at the epoxyangeloyl moiety could not be connected to that of stereogenic centers belonging to the germacrane ring.

Table 4.2. ^{13}C NMR data (125 MHz) in $CDCl_3$ of selected daucovirgolides

Pos.	Daucovirgolide A (**1**)	Daucovirgolide C (**3**)	Daucovirgolide D (**4**)	Daucovirgolide G (**7**)
	δ_C, mult.	δ_C, mult.	δ_C, mult.	δ_C, mult.
1	62.2, CH	85.2, CH	39.1, CH_2	131.5, CH
2	24.3, CH_2	25.7, CH_2	34.5, CH_2	24.4, CH_2
3	36.7, CH_2	33.9, CH_2	71.5, CH	38.4, CH_2
4	136.4, C	58.4, C	149.7, C	138.7, C
5	126.7, CH	65.5, CH	40.6, CH_2	126.0, CH,
6	68.8, CH	68.8, CH	68.5, CH	70.6, CH
7	51.4, CH	50.1, CH	50.6, CH	50.0, CH
8	75.8, CH	78.7, CH	74.2, CH	79.0, CH
9	42.6, CH_2	40.1, CH_2	118.4, CH	39.3, CH_2
10	57.1, C	139.8, C	146.7, C	138.2, C
11	71.7, C	72.4, C	74.3, C	77.5, C
12	178.8, C	177.9, C	179.0, C	174.0, C
13	29.1, CH_3	29.4, CH_3	22.8, CH_3	24.7, CH_3
14	22.1, CH_3	121.0, CH_2	17.3, CH_3	20.7, CH_3
15	17.3, CH_3	17.1, CH_3	111.3, CH_3	16.9, CH_3
1'	166.7, C	166.3, C	167.6, C	167.2, C
2'	127.2, C	127.2, C	127.5, C	126.8, C
3'	140.8, CH	140.6, CH	139.4, CH	140.7, CH
4'	16.0, CH_3	16.1, CH_3	15.9, CH_3	15.9, CH_3
5'	20.5, CH_3	20.5, CH_3	20.5, CH_3	20.4, CH_3
1"				168.2, C
2"				59.3, C
3"				59.6, CH
4"				13.2, CH_3
5"				18.4, CH_3

Daucovirgolide E (**5**) was determined to possess the same 1,10-epoxygermacranolide core of (**1**) on the basis of a parallel pattern of H/C resonances (with the exception of those belonging to the γ-lactone ring) and 2D NMR correlations, including the ROESY spectrum. Similar reasoning was applied to assign the structure of daucovirgolide F (**6**), which was found to possess the same 4,5-epoxygermacranolide core as (**2**).

Daucovirgolide G (**7**), $C_{25}H_{34}O_7$ by HRESIMS, was identified as the likely biogenetic precursor of the daucovirgolides E (**5**) and F (**6**), since it shared epoxyangeloylation at C-6 and angeloylation at C-11 and included two trisubstituted double bonds at $\Delta^{1(10)}$ and $\Delta^{4(5)}$ (δ_H 4.98, δ_C 131.5; δ_H 4.80, δ_C 126.0, respectively). The ROESY cross-peaks CH_3-14/H_2-2 and H-5/H_2-3 defined the *E*- geometry at both these centers.

Finally, minute amounts of daucovirgolide H (**8**), $C_{25}H_{32}O_8$ by HRESIMS, were also isolated. The additional unsaturation degree and the additional oxygen atom, when compared to (**7**), implied by this molecular formula, were rationalized by the presence of a ketone carbonyl (δ_C 204.1) at position 1, conjugated with the $\Delta^{10(14)}$ exocyclic double bond. Accordingly, the deshielded sp^2 methylene protons resonated at δ_H 5.88 (bs) and 6.06 (bs), and a marked downfield shift was also experienced by protons at C-2 (δ_H 3.36 and 2.28) and C-9.

The stereostructure of the remaining part of the molecule was the same as that of daucovirgolide G (**7**).

4.5 Absolute configuration of daucovirgolides

Germacranes are an extremely diverse class of sesquiterpenoids, and their variability is not limited to their structural architecture; it also includes stereochemical features. For example, molecules containing a 1,5-cyclodecadienes moiety in their structure can exist in different conformers that are very close in energy, showing the possibility to be interchangeable, given the small energy barriers. Germacranolides are endowed with large conformational freedom, but this freedom is primarily restricted by the γ-lactone ring fused to the cyclodecadiene core. Four principal conformational forms have been proposed (**Fig. 4.9**).

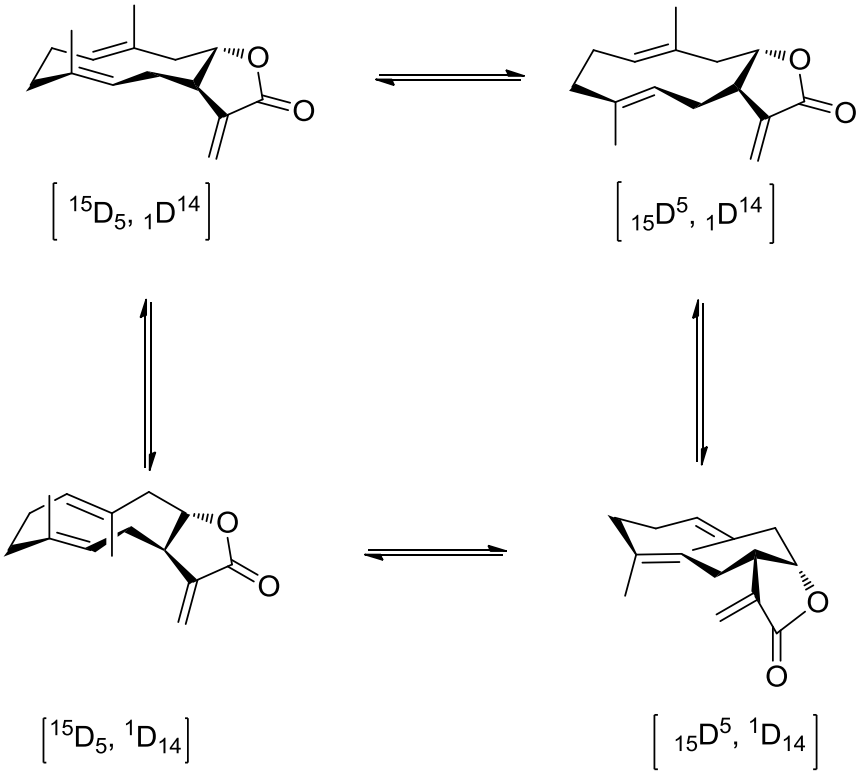

Figure 4.9 Conformational equilibrium of germacranolides

Following Samek's nomenclature, these conformers are indicated as [$^{15}D_5$, $_1D^{14}$] and [$_{15}D^5$, $^1D_{14}$], meaning that the two double bonds C1-C10 and C4-C5 are cross oriented, while the conformers [$_{15}D^5$,$_1D^{14}$] and [$^{15}D_5$, $^1D_{14}$] possess the double bonds in parallel position (**Fig 4.9**). The four conformers exist in a dynamic equilibrium through rotation of the bonds close to the C1-C10 and C4-C5 double bonds. For example, the stereostructure of the sesquiterpene lactone 6-epidesacetyllaurenobiolide, a germacranolide isolated from *Montanoa grandiflora*, was determined by X-ray diffraction. The X-ray data clearly proved that the 10-membered ring exists in a [$_{15}D^5$,$_1D^{14}$] conformation, showing that the methyl group at C-4 is α-oriented, while the methyl group at C-10 is β-oriented. Conversely, the common conformation [$^{15}D_5$,$_1D^{14}$] of the costunolide-type germacranolides, display both methyl groups above the plane of the 10-membered ring (β-oriented).[27]

Germacranolides related to daucovirgolides and belonging to two enantiomeric stereochemical series have been found in different plants; thus, an unambiguous experimental determination of absolute configuration for the isolated compounds appeared necessary. Analyzing daucovirgolide A (**1**), for example, a simple

derivatization with chiral auxiliaries was not applicable in this case, consequently a computational approach was applied. Thus, a molecular modeling analysis on compound (**1**) (with simulations carried out for 500 ps by using the CVFF force field as implemented in Discover software) afforded three reasonably populated conformers (**Fig. 4.10**).

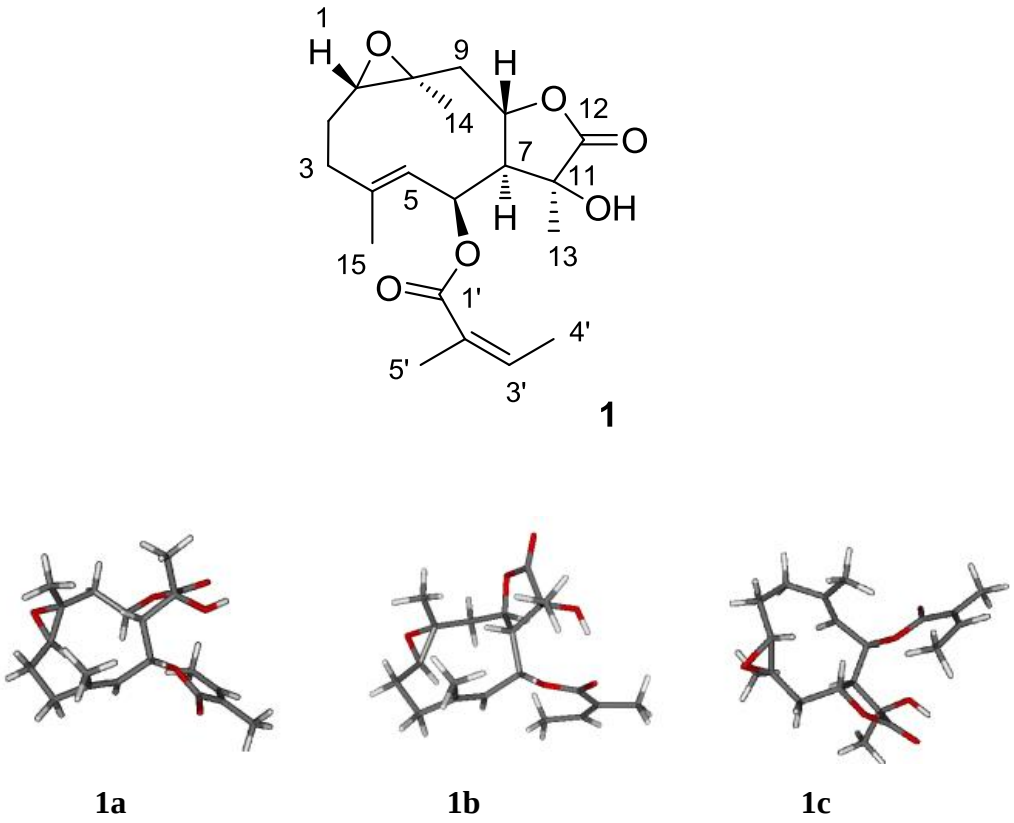

Figure 4.10 Structure of daucovirgolide A (**1**) and its three populated conformers

The Boltzmann-averaged CD curves for the two enantiomers of (**1**) were calculated using the TDDFT approach, with Gaussian03 software, and then compared to the experimental data (**Fig. 4.11**), thus indicating the absolute configuration of daucovirgolide A.

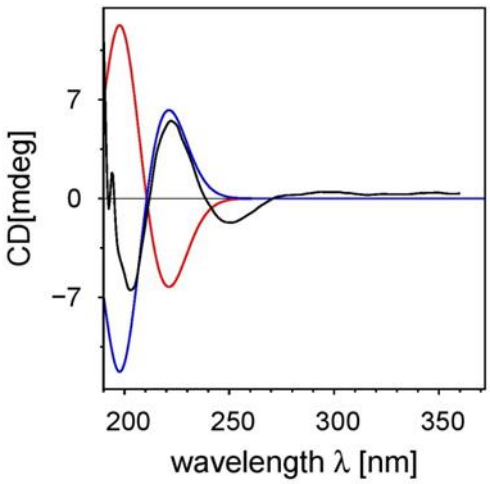

Figure 4.11. Experimental ECD curve of daucovirgolide A (**black**) and calculated ECD curves for *1S,6S,7R,8S,10S,11S*-**1** (blue) and its enantiomer (red).

Given the structural relationship between daucovirgolide A (**1**), B (**2**), and C (**3**), the absolute configuration could be assigned for all indicated compounds.

The Mosher ester method was applied to determine the absolute configuration of daucovirgolide D (**4**), by making use of a secondary alcohol present in the structure of this metabolite.[28] Thus, compound (**4**) was treated with *R*-(−)-and *S*-(+)-MTPA chloride to give the *S*-MTPA (**4a**) and *R*-MTPA (**4b**) ester, respectively (**Fig. 4.12**). Analysis of the $\Delta\delta_{(S-R)}$ values, following the Mosher's model, suggested the assignment of the *S* configuration at C-3 of (**4**). Given the above-determined relative arrangement, the absolute configuration of the entire molecule was assigned.

Since the same absolute configuration was assigned for common stereogenic centers to two different daucovirgolides (**1** and **4**), by means of different methods (comparison of experimental and calculated ECD and Mosher derivatization), it can be reasonably assumed that all the members of this family of germacranolides belong to the same stereochemical series.

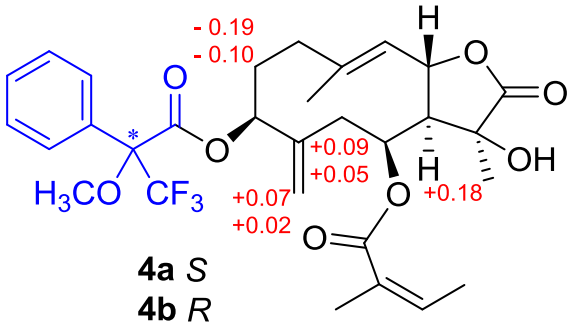

Figure 4.12 Application of the Mosher's method to daucovirgolide D (**4**). Selected $\Delta\delta_{(S-R)}$ values (in ppm) are shown.

4.6 *Plasmodium* transmission-blocking activity

The isolated germacranolides (with the exception of compounds (**4**) and (**8**), which were isolated in too minute amounts or needed for stereostructural determination) were investigated *in vitro* for inhibition of *Plasmodium* early sporogonic stages development, using the rodent malaria parasite *P. berghei* (CTRPp.GFP strain).[29] Parasitized gametocytemic mouse blood was incubated in microtiter plates with daucovirgolides at a concentration of 50 µg/mL, and vernodalol was used as a positive control.[21] The sesquiterpene lactone vernodalol (see **Fig. 4.15**) is an elemanolide isolated from the leaves of *Vernonia amygdalina*; as mentioned before (See paragraph 4.2.1), this plant is largely used to treat malaria infections in many African countries, and vernodalol showed to inhibit the *in vitro* ESS development by 70–90% at tested concentration (50 µM). Dose range experiments conducted with vernodalol allowed to determine an IC_{50} value of 18.7 µM.[21] Given this remarkable pharmacological result, vernodalol was chosen to be a positive control in our biological test for the evaluation of the *Plasmodium* transmission-blocking activity of the isolated daucovirgolides. This test was carried out by the group of prof. A. Habluetzel at the University of Camerino (Italy). As illustrated in **Fig. 4.13**, daucovirgolide G (**7**) showed a marked inhibition (about 92%) of ESS development at the tested concentration, while all the others daucovirgolides exhibited moderate bioactivity, with inhibition percentages ranging from 22% to 35%. Dose-range experiments and stage-specific impact assessment conducted with daucovirgolide G (**7**) permitted to determine the IC_{50} values, which were of 82.3 µM

(CI95 69.0−96.8 μM) on overall ESS development and of 48.4 μM (CI95 44.5−52.8 μM) on the capacity of zygotes to undergo ookinete maturation. It should be noted that daucovirgolide G (**7**) proved to be noncytotoxic (IC_{50} > 100 μM) toward the HACAT (keratinocyte) and A375 (melanoma) cell lines, proving to possess an interestingly high bioactivity that deserve further investigation.

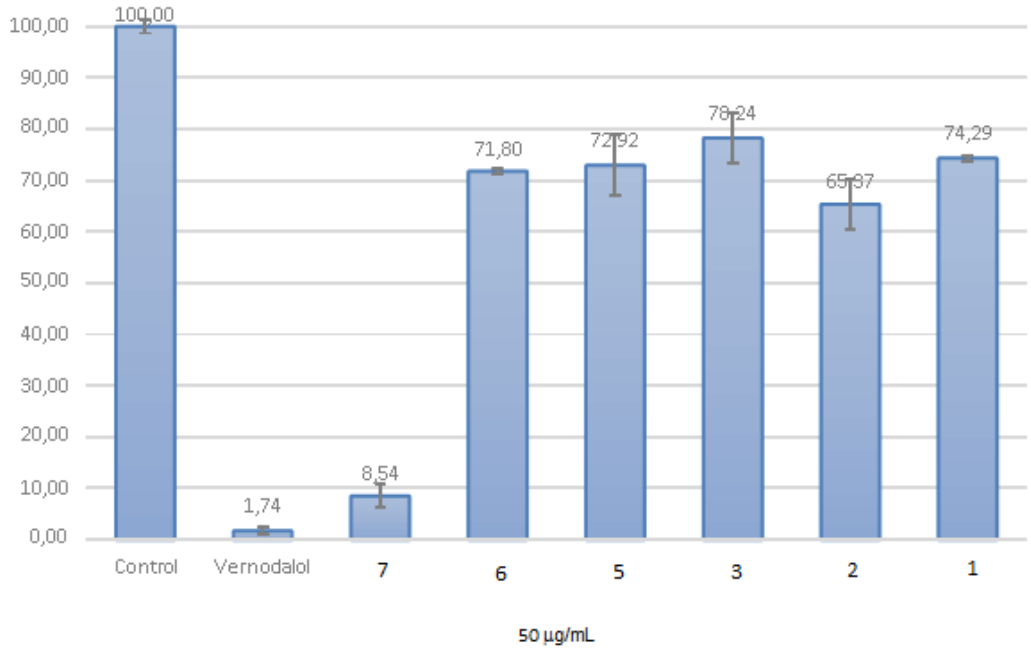

Figure 4.13. Activity of daucovirgolides against *P.bergehi* CTRPp.GFP ESS expressed as percentage of ESS development. Vernodalol was used as positive and DMSO 0.1% as negative solvent control. Vertical bars indicate S.E.M. Results derive from two experimental replicates, testing the molecules in triplicate wells.

Although numerically limited, the series of compounds tested was structurally homogeneous; thus, the selective activity of daucovirgolide G (**7**) points to the occurrence of strict structural requirements for the transmission-blocking activity. In fact, the presence of the epoxide group in place of one of the two double bonds, as in daucovirgolides E (**5**) and F (**6**), dramatically affected the activity, which also was not evident for the monoacylated analogues (**1**) and (**2**).

Interestingly, a similar deleterious effect associated with the presence of the epoxide ring has been recently observed by Gertsch and co-workers for the potent

cannabinoid CB_2 receptor agonism of β-caryophyllene; selective activation of the CB_2 receptor could lead to the development of a potential therapeutic strategy for the treatment of inflammation, pain, osteoporosis, and atherosclerosis. Similarly to what has been observed for daucovirgolides, in the case of β-caryophyllene the activity is completely lost by caryophyllene monoepoxide (**Fig. 4.14**). This selectivity was rationalized on the basis of the existence of a crucial ligand-binding site π–π stacking interaction.[30] Thus, the existence of a well-defined (although not yet identified) biological target within the *Plasmodium* cells of the early sporogonic stages can be postulated also for daucovirgolide G (**7**).

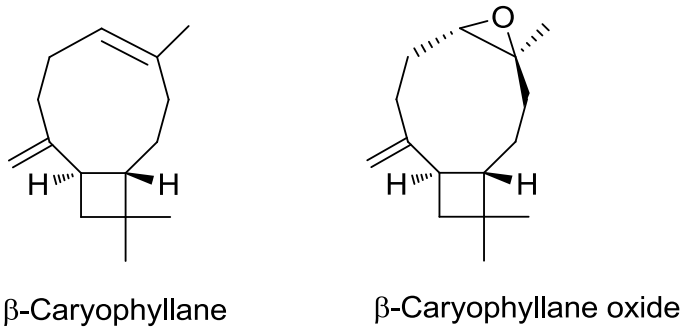

Figure 4.14 Structures of β-caryophyllene and caryophyllene monoepoxide

Daucovirgolide G becomes part of the small family of terpenoids active against *Plasmodium* transmissible stages, which includes azadirachtin A and vernodalol, whose transmission blocking activity was described before (See paragraph 4.2.1), along with parthenin, and parthenolide (**Fig. 4.15**). Parthenin is a sesquiterpene lactone isolated from *Parthenium hysterophorus*, an invasive weed that causes a significant decrease of the agricultural productivity because inhibit the growth of neighbouring plants, and it is also responsible for allergic contact dermatitis. Further studies have proved that these detrimental effects can be attributed to parthenin, a secondary metabolite produced by the plant. This compound has shown a broad variety of biological effects, including antiparasitic and anticancer activities, but the cytotoxicity of parthenin shall be considered as a negative side. Parthenolide is another compound that possesses properties similar to those of parthenin; it derives from *Tanacetum parthenium* and in contrast to parthenin, parthenolide is less

cytotoxic. A recent study has been demonstrated that both parthenin and parthenolide was able to inhibit the development of the stage V gametocytes of *Plasmodium* life cycle.[31] Although daucovirgolide G (**7**) is less potent than the densely functionalized limonoid azadirachtin A, the strongly electrophilic vernodalol and then parthenin and parthenolide, it is also considerably less toxic, lacking general toxicity against both normal and tumor cell lines. Thus, studies addressed toward investigation of the mechanism of action and lead optimization could disclose the antimalarial potential of daucovirgolide G (**7**) and related germacranolides. The biological results presented in this study, provided a strong argument for further insights into the possibility to synthesize some germacranolides analogs as potential transmission-blocking drugs. In the next chapter, the synthetic studies performed towards the total synthesis of the most active angeloylated germacranolide isolated from *Daucus virgatus* will be reported.

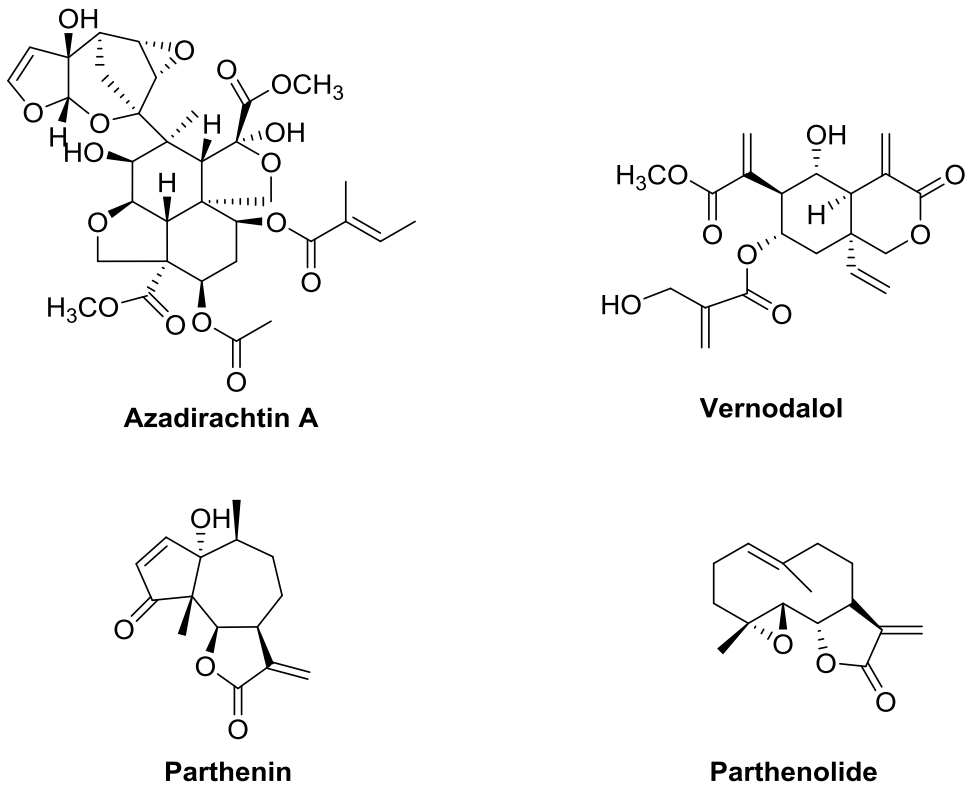

Figure 4.15 Structures of terpenoids active against *Plasmodium* transmissible stages

4.7 Antiproliferative metabolites from *Daucus virgatus* apolar extract

Given the total lack of data about the phytochemical characterization of *Daucus virgatus*, our interest was directed to complete the study of the plant apolar extract. For this purpose, further purifications of CH_2Cl_2 phase, led to the isolation of three previously undescribed sesquiterpenoids, namely the daucane vaginatin B (**14**), a eudesmane (**15**) and the elemane elemavirgolide (**16**), along with five known metabolites. The isolated compounds were evaluated for antiproliferative activity against three human cell lines, A375 (melanoma), MCF-7 (breast adenocarcinoma), and HACAT (keratinocyte).

4.7.1 Structural elucidation of the isolated metabolites

After the isolation of secondary metabolites in their pure form, the structures of the known compounds (**9-13**) were assigned by comparison of their spectroscopic data with those reported in the literature,[32-40] while the structures of the new natural products (**14-16**) were determined by a detailed MS and NMR analysis (**Fig. 4.16**).
Compound (**9)** was identified as 6-methoxymellein, a dihydroisocoumarin involved in the defense mechanisms of plants, and believed to be responsible for the bitter taste of wild carrot (*D. carota*); although a recent work based on sensory and quantitative studies, has questioned this function.[32]
Compound (**10)** is represented by matairesinol, a dibenzylbutyrolactone plant lignan, possessing several biological activities, such as antifungal, anti-oxidative and estrogenic ones. Additionally, a recent study showed the anti-inflammatory activity of matairesinol, which is able to decrease LPS-stimulated NO production, and the expression of pro-inflammatory mediators (iNOS and COX_2) in the microglia. Moreover, it displayed to possess the capability to down-regulate NF-Kb activation.[33]
Compound (**11)** was identified as the phenylpropanoid diester laserine oxide, first isolated from *Laserpitium scabrum* Cav., a pubescent perennial umbelliferous species.[34]

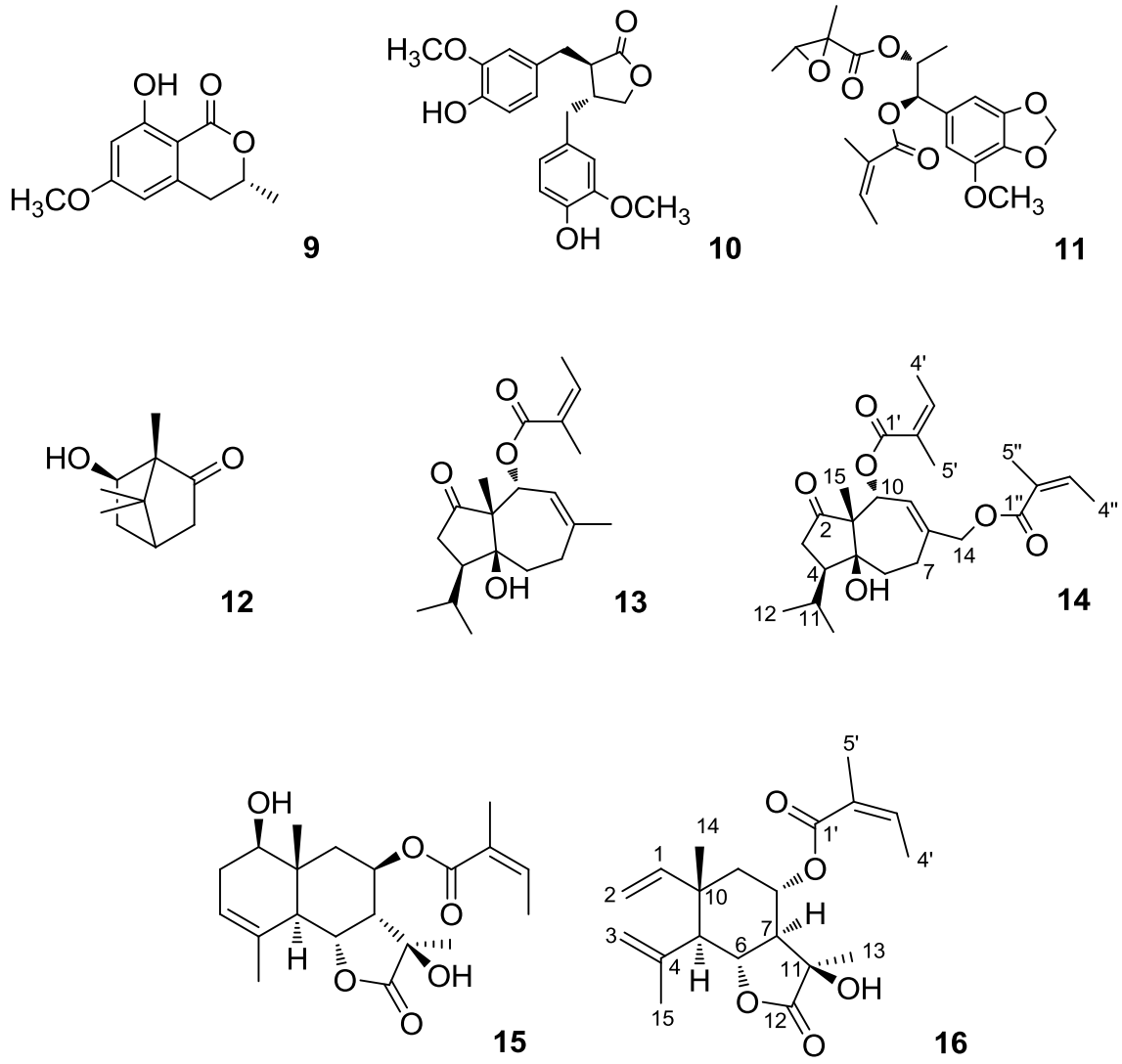

Figure 4.16 Chemical structures of antiproliferative metabolites isolated from *Daucus virgatus*

Compound (**12**), 6-hydroxycamphor, constitutes a catabolic product deriving from (+)-camphor, a monoterpene present in large amount in the essential oil of *Salvia officinalis*; as well as other monoterpenes, (+)-camphor plays a key role in plant-plant or plant-insect interactions.[35]

The last known compound is the daucane sesquiterpene vaginatin (**13**), first isolated from the roots of *Selinum vaginatum*, but later found also as antimicrobial metabolite in *Ferula hermonis*.[36] As outlined in a recent work, vaginatin displayed a selective

activity as glucocorticoid receptor (GR) modulator, along with the capacity to inhibit AP-1, a pro-inflammatory factor.[37]

Vaginatin B (**14**) was isolated as an optically active colorless oil. Its molecular formula, $C_{25}H_{36}O_6$, determined by HR-ESIMS, indicated eight unsaturation degrees. Spectral data of (**14**) suggested that vaginatin B was a sesquiterpene bearing two C_5 acyl groups. In fact, NMR data of vaginatin B and vaginatin (**13**) were almost superimposable, but some relevant differences could be detected:[38]

1) the deshielded methyl at δ_H 1.84 (H_3-14) was replaced by a pair of doublets resonating at δ_H 4.57 and 4.51 (J = 13.2 Hz);

2) the resonances of an additional angeloyl group were present, flanking those attributable to the acyl group attached at C-10.

Inspection of 2D NMR COSY and HSQC spectra of (**14**) confirmed this assignment, displaying the presence of the same spin systems present in vaginatin. The HSQC spectrum associated the oxymethylene proton signals resonating in the midfield region of the ^{1}H NMR spectrum to the carbon at δ_C 69.1. Finally, the HMBC spectrum confirmed the structure of vaginatin B, allowing the unambiguous linkage of the two angelate groups at C-10 (cross-peak H-10/C-1') and C-14 (cross-peaks H_2-14/C1''), respectively. Since the ^{13}C NMR resonances at the four stereogenic carbons of vaginatin B (**14**) were almost completely superimposable to those reported for (**13**) (δ_C values of (**13**) in ppm: C-1 = 60.1, C-4 = 50.8, C-5 = 82.3, C-10 = 75.5; δ_C values of (**14**) in ppm: C-1 = 60.2, C-4 = 51.0, C-5 = 82.6, C-10 = 75.1), we easily concluded that these two compounds possess the same relative configuration. Given the co-occurrence in the plant of vaginatins A (**13**) and B (**14**), we assume that the two compounds also share the same absolute configuration.

Compound (**15**), $C_{20}H_{28}O_6$ by HR-ESIMS, was isolated as a yellow-brown amorphous solid. The ^{1}H NMR spectrum of (**15**) showed the typical signals of an angelate ester, along with three multiplets at relatively low fields (δ_H 5.42, 5.26 and 4.84), an oxymethine signal at δ_H 3.60, a series of multiplets between δ_H 3.0 and 1.95, and three methyl singlets at δ_H 1.84, 1.47 and 1.01. The inspection of 2D NMR spectra (COSY, HSQC and HMBC) led to build up three spin systems, to join them and assign all the proton and carbon resonances. This allowed the definition of the structure of (**15**) as a C-8 angeloylated eudesmane bearing free hydroxyl groups at C-1 and C-11. A literature search displayed that this compound had already been reported by Appendino *et al.*,[39] as a semisynthetic product obtained from

saponification reaction of the sesquiterpene lactone mixture extracted from *Laserpitium gallicum* (Apiaceae). Furthermore, eudesmane (**15**) had never been obtained before as a natural product.

HR-ESIMS data indicated the molecular formula $C_{20}H_{28}O_5$, implying seven degrees of unsaturation, for compound (**16**). ^{1}H NMR spectrum showed a series of well resolved signals distributed in the regions between δ_H 6.15 and 4.80 (including six multiplets and two broad singlets), and between δ_H 2.85 and 1.07, including four multiplets and five methyl signals (a doublet and four singlets). The assignments of ^{1}H and ^{13}C NMR resonances ($CDCl_3$, **Table 4.3**) were assisted by COSY, HSQC, and HMBC spectra. In particular, inspection of the COSY spectrum allowed to combine the multiplet resonances of the ^{1}H NMR spectrum into three spin systems (**Fig. 4.17**), next associated to their corresponding carbon atoms by the HSQC spectrum. The first fragment, connecting H-1 to H_2-2, features a sp^2 methine (δ_C 146.3; δ_H 5.83) coupled to a sp^2 methylene C-2 (δ_C 112.3; δ_H 5.06 and 5.14), respectively. The second fragment, connecting H-5 to H_2-9, comprised two oxymethines at C-6 (δ_C 78.5, δ_H 4.98) and C-8 (δ_C 67.0, δ_H 5.23) and a further branching at C-7. The third fragment included a methyl doublet coupled to a sp^2 methine and was clearly part of an angeloyl group, whose H/C resonances closely resembled those detected for compounds (**14**) and (**15**), including also the methyl singlet at δ_H 1.90. Three uncoupled methyl groups (δ_H 1.07, 1.49, 1.84) and a sp^2 methylene (δ_H 4.83 and 5.05, bs) completed the series of the proton signals, leaving only three unprotonated carbon atoms of the sesquiterpenoid core to assign. Analysis of the HMBC $^{2,3}J_{C-H}$ correlations connected the above proton spin systems (**Fig. 4.17**).

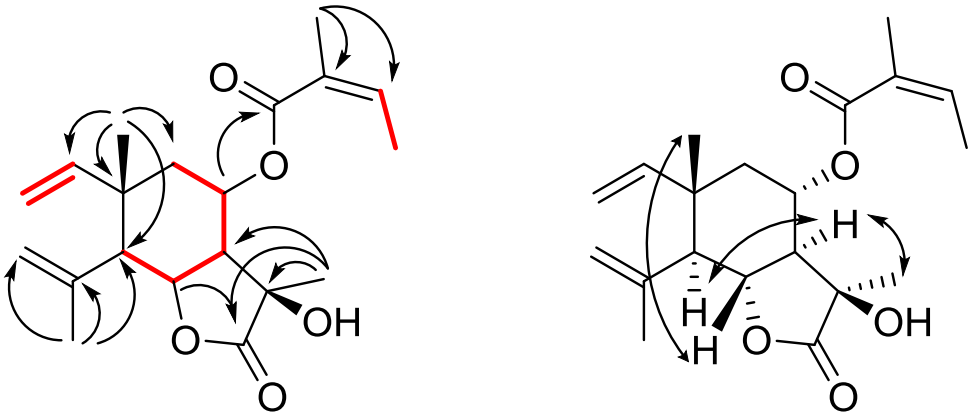

Figure 4.17 Left: COSY (red) and HMBC (arrows) correlations of elemanolide (**16**); right: ROESY correlations

Table 4.3

^{1}H (500 MHz) and ^{13}C (125 MHz) NMR data of elemavirgolide (**16**) in $CDCl_3$.

Pos.	δ_H, mult., *J* in Hz	δ_C, mult.	Pos.	δ_H, mult., *J* in Hz	δ_C, mult.
1	5.83, dd, 17.5, 10.7	146.3	10		39.5
2a	5.06, d, 10.7	112.3	11		75.1
2b	5.14, d, 17.5		12		177.6
3a	5.05, bs	115.7	13	1.49, s	22.6
3b	4.83, bs		14	1.07, s	24.3
4		142.4	15	1.84, s	25.3
5	2.36, d, 8.1	52.6	1’		167.0
6	4.98, t, 8.1	78.5	2’		127.9
7	2.86, t, 8.1	49.4	3’	6.13, q, 7.2	139.7
8	5.23, m	67.0	4’	2.02, d, 7.2	16.4
9a	2.02, overlapped	38.3	5’	1.90, s	20.8
9b	1.73, dd, 14.2, 8.1				

Thus, the cross-peaks of Me-14 and Me-15 furnished a link between the first two fragments and defined the elemane nucleus; correlations of Me-13 to C-7, C-12 (δ_C 177.6) and the oxygenated C-11 (δ_C 75.1), along with the cross-peak H-6/C-12 indicated the presence of a γ-lactone group. Finally, the HMBC cross-peaks between H-8 and C-10 unambiguously attached the angeloyl group at C-8, allowing us to identify elemavirgolide (**16**) as an 8-angeloyl-11-hydroxy-elemanolide derivative. To our knowledge, elemavirgolide (**16**) is the first elemanolide to be reported from a *Daucus* species. The relative configuration of (**16**) was assigned on the basis of scalar ($^3J_{HH}$) and dipolar (ROESY correlations) couplings of the ring protons (**Fig. 4.17**). In particular, the values of $J_{H\text{-}5/H\text{-}6}$, $J_{H\text{-}6/H\text{-}7}$ and $J_{H\text{-}7/H\text{-}8}$ (all 8.1 Hz) was clearly indicative of trans-diaxial orientation of these protons. The ROESY cross-peaks H-5/H-7 Me-14/H-6 and Me- 13/H-7, further confirmed the trans orientation of all the methines belonging to the six-membered ring and indicated the relative configurations at C-10 and C-11, thus completing the definition of the relative stereostructure of elemavirgolide (**16**). Since a 5*S*, 10*S* configuration has been almost invariably associated to natural elemanolides, we can confidently extend this relative configuration to the absolute one.

4.8 Antiproliferative activity

All the isolated metabolites except vaginatin B (**14**), obtained in too minute amounts, were evaluated for their antiproliferative activity against A375 (human melanoma). In order to determine their selectivity, compounds were also tested against two additional human cell lines, MCF-7 (breast adenocarcinoma) and HACAT (keratinocyte). Results of this evaluation are reported in **Table 4.4**.

Table 4.4

Antiproliferative activity of *D. virgatus* metabolites against A375, MCF-7, and HACAT cell lines. Results are expressed as IC_{50} (μM, means ± SEM). [a]

Compounds	A375	MCF-7	HACAT
6-methoxymellein (**9**)	77.3 ± 1.0	123.3 ± 0.5	131.2 ± 0.8
Matairesinol (**10**)	96.5 ± 0.8	117.1 ± 0.7	155.0 ± 1.0
Laserine oxide (**11**)	181.2 ± 0.6	227.9 ± 0.6	576.3 ± 0.8
6-hydroxycamphor (**12**)	207.1 ± 1.2	270.1 ± 0.9	367.0 ± 0.9
Vaginatin (**13**)	126.0 ± 0.6	165.2 ± 0.7	273.4 ± 1.4
Eudesmane (**15**)	32.9 ± 0.6	213.0 ± 0.9	366.1 ± 0.6
Elemavirgolide (**16**)	197.0 ± 0.8	194.4 ± 0.3	646.0 ± 0.7

[a] $P < 0.001$ vs. control.

Among the isolated phenolic compounds (**9-11**), 6-methoxymellein (**9**) was the most active derivative, but it showed only a low selectivity for tumor cell lines. As mentioned, 6-methoxymellein is a phytoalexin produced by *Daucus* tissues in response to microbial invasions or after treatment with several elicitors,[40] but 6-methoxymellein has been demonstrated to be toxic also toward the producing plant cells, showing a higher potency compared to its precursor 6-hydroxymellein. To our knowledge, this is the first report about antiproliferative activity of (**9**) on human cell lines. It is also important to note that all the three tested sesquiterpenoids showed a remarkable higher antiproliferative activity against tumor cell lines compared to that against non-tumor keratinocytes, with a potency three times (in the case of elemavirgolide) and eleven times (in the case of eudesmane) higher.

The selective activity on human melanoma showed by compound (**15**) opens the way to further investigation. In this regard, the skeletons of eudesmane (**15**) and elemavirgolide (**16**) differ only for some stereochemical details, but they almost

completely share the structures of rings B and C, including their substituents. This seems to outline that the structure of ring A, which includes a six-membered ring and a free hydroxyl group, plays an important role in determining the antiproliferative activity of (**15**) against melanoma cell lines. Therefore, on the basis of the reported pharmacological results, further investigations could be performed in order to achieve additional information on the structure-activity relationship of these class of sesquiterpenoids; given the selectivity of the eudesmane, for example, some analogues can be designed and tested, to obtain derivatives with higher potency and selectivity, for the development of new antiproliferative lead compounds.

4.9 Experimental section

4.9.1 Plant material, extraction and isolation

The aerial parts of six *Daucus virgatus* (Poir.) Maire species (weight approx. 2.0 Kg) were collected during the flowering stage in the Northwest of Tunisia (Biserta, GPS coordinates 37°18’19’’N, 9°51’15’’E) on May 2013 and identified by one of the authors (R. E. M.). Voucher specimens [AP; 00117/2013] were deposited in local Herbaria of both the Faculty of Pharmacy of Monastir and the Faculty of Sciences of Biserta.

2.0 Kg of aerial parts were dried in the shade for 4-5 days at room temperature in a well-ventilated area (dry weight 0.95 g), then comminuted to powder, and exhaustively extracted by maceration in methanol (3 x 6L) to afford 130 g of crude extract after removal of the solvent in vacuum. The whole methanol extract was dissolved in water (500 mL) and then successively partitioned against *n*-hexane (2 x 400 mL) CH_2Cl_2 (3 x 500 mL), and *n*-butanol (3 x 500 mL) to yield 40 g, 14 g and 45 g of organic phases, respectively. The CH_2Cl_2 extract (14 g) was subjected to MPLC over a silica gel column (230-400 mesh) and eluted with the following solvent gradient: *n*-hexane (0.8 L), *n*-hexane/EtOAc 8:2 (1.0 L), *n*-hexane/EtOAc 7:3 (1.0 L), *n*-hexane/EtOAc 6:4 (1.0 L), *n*-hexane/EtOAc 4:6 (1.0 L), *n*-hexane/EtOAc 2:8 (1.0 L), EtOAc (0.8 L), EtOAc/MeOH 9:1 (1.0 L), EtOAc/MeOH 7:3 (1.0 L, EtOAc/MeOH 1:1 (1.0 L), MeOH (2.0 L). Four subfractions were collected for each elution solvent/mixture and the 44 subfractions thus obtained were pooled together

on the basis of their TLC profile. Fifteen fractions (1-15) resulted from this procedure and they were further purified by normal- and reverse-phase HPLC.

Fraction 5 (93 mg), eluted with *n*-hexane−EtOAc, 8:2, was separated first by normal-phase HPLC (*n*-hexane−EtOAc, 85:15, flow rate 1.0 mL/min) and then by RP-HPLC (MeOH−H2O, 75:25, flow rate 1.0 mL/min), yielding Daucovirgolide G (**7**, 21.5 mg). Fraction 7 (116 mg), eluted with *n*-hexane−EtOAc, 7:3, was separated by HPLC (*n*-hexane−EtOAc, 7:3, flow rate 1.0 mL/min) to afford pure daucovirgolide E (**5**, 28.1 mg), daucovirgolide F (**6**, 21.2 mg), and daucovirgolide H (**8**, 1.1 mg). Fraction 8 (161 mg), eluted with *n*-hexane−EtOAc, 7:3, was separated by HPLC (*n*-hexane−EtOAc, 6:4, flow rate 1.0 mL/min) to afford daucovirgolide C (**3**, 4.3 mg). Fraction 9 (906 mg), eluted with *n*-hexane−EtOAc, 6:4, was subjected to chromatography over a silica gel column (70−230 mesh) eluting with a solvent gradient of increasing polarity from *n*-hexane−EtOAc 7:3 to EtOAc 100%, and finally EtOAc−MeOH, 1:1. Fraction 5 (132 mg) of the latter column, eluted with *n*-hexane−EtOAc, 6:4, was further fractionated by HPLC (*n*-hexane−EtOAc, 7:3, flow 3.0 mL/min) to obtain daucovirgolide B (**2**, 30.0 mg) and daucovirgolide A (**1**, 22.2 mg) in the pure state. Fraction 10 (1.08 g), eluted with *n*-hexane−EtOAc, 5:5, was subjected to chromatography over a silica gel column (70−230 mesh) eluting with a solvent gradient of increasing polarity from *n*-hexane−EtOAc, 7:3, to EtOAc, and finally EtOAc−MeOH (1:1). Fraction 4 (84.5 mg), eluted with *n*-hexane EtOAc, 7:3, was further purified by HPLC (*n*-hexane−EtOAc, 65:35, flow 1.0 mL/min) to obtain daucovirgolide D (**4**, 3.5 mg).

Fraction 5 (93 mg), eluted with *n*-hexane/ EtOAc 8:2, was separated by HPLC (*n*-hexane/EtOAc 85:15, flow rate 1.0 mL/min) to afford vaginatin (**13**, 7.2 mg, rt 4.2 min) and 6-methoxymellein (**9**, 2.6 mg, rt 6.1 min) in the pure state and a subfraction (subfraction 10) whose further purification by RP-HPLC (MeOH/H2O 7:3, flow rate 0.5 mL/min) yielded laserine oxide (**11**, 1.6 mg, rt 8.3 min), elemavirgolide (**16**, 4.4 mg, rt 9.5 min) and vaginatin B (**14**, 0.8 mg, rt 9.9 min). Fraction 6 (193 mg), eluted with *n*-hexane/EtOAc 6:4, was separated by HPLC (*n*-hexane/EtOAc 65:35, flow rate 1.0 mL/min) to afford pure matairesinol (**10**, 3.0 mg, rt 5.1 min) and a fraction that was further purified by RP-HPLC (MeOH/H2O 6:4, flow rate 1.0 mL/min) to obtain eudesmane (**15**) (1.3 mg, rt 6.2 min). Fraction 7 (116 mg), eluted with *n*-

hexane/EtOAc 7:3, was separated by HPLC (*n*-hexane/EtOAc 7:3, flow rate 1.0 mL/min) and a subfraction (subfraction 14) was further purified by RP-HPLC (MeOH/H2O 7:3, flow rate 1.0 mL/min) to obtain pure 6-hydroxycamphor (**12**, 2.2 mg, rt 4.4 min).

4.9.2 Spectroscopic data for the isolated compounds

Daucovirgolide A (1): colorless oil, $[\alpha]_D$ +42.6 (c 0.09, $CHCl_3$); ECD (MeOH) λmax (Δε) 208 (−6.8), 229 (+5.2) nm; ^{1}H NMR ($CDCl_3$, 500 MHz), see Table 1; ^{13}C NMR ($CDCl_3$, 125 MHz), see Table 2; ESIMS m/z 387 $[M + Na]^+$; HRESIMS m/z found 387.1773 ($C_{20}H_{28}O_6Na$ requires 387.1784).

Daucovirgolide B (2): colorless oil; $[\alpha]_D$ +59.0 (c 0.01, $CHCl_3$); ECD (MeOH) λmax (Δε) 211 (−6.5), 232 (+5.8) nm; ^{1}H NMR ($CDCl_3$, 500 MHz) δ_H 6.08 (1H, qq, J = 7.3, 1.1 Hz, H-3′), 5.35 (1H, m, H-1), 5.12 (1H, dd, J = 7.6, 1.3 Hz, H-6), 4.79 (1H, dd, J = 10.3, 1.1 Hz, H-8), 2.80 (1H, bs, OH-11), 2.60 (1H, bs, H-5), 2.33 (1H, dd, J = 1.3, 1.1 Hz, H-7), 2.32 (2H, overlapped, H-2), 2.13 (1H, m, H-3b), 2.06 (1H, m, H-9b), 2.01 (1H, m, H-9a), 1.98 (3H, d, J = 7.3 Hz, H- 4′), 1.82 (3H, s, H-5′), 1.78 (3H, s, H-14), 1.56 (3H, s, H-13), 1.30 (3H, s, H-15), 1.22 (1H, m, H-3a); ^{13}C NMR ($CDCl_3$, 125 MHz) δ_C 179.2 (C-12), 166.2 (C-1′), 140.5 (C-3′), 130.8 (C-10), 128.6 (C-1), 127.3 (C-2′), 77.3 (C-8), 71.6 (C-11), 70.7 (C-6), 65.7 (C-5), 59.5 (C-4), 49.2 (C-7), 40.7 (C-9), 37.3 (C-3), 30.0 (C-13), 25.2 (C-14), 23.6 (C-2), 20.3 (C-5′), 16.7 (C-15), 16.1 (C-4′); ESIMS m/z 387 $[M + Na]^+$; HRESIMS m/z found 387.1795 ($C_{20}H_{28}O_6Na$ requires 387.1784).

Daucovirgolide C (3): colorless oil, $[\alpha]_D$ +68.8 (c 0.03, $CHCl_3$); ECD (MeOH) λmax (Δε) 210 (−6.2), 227 (+5.4) nm; ^{1}H NMR ($CDCl_3$, 500 MHz), see Table 1; ^{13}C NMR ($CDCl_3$, 125 MHz), see Table 2; ESIMS m/z 419 $[M + Na]^+$; HRESIMS m/z found 419.1681 ($C_{20}H_{28}O_8Na$ requires 419.1682).

Daucovirgolide D (4): colorless oil, $[\alpha]_D$ + 4.9 (c 0.01, $CHCl_3$); ^{1}H NMR ($CDCl_3$, 500 MHz), see Table 1; ^{13}C NMR ($CDCl_3$, 125 MHz), see Table 2; ESIMS m/z 387 $[M + Na]^+$; HRESIMS m/z found 387.1774 ($C_{20}H_{28}O_6Na$ requires 387.1784).

Mosher Ester Derivatization of Daucovirgolide D. Two aliquots of daucovirgolide D (**4**) (1.0 mg, 2.6 μmol) were treated with R-MTPA and S-MTPA chloride (30 μL)

in 400 μL of dry pyridine with a catalytic amount of DMAP overnight at rt. Then, the solvent was removed and the products were purified by HPLC (*n*-hexane−EtOAc, 97:3) to obtain, respectively, the S-MTPA ester **4a** (0.9 mg) and the R-MTPA ester **4b** (1.1 mg).

S-MTPA ester 4a: colorless, amorphous solid; ^{1}H NMR ($CDCl_3$, 500 MHz) δ_H 6.10 (1H, qq, J = 6.8, 1.1 Hz, H-3′), 5.55 (1H, d, J = 10.8 Hz, H-9), 5.48 (1H, overlapped, H-3), 5.48 (1H, overlapped, H- 6), 5.30 (1H, t, J = 10.8 Hz, H-8), 5.14 (1H, bs, H-15a), 5.01 (1H, bs, H-15b), 3.29 (1H, t, J = 10.8 Hz, H-7), 2.60 (1H, m, H-1a), 2.41 (1H, overlapped, H-5a), 2.39 (1H, overlapped, H-5b), 2.31 (1H, m, H-1b), 1.98 (3H, d, J = 6.8 Hz, H3-4′), 1.95 (3H, bs, H3-5′), 1.95 (1H, overlapped, H-2a), 1.88 (1H, m, H-2b), 1.76 (3H, s, H3-14), 1.51 (3H, s, H3-13); (+)-ESIMS m/z 581 $[M + H]^+$, 603 $[M + Na]^+$.

R-MTPA ester 4b: colorless, amorphous solid; ^{1}H NMR ($CDCl_3$, 500 MHz) δ_H 6.10 (1H, qq, J = 6.8, 1.1 Hz, H-3′), 5.48 (1H, d, J = 10.8 Hz, H-9), 5.46 (1H, overlapped, H-3), 5.46 (1H, overlapped, H- 6), 5.14 (1H, t, J = 10.8 Hz, H-8), 5.07 (1H, bs, H-15a), 4.99 (1H, bs, H-15b), 3.11 (1H, t, J = 10.8 Hz, H-7), 2.47 (1H, m, H-1a), 2.36 (1H, overlapped, H-5a), 2.30 (1H, overlapped, H-5b), 2.21 (1H, m, H-1b), 2.07 (1H, overlapped, H-2a), 2.05 (1H, m, H-2b), 1.95 (3H, d, J = 6.8 Hz, H3-4′), 1.89 (3H, bs, H3-5′), 1.68 (3H, s, H3-14), 1.46 (3H, s, H3- 13); (+)-ESIMS m/z 581 $[M + H]^+$, 603 $[M + Na]^+$.

Daucovirgolide E (5): colorless oil; $[\alpha]_D$ +59.7 (c 0.01, $CHCl_3$); ^{1}H NMR ($CDCl_3$, 500 MHz) δ_H 6.22 (1H, qq, J = 7.3, 1.3 Hz, H-3′), 5.71 (1H, dd, J = 6.0, 1.3 Hz, H-6), 5.12 (1H, d, J = 6.0 Hz, H-5), 4.83 (1H, ddd, J = 11.9, 6.2, 1.9 Hz, H-8), 3.01 (1H, overlapped, H-3″), 3.01 (1H, overlapped, H-7), 2.81 (1H, dd, J = 11.0, 1.3 Hz, H-1), 2.26 (1H, m, H-3b), 2.25 (1H, m, H-3a), 2.18 (2H, m, H-9), 2.07 (1H, overlapped, H-2b), 2.06 (3H, d, J = 7.3 Hz, H-4′), 1.91 (3H, s, H-5′), 1.86 (3H, s, H-13), 1.75 (3H, s, H-15), 1.50 (1H, m, H-2a), 1.47 (3H, s, H-5″), 1.41 (3H, s, H-14), 1.26 (3H, d, J = 5.4 Hz, H-4″); ^{13}C NMR ($CDCl_3$, 125 MHz) δ_C 173.7 (C-12), 168.6 (C-1″), 167.6 (C-1′), 141.7 (C-3′), 138.6 (C-4), 127.1 (C-2′), 125.1 (C-5), 77.7 (C-11), 76.0 (C-8), 70.9 (C-6), 62.2 (C-1), 60.2 (C-3″), 59.7 (C-2″), 57.1 (C- 10), 50.7 (C-7), 42.5 (C-9), 36.6 (C-3), 25.0 (C-13), 24.1 (C-2), 22.1 (C-14), 20.8 (C-5′), 19.0

(C-5″), 17.5 (C-15), 16.4 (C-4′), 13.6 (C- 4″); ESIMS m/z 485 $[M + Na]^+$; HRESIMS m/z found 485.2158 ($C_{25}H_{34}O_8Na$ requires 485.2151).

Daucovirgolide F (6): colorless oil; $[\alpha]_D$ +91.7 (c 0.01, $CHCl_3$); ^1H NMR ($CDCl_3$, 500 MHz) δ_H 6.21 (1H, qq, J = 7.3, 1.1 Hz, H-3′), 5.34 (1H, m, H-1), 5.00 (1H, dd, J = 6.6, 1.3 Hz, H-6), 4.82 (1H, m, H-8), 3.01 (1H, q, J = 5.4 Hz, H-3″), 2.89 (1H, t, J = 1.3 Hz, H-7), 2.58 (1H, d, J = 6.6 Hz, H-5), 2.35 (2H, m, H2-2), 2.13 (1H, dt, J = 13.3, 3.4 Hz, H-3b), 2.09 (1H, overlapped, H-9b), 2.04 (1H, overlapped, H-9a), 2.03 (3H, d, J = 7.5 Hz, H-4′), 1.88 (3H, s, H-5′), 1.87 (3H, s, H-13), 1.83 (3H, s, H-14), 1.49 (3H, s, H-5″), 1.33 (3H, s, H-15), 1.28 (3H, d, J = 5.4 Hz, H-4″), 1.18 (1H, q, J = 11.4 Hz, H-3a); ^{13}C NMR ($CDCl_3$, 125 MHz) δ_C 174.1 (C-12), 168.1 (C-1″), 167.3 (C-1′), 141.9 (C-3′), 130.2 (C-10), 128.9 (C-1), 126.9 (C-2′), 77.6 (C-11), 77.3 (C-8), 72.8 (C-6), 65.2 (C-5), 60.0 (C-3″), 59.8 (C-2″), 59.6 (C- 4), 48.0 (C-7), 40.7 (C-9), 37.5 (C-3), 25.5 (C-13), 25.2 (C-14), 24.0 (C-2), 20.6 (C-5′), 18.6 (C-5″), 16.4 (C-15), 16.2 (C-4′), 13.5 (C- 4″); ESIMS m/z 485 $[M + Na]^+$; HRESIMS m/z found 485.2160 ($C_{25}H_{34}O_8Na$ requires 485.2151).

Daucovirgolide G (7): colorless oil, $[\alpha]_D$ +49.1 (c 0.03, $CHCl_3$); ^1H NMR ($CDCl_3$, 500 MHz), see Table 1; ^{13}C NMR ($CDCl_3$, 125 MHz), see Table 2; ESIMS m/z 469 $[M + Na]^+$; HRESIMS m/z found 469.2195 ($C_{25}H_{34}O_7Na$ requires 469.2202).

Daucovirgolide H (8): colorless oil; $[\alpha]_D$ +49.1 (c 0.03, $CHCl_3$); ^1H NMR ($CDCl_3$, 500 MHz) δ_H 6.19 (1H, qq, J = 7.3, 1.1 Hz, H-3′), 6.06 (1H, s, H-14a), 5.88 (1H, s, H-14b), 5.57 (1H, dd, J = 5.6, 1.1 Hz, H- 6), 4.94 (1H, dd, J = 12.2, 4.6 Hz, H-8), 4.87 (1H, d, J = 5.6 Hz, H-5), 3.54 (1H, m, H-9a), 3.36 (1H, m, H-2a), 3.01 (1H, q, J = 10.8 Hz, H- 3″), 2.69 (1H, m, H-7), 2.48 (1H, m, H-3a), 2.28 (1H, overlapped, H-2b), 2.28 (1H, overlapped, H-3b), 2.15 (1H, m, H-9b), 2.05 (3H, d, J = 7.3 Hz, H-4′), 1.89 (3H, s, H-5′), 1.83 (3H, s, H-13), 1.74 (3H, s, H- 15), 1.46 (3H, s, H-5″), 1.24 (3H, d, J = 5.4 Hz, H-4″); ^{13}C NMR ($CDCl_3$, 125 MHz) δ_C 204.1 (C-1), 174.0 (C-12), 168.5 (C-1″), 167.4 (C-1′), 141.2 (C-3′), 136.4 (C-4), 127.5 (C-5), 127.0 (C-2′), 77.6 (C- 11), 70.7 (C-6), 59.9 (C-3″), 59.7 (C 2″), 49.6 (C-7), 38.2 (C-3), 38.1 (C-9), 26.1 (C-2), 25.4 (C-13), 20.4 (C-5′), 18.5 (C-5″), 17.1 (C-15), 16.2 (C-4′), 13.5 (C-4″); ESIMS m/z 483 $[M + Na]^+$; HRESIMS m/z found 483.1987 ($C_{25}H_{32}O_8Na$ requires 483.1995).

Vaginatin B (14): colorless oil, $[\alpha]_D$ -31 (c 0.04, $CHCl_3$); ^1H NMR ($CDCl_3$, 500 MHz): δ_H 6.09 (1H, qq, *J* = 7.2, 1.3 Hz, H-3'), 6.04 (1H, qq, *J* = 7.5, 1.6 Hz, H-3''), 5.99 (1H, d, *J* = 7.8 Hz, H-9), 5.34 (1H, d, *J* = 7.8 Hz, H-10), 4.57 (1H, d, *J* = 13.2 Hz, H-14a), 4.51 (1H, d, *J* = 13.2 Hz, H-14b), 2.43 (1H, overlapped, H-6a), 2.42 (1H, overlapped, H-3a), 2.26 (1H, m, H-4), 2.24 (1H, m, H-7a), 2.21 (1H, m, H-3b), 2.10 (1H, overlapped, H-6b), 2.10 (1H, overlapped, H-7b), 2.05 (1H, m, H-11), 1.98 (3H, dd, *J* = 7.2, 1.5 Hz, H-40), 1.96 (3H, dd, *J* = 7.5, 1.4 Hz, H-4''), 1.90 (3H, s, H_3-5'), 1.84 (3H, s, H_3-5''), 1.07 (3H, s, H_3-15), 1.06 (3H, d, *J* = 6.8 Hz, H_3-12), 0.99 (3H, d, *J* = 6.8 Hz, H_3-13); ^{13}C NMR ($CDCl_3$, 125 MHz) δ_C 219.7 (C-2), 167.9 (C-1'), 166.1 (C-1''), 146.5 (C-8), 140.3 (C-3''), 138.8 (C-3'), 127.9 (C-2'), 126.9 (C-2''), 119.9 (C-9), 82.6 (C-5), 75.1 (C-10), 69.1 (C-14), 60.2 (C-1), 51.0 (C-4), 38.5 (C-3), 37.3 (C-6), 29.3 (C-7), 26.7 (C-11), 25.0 (C-12), 21.2 (C-13), 20.7 (C-4'), 20.5 (C-4''), 18.2 (C-15), 15.7 (C-5''), 15.5 (C-5'). ESIMS (positive ions) *m/z* 455 $[M + Na]^+$; HR-ESIMS *m/z* 455.2412; calcd. for $C_{25}H_{36}NaO$ *m/z* 455.2410.

Compound (15): brown gum, $[\alpha]_D$ +28.0 (c 0.01, $CHCl_3$); ^1H and ^{13}C NMR: see Appendino *et al.*, 1993 (Please notice that the resonances reported for C-1 and C-8 must be inverted). ESIMS (positive ions) *m/z* 387 $[M + Na]^+$; HR-ESIMS *m/z* 387.1779; calcd. for $C_{20}H_{28}NaO_6$ *m/z* 387.1784.

Elemavirgolide (16): colorless oil; $[\alpha]_D$ - 2 (c 0.5, $CHCl_3$); ^1H NMR and ^{13}C NMR ($CDCl_3$): see Table 3.1. ESI-MS (positive ions) *m/z* 371 $[M + Na]^+$; HRESIMS *m/z* 371.1830; calcd. for $C_{20}H_{28}NaO_5$ *m/z* 371.1834.

4.9.3 Evaluation of Transmission Blocking Activity

Assessment of *in Vitro* Transmission-Blocking Activity. The effects of daucovirgolides **1**–**3** and **5**–**7** on the development *in vitro* of *P. berghei* early sporogonic stages, i.e., on gametes, zygotes, and ookinetes developing within 24 h in the mosquito midgut after ingestion of gametocytemic blood, were evaluated by employing the rodent malaria strain *P. berghei* CTRPp.GFP and the ookinete development assay, according to Delves et al., with slight modifications.

To obtain mouse blood with high numbers of mature gametocytes, mice were pretreated with phenylhydrazine (120 mg/kg ip) 4 days prior to infection with *P. berghei* CTRPp.GFP through ip injection of 107 infected red blood cells (RBCs).

Gametocytemia was then checked 4 days postinfection by microscopic examination of thin blood films, and the maturity of microgametocytes verified by testing their capacity to generate flagellate microgametes in the exflagellation assay. Mice with mature female and male gametocytes according to thin Giemsastained films and showing more than three exflagellation centers per 1000 RBCs were used as blood donors for the subsequent ookinete development assay.

Permission to perform animal experiments was obtained by University Research Ethics Committee (protection of animals used for experimental and other scientific purposes) of the University of Camerino, protocol number UREC_CAM_2015/18.

Ookinete Development Assay. The culture medium was composed of RPMI 1640 containing 25 mM HEPES, 25 mM sodium bicarbonate, 50 mg/L hypoxanthine, 100 μM xanthurenic acid, and 20% heat-inactivated fetal bovine serum, supplemented with 100 units/mL penicillin and 100 μg/mL streptomycin and set at pH 7.4. For the ookinete cultures, 96-well microplates (Nunc, Roskilde, Denmark) were employed; dimethyl sulfoxide (DMSO) was used as negative control and vernodalol as positive reference. In brief, 10 μL of each dilution was added to the microplate wells containing 80 μL of ookinete culture medium to obtain the desired test concentrations. Then, 10 μL aliquots of blood obtained by cardiac puncture from gametocytemic mice were transferred to the microplate wells containing test compounds or solvent controls and mixed rapidly.

Plates were then incubated at 19 °C for 24 h. At the end of incubation, well contents were mixed and 3.5 μL of cell suspension from each well was withdrawn and diluted with serum-free medium at a ratio of 1:25 in a separate 96-well microplate. This dilution step permitted, after cell settlement, obtaining a monolayer of blood cells and parasites, a condition that was required for an accurate microscopic examination. Green fluorescent protein-expressing zygotes and ookinetes were visualized and counted using a Zeiss fluorescence microscope (400× magnification). Each test substance was examined in three replicate wells, and experiments were repeated at least twice. The percent inhibition of ESS development induced by the extracts/molecules was calculated as follows:

(1 - mean ESS count test wells/mean ESS count solvent control wells) x 100

Distinct counts of zygotes and ookinetes were effected based on the shape of the ESS: round-shaped forms were counted as zygotes, while roundish forms with nose-like protrusions and banana-like elongated forms were considered as maturing and mature ookinetes.

4.9.4 Antiproliferative activity

Human immortalized keratinocytes (Hacat) were purchased from Lonza (Walkersville, MD, USA). The melanoma cell line A375 and the human breast adenocarcinoma cell line MCF-7 were purchased from Sigma-Aldrich (Milan, Italy). All cell lines were cultured in Dulbecco's modified Eagle's medium (DMEM) containing 10% fetal bovine serum, 2 mmol/L L-glutamine, 100 µmol/L non-essential amino acids, penicillin (100 U/mL), streptomycin (100 µg/mL) and 1 mmol/L sodium pyruvate (all from Sigma-Aldrich, Milan, Italy). Compounds 1-5, 7 and 8 were diluted in DMSO to prepare a stock solution of 100 µM. All cell lines used in this study were characterized by the cell bank where they were purchased. Cell proliferation was measured by the 3-[4,5-dimethyltiazol-2yl]-2,5 diphenyl tetrazolium bromide (MTT) assay as previously described (De Cicco et al., 2017). The cells were seeded on 96 well plates (1 104 cells/well) and treated with the compounds (1-3-10-30-100 µM) for 24-48-72 h before adding 25 µL of MTT (Sigma, Milan, Italy) (5 mg/mL in saline). Cells were incubated for additional 3 h at 37° C. Thereafter, cells were lysed and dark blue crystals were dissolved in a solution containing 50% (vol/vol) N, N-dimethylformamide, 20% (w/vol) sodium dodecylsulfate with an adjusted pH of 4.5. The OD of each well was measured with a microplate spectrophotometer (TitertekMultiskan MCC/340) equipped with a 620-nm filter. Results were expressed as IC_{50} (µM). ADA (De Cicco *et al*., 2017) was used as a positive control (IC_{50} on A375 = 51.4 µM).

4.9.5 Computational Calculations

A preliminary conformational search on each pair of enantiomers of daucovirgolide A (**1**) was performed by Simulated Annealing in the INSIGHT II

package. Using the steepest descent followed by the quasi-Newton−Raphson method (VA09A), the conformational energy was minimized. Restrained simulations were carried out for 500 ps using the CVFF force field as implemented in Discover software (Accelrys, San Diego, CA, USA).

The simulation started at 1000 K, and then the temperature was decreased stepwise to 300 K. The final step was again the energy minimization, performed in order to refine the structures obtained, using the steepest descent and the quasi-Newton−Raphson (VA09A) algorithms successively. Both dynamic and mechanic calculations were carried out using 1 (kcal/mol)/Å 2 flat well distance restraints. One hundred structures were thus generated. To simulate the solvent chosen for ECD analysis, a distance-dependent dielectric constant set to the value of MeOH at 298 K (ε 33.10) was used during the calculations. All optimizations were performed with the software package Gaussian 03, using the DFT functional mpw1pw91 and the basis set 6-31G(d). TDDFT calculations were run using the functional CAM-B3LYP and the basis sets 6-31G(d,p) including at least 30 excited states in all cases and using IEF-PCM for MeOH with Gaussian 03. The rotatory strength values were summed after a Boltzmann statistical weighting, and $\Delta\varepsilon$ values were calculated by forming sums of Gaussian functions centered at the wavelengths of the respective electronic transitions and multiplied by the corresponding rotatory strengths. The obtained ECD spectra were UV-corrected and compared to the experimental ones.

References

1. Rokbeni, N., M'rabet, Y., Dziri, S., Chaabane, H., Jemli, M., Fernandez, X., & Boulila, A. (**2013**). Variation of the chemical composition and antimicrobial activity of the essential oils of natural populations of Tunisian *Daucus carota* L. (Apiaceae). *Chem. Biodivers.*, *10*(12), 2278-2290.

2. Hammami, S., Salem, A. B., Ashour, M. L., Cheriaa, J., Graziano, G., & Mighri, Z. (**2013**). A novel methylated sesquiterpene from seagrass *Posidonia oceanica* (L.) Delile. *Nat. Prod. Res.*, *27*(14), 1265-1270.

3. Hammami, S., Li, Z., Huang, M., El Mokni, R., Dhaouadi, H., & Yin, S. (**2016**). New bioactive labdane diterpenoids from *Marrubium aschersonii*. *Nat. Prod. Res.*, *30*(19), 2142-2148.

4. Faidi, K., Hammami, S., Salem, A. B., El Mokni, R., Garrab, M., Mastouri, M., & Mighri, Z. (**2014**). Polyphenol derivatives from bioactive butanol phase of the Tunisian narrow-leaved asphodel (*Asphodelus tenuifolius* Cav., Asphodelaceae). *J. Med. Plants Res.*, *8*(14), 550-557.

5. Akhtar, S., Rauf, A., Imran, M., Qamar, M., Riaz, M., & Mubarak, M. S. (**2017**). Black carrot (*Daucus carota* L.), dietary and health promoting perspectives of its polyphenols: A review. *Trends Food Sci. Technol.*, 66, 36-47.

6. Chen, Y., Peng, S., Luo, Q., Zhang, J., Guo, Q., Zhang, Y., & Chai, X. (**2015**). Chemical and pharmacological progress on polyacetylenes isolated from the family Apiaceae. *Chem. Biodivers.*, 12(4), 474-502.

7. Negri, R. (**2015**). Polyacetylenes from terrestrial plants and fungi: recent phytochemical and biological advances. *Fitoterapia*, 106, 92-109.

8. Yahyaa, M., Ibdah, M., Marzouk, S., & Ibdah, M. (**2016**). Profiling of the terpene metabolome in carrot fruits of wild (*Daucus carota* L. ssp. *carota*)

accessions and characterization of a geraniol synthase. *J. Agric. Food Chem.*, 66(10), 2378-2386.

9. Fu, Z. Z., Han, H. T., Liu, N., Xu, X. B., Zhu, W., Gong, M. H., & Tian, J. K. (**2015**). Two new eudesmane sesquiterpenoids from *Daucus carota* L. *Phytochem. Lett.*, *14*, 35-38.

10. Fu, H. W., Zhang, L., Yi, T., Chen, R. Z., Wang, X., & Tian, J. K. (**2010**). Two new guaiane-type sesquiterpene glycosides from the fruits of *Daucus carota* L. *Chem. Pharm. Bull.*, *58*(1), 125-128.

11. Cherng, J. M., Chiang, W., & Chiang, L. C. (**2008**). Immunomodulatory activities of common vegetables and spices of Umbelliferae and its related coumarins and flavonoids. *Food Chem.*, *106*(3), 944-950.

12. Almela, M. J., Lozano, S., Lelièvre, J., Colmenarejo, G., Coterón, J. M., Rodrigues, J., & Herreros, E. (**2015**). A new set of chemical starting points with *Plasmodium falciparum* transmission-blocking potential for antimalarial drug discovery. *PloS One*, *10*(8), e0135139.

13. Gonçalves, D., & Hunziker, P. (**2016**). Transmission-blocking strategies: the roadmap from laboratory bench to the community. *Malar. J.*, *15*(1), 95.

14. Abdul-Ghani, R., Basco, L. K., Beier, J. C., & Mahdy, M. A. (**2015**). Inclusion of gametocyte parameters in anti-malarial drug efficacy studies: filling a neglected gap needed for malaria elimination. *Malar. J.*, *14*(1), 413.

15. WHO World Malaria Report 2016. http://www.who.int/malaria/publications/world-malaria-report-2016/report/en/. Accessed on July 7, **2017**.

16. Chotivanich, K., Sattabongkot, J., Udomsangpetch, R., Looareesuwan, S., Day, N. P., Coleman, R. E., & White, N. J. (**2006**). Transmission-blocking activities of quinine, primaquine, and artesunate. *Antimicrob. Agents Chemother.*, *50*(6), 1927-1930.

17. Adebayo, J. O., & Krettli, A. U. (**2011**). Potential antimalarials from Nigerian plants: a review. *J. Ethnopharmacol.*, *133*(2), 289-302.

18. Karunamoorthi, K., Sabesan, S., Jegajeevanram, K., & Vijayalakshmi, J. (**2013**). Role of traditional antimalarial plants in the battle against the global malaria burden. *Vector Borne Zoonotic Dis.*, *13*(8), 521-544.

19. Tapanelli, S., Chianese, G., Lucantoni, L., Yerbanga, R. S., Habluetzel, A., & Taglialatela-Scafati, O. (**2016**). Transmission blocking effects of neem (*Azadirachta indica*) seed kernel limonoids on *Plasmodium berghei* early sporogonic development. *Fitoterapia*, *114*, 122-126.

20. Bhatnagar, S., & Das, P. (**2007**). Antimalarial activity in tropical plants: a review. *J. Herbs Spices Med. Plants*, *13*(1), 103-132.

21. Abay, S. M., Lucantoni, L., Dahiya, N., Dori, G., Dembo, E. G., Esposito, F., & Taglialatela-Scafati, O. (**2015**). *Plasmodium* transmission blocking activities of *Vernonia amygdalina* extracts and isolated compounds. *Malar. J.*, *14*(1), 288.

22. Frank, A., & Groll, M. (**2016**). The methylerythritol phosphate pathway to isoprenoids. *Chem. Rev.*, *117*(8), 5675-5703.

23. Vattekkatte, A., Garms, S., Brandt, W., & Boland, W. (**2018**). Enhanced structural diversity in terpenoid biosynthesis: enzymes, substrates and cofactors. *Org. Biomol. Chem.*, *16*(3), 348-362.

24. Eljounaidi, K., Cankar, K., Comino, C., Moglia, A., Hehn, A., Bourgaud, F., & Beekwilder, J. (**2014**). Cytochrome P450s from *Cynara cardunculus* L. CYP71AV9 and CYP71BL5, catalyze distinct hydroxylations in the sesquiterpene lactone biosynthetic pathway. *Plant Sci.*, *223*, 59-68.

25. Minnaard, A. J., Wijnberg, J. B., & de Groot, A. (**1999**). The synthesis of germacrane sesquiterpenes and related compounds. *Tetrahedron*, *55*(8), 2115-2146.

26. De Kraker, J. W., Franssen, M. C., Joerink, M., De Groot, A., & Bouwmeester, H. J. (**2002**). Biosynthesis of costunolide, dihydrocostunolide, and leucodin. Demonstration of cytochrome P450-catalyzed formation of the lactone ring present in sesquiterpene lactones of chicory. *Plant Physiol.*, *129*(1), 257-268.

27. Barquera-Lozada, J. E., Quiroz-García, B., Quijano, L., & Cuevas, G. (**2010**). Conformational properties of the germacradienolide 6-epidesacetyllaurenobiolide by theory and NMR analyses. *J. Org. Chem.*, *75*(7), 2139-2146.

28. Ohtani, I., Kusumi, T., Kashman, Y., & Kakisawa, H. (**1991**). High-field FT NMR application of Mosher's method. The absolute configurations of marine terpenoids. *J. Am. Chem. Soc.*, *113*(11), 4092-4096.

29. Sinisi, A., Millán, E., Abay, S. M., Habluetzel, A., Appendino, G., Muñoz, E., & Taglialatela-Scafati, O. (**2015**). Poly-electrophilic sesquiterpene lactones from *Vernonia amygdalina*: new members and differences in their mechanism of thiol trapping and in bioactivity. *J. Nat. Prod.*, *78*(7), 1618-1623.

30. Gertsch, J., Leonti, M., Raduner, S., Racz, I., Chen, J. Z., Xie, X. Q., & Zimmer, A. (**2008**). Beta-caryophyllene is a dietary cannabinoid. *Proc. Natl. Acad. Sci.*, 105(26), 9099-9104.

31. Balaich, J. N., Mathias, D. K., Torto, B., Jackson, B. T., Tao, D., Ebrahimi, B., & Dinglasan, R. R. (**2016**). The non-artemisinin sesquiterpene lactones parthenin and parthenolide block *Plasmodium falciparum* sexual stage transmission. *Antimicrob. Agents Chemother.*, AAC-02002.

32. Schmiech, L., Uemura, D., & Hofmann, T. (**2008**). Reinvestigation of the bitter compounds in carrots (*Daucus carota* L.) by using a molecular sensory science approach. *J. Agric. Food Chem.*, *56*(21), 10252-10260.

33. Xu, P., Huang, M. W., Xiao, C. X., Long, F., Wang, Y., Liu, S. Y., & Liu, X. H. (**2017**). Matairesinol suppresses neuroinflammation and migration associated with Src and ERK1/2-NF-κB pathway in activating BV2 microglia. *Neurochem. Res.*, *42*(10), 2850-2860.

34. Pinar, M., Rico, M., & Rodríguez, B. (**1982**). Laserine oxide, an epoxide from *Guillonea scabra*. *Phytochemistry*, *21*(3), 735-737.

35. Funk, C., Koepp, A. E., & Croteau, R. (**1992**). Catabolism of camphor in tissue cultures and leaf disks of common sage (*Salvia officinalis*). *Arch. Biochem. Biophys.*, *294*(1), 306-313.

36. Mesta, C. K., Paknikar, S. K., & Bhattacharyya, S. C. (**1968**). The structure of vaginatin: a new sesquiterpene from the root extractive of *Selinum vaginatum*. *Chem. Comm. (London)*, (10), 584b-585.

37. Popović, V., Goeman, J. L., Bougarne, N., Eyckerman, S., Heyerick, A., De Bosscher, K., & Van der Eycken, J. (**2017**). Involvement of the Glucocorticoid Receptor in pro-inflammatory transcription factor inhibition by daucane esters from *Laserpitium zernyi*. *J. Nat. Prod.*, *80*(5), 1505-1513.

38. Ibraheim, Z. Z., Abdel-Mageed, W. M., Dai, H., Guo, H., Zhang, L., & Jaspars, M. (**2012**). Antimicrobial antioxidant daucane sesquiterpenes from *Ferula hermonis* Boiss. *Phytother. Res.*, *26*(4), 579-586.

39. Appendino, G., Cravotto, G., & Nano, G. M. (**1993**). Sesquiterpene lactones from *Laserpitium gallicum*. *Phytochemistry*, *33*(4), 883-886.

40. Marinelli, F., Zanelli, U., & Ronchi, V. N. (**1996**). Toxicity of 6-methoxymellein and 6-hydroxymellein to the producing carrot cells. *Phytochemistry*, *42*(3), 641-6

CHAPTER 5:

STUDIES TOWARDS THE TOTAL SYNTHESIS OF DAUCOVIRGOLIDE G

5.1 Total synthesis of germacrane sesquiterpenes

Total synthesis of germacranes and germacranolides has attracted the attention of synthetic chemists for many years, given their promising pharmacological activities and the possibility to employ the germacrane skeleton as intermediate to obtain sesquiterpene subclasses, such as elemanes, guaianes and eudesmanes.[1] Despite all the positive aspects, a drawback is represented by the instability of germacrane core to acidic, basic and thermal conditions, resulting in the formation of undesirable rearranged compounds.[2] To date, there are several publications about the total synthesis of these molecules, but in many cases, the adopted approach is not readily reproducible or it does not result in a reasonable yield of the synthesized products; hence the challenge to perform an efficient synthetic route leading to target sesquiterpenes in bulk quantities.

In the first part of this chapter, some relevant procedures for the total synthesis of germacrane derivatives will be reported, with particular attention to the formation of (*E, E*)-compounds. Then, the retrosynthetic and synthetic studies towards the total synthesis of daucovirgolide G, the most promising metabolite isolated from *D. virgatus*, will be described.

5.1.1 The first total synthesis of a germacranolide: (+)-dihydrocostunolide

The first germacrane sesquiterpene was synthesized by Corey and Hortmann in 1963, employing a photolytic cleavage as strategy to forge the ten-membered carbocycle of (+)-dihydrocostunolide (**4**) (**Scheme 5.1**).[3] Santonin (**1**), a natural product isolated from flowers of *Artemisia cina* possessing anthelmintic activity, was utilized as starting material to obtain a bicyclic conjugated diene (**2**); the latter was irradiated to give a mixture of starting bicyclic compound and cyclodecatriene (**3**), which was hydrogenated over Raney nickel to afford (+)-dihydrocostunolide in a very low yield (10%).

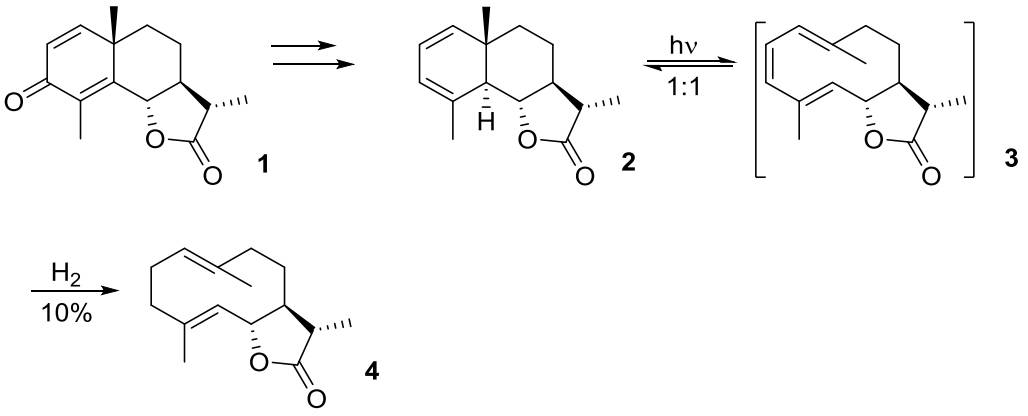

Scheme 5.1. The first total synthesis of (+)-dihydrocostunolide (**4**)

In 1986, J. E. Burks, Jr. *et al*. reported the total synthesis of (+)-dihydrocostunolide (**4**) *via* tandem Cope-Claisen rearrangement (**Scheme 5.2**).[4] The starting material of reaction, in this case, is represented by the triisopropylsilyl ketene acetal (**5**), which was obtained by treatment of the corresponding propionate ester with LDA and then with (*i*-Pr)$_3$SiCl. Thermolysis of (**5**) at 200°C provided compound (**7**), after a tandem Cope-Claisen rearrangement; the latter, after hydrolysis with KF·2H_2O and esterification with CH_2N_2 afforded (**8**) in 30% yield. The trisubstituted double bond of (**8**) was subjected to an epoxidation to give (**9**), which was in turn treated with OsO_4 to obtain the hydroxyl lactone (**10**). After oxidation of (**10**) with pyridinium dichromate (PDC), followed by a diasteroselective reduction with $NaBH_4$, mesylate (**13**) was prepared by treatment with MsCl. Compound (**13**) was deoxygenated with dimethyl diazomalonate and [(*n*-$C_7H_{15}C0_2$)$_2$Rh]$_2$ to give (**14**) in 66% yield. The anti-elimination of (**14**) utilizing tetra-*n*-butylammonium oxalate led to the desired final product (**4**) in 48% yield.

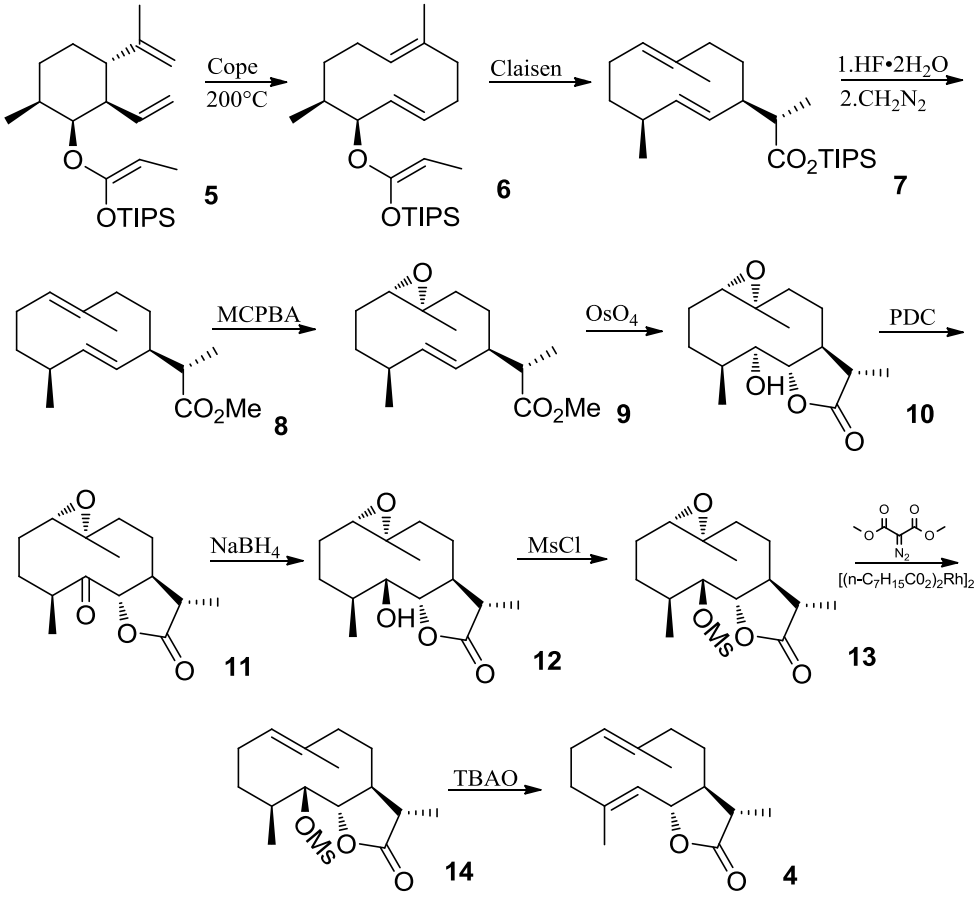

Scheme 5.2. Synthesis of (+)-dihydrocostunolide (4) via tandem Cope-Claisen rearrangement.

5.1.2 The total synthesis of (+)-costunolide

In 1977, Grieco and Nishizawa reported the first total synthesis of (+)-costunolide (**24**) (**Scheme 5.3**), a germacranolide isolated from the roots of *Saussurea costus*.[5] Santonin (**1**) was utilized as starting material to obtain keto lactone (**15**), after the hydrogenation of two double bonds and epimerization at C-4. The keto lactone (**15**) was treated with tosylhydrazine to give the corresponding hydrazone, which was in turn treated with an excess of lithium diisopropylamide in dry tetrahydrofuran at 0 °C to afford the crystalline olefin (**16**). Ozonolysis of olefin (**16**) and subsequent use of sodium borohydride led to the diol (**17**), which was subjected to treatment with o-nitrophenyl selenocyanate in pyridine-tetrahydrofuran (1:1), containing tributylphosphine, to give monoselenide (**18**). Oxidation of monoselenide (**18**) into olefinic alcohol (**19**) and conversion of the latter into selenide

(**20**), led to saussurea lactone (**21**) upon elimination of the 0-nitrophenylselenoxide. Subsequently, selenenylation of (**21**) afforded selenide (**22**); compound (**22**) was treated with hydrogen peroxide in tetrahydrofuran to obtain dehydrosaussurea lactone (**23**), which was subjected to thermolysis to give a 20% yield of crystalline (+)-costunolide (**24**).

This synthetic approach is based on the naturally occurring equilibrium between germacrane and elemane sesquiterpenes; thus, drawing on thermal conversion from 1,2-divinylcyclohexanes to cyclodecadienes, it was used a Cope rearrangement to obtain a germacrane derivative.

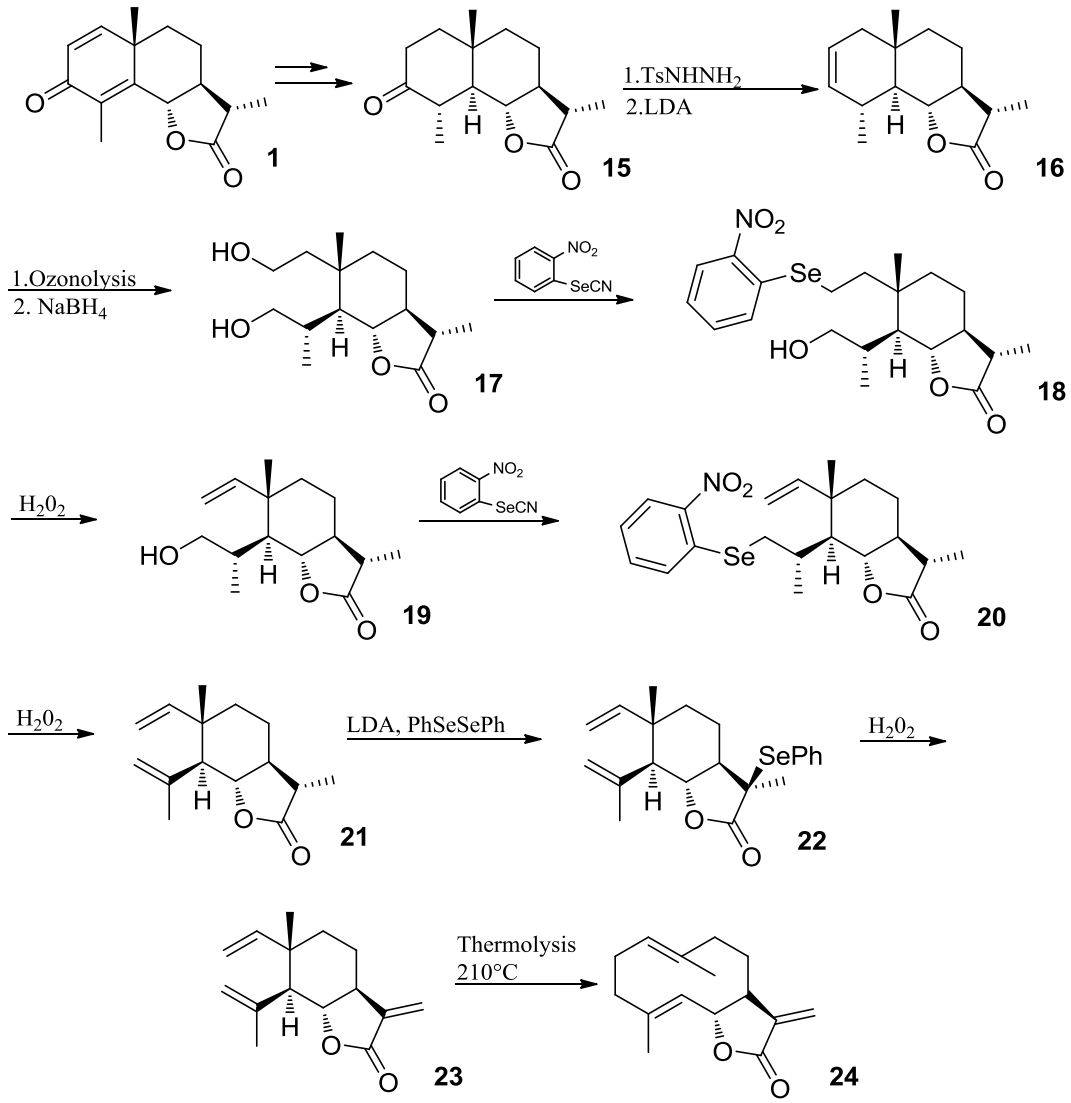

Scheme 5.3. Total synthesis of (+)-costunolide (24).

In 1986, Kitagawa *et al.* described an alternative route to synthesize (+)-costunolide;[6] as outlined in **Scheme 5.4**, it was employed a low-valent chromium reagent to synthesize the ten-membered carbocycle, starting from *E,E*-farnesyl acetate (**25**), which was treated with selenium dioxide to obtain ω-hydroxy-farnesyl acetate (**26**) in 53% yield. The latter was subjected to a bromination utilizing carbon tetrabromide and trioctyl phosphine in ether to afford ω-bromo-farnesyl acetate (**27**) in 72% yield. Upon alkaline hydrolysis and oxidation with PCC-AcONa in CH_2Cl_2, ω-bromo-farnesal (**28**) was obtained in 88% yield. As mentioned, the cyclization of the carbocyclic ring (**29**) was obtained with $CrCl_3$-$LiAlH_4$ (2:1) in N,N-dimethylformamide at room temperature in 42% yield, as racemic mixture. Thus, the treatment of (**29**) with t-butyldimethylsilyl chloride (TBDMSCI), hydroboration-oxidation with 9- borabicyclo [3.3.1] nonane (9-BBN), and alkaline hydrogen peroxide oxidation, afforded the diol-monosilyl ether (**30**). Subsequent oxidation with pyridinium dichromate (PDC) and desilylation using tetrabutylammonium fluoride followed by lactonization in acidic conditions, led to (+)- dihydrocostunolide (**4**) in 68% yield. The last step involved the use of lithium diisopropylamide (LDA) and diphenyl diselenide, followed by the treatment with hydrogen peroxide to give (+)-costunolide (**24**) in 49% yield.

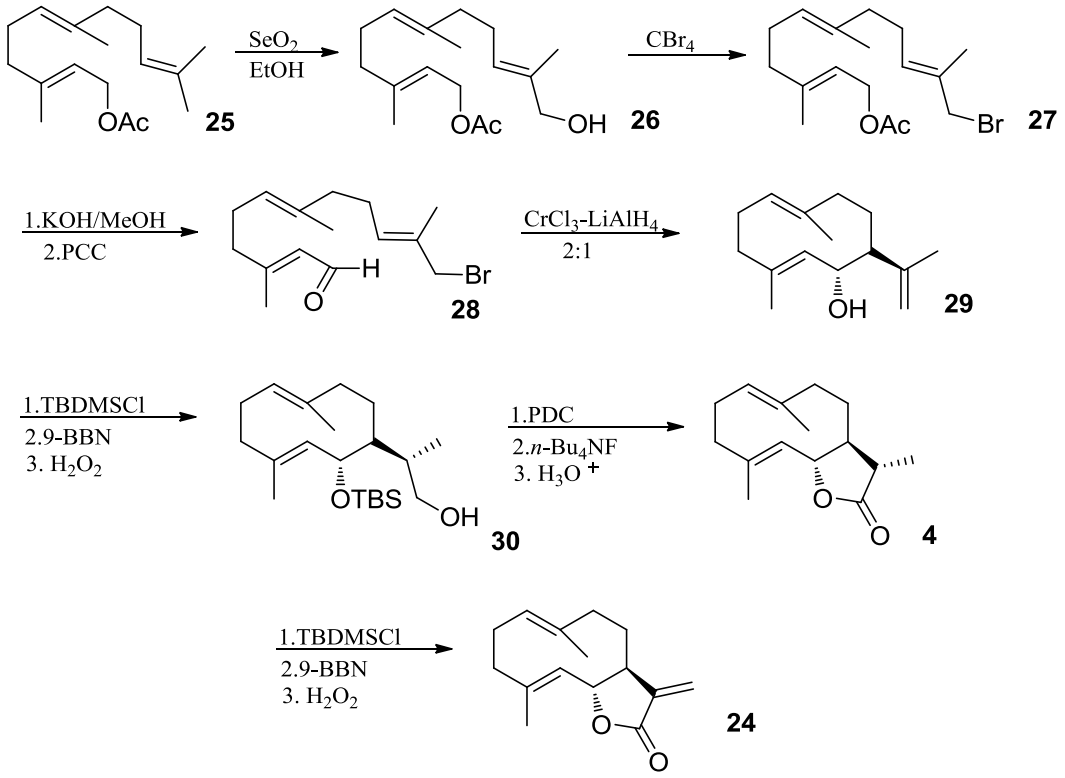

Scheme 5.4. Alternative route for the synthesis of (+)-costunolide

5.1.3 Total synthesis of (±)-acoragermacrone

In 1983, Takahashi *et al.* reported a new method for the synthesis of (±)-acoragermacrone (**39**) (**Scheme 5.5**),[7] founded on an intramolecular alkylation of cyanohydrins protected as 1-ethoxyethyl ether (EEO). Aldehyde (**32**), prepared starting from geranyl acetate (**31**), was subjected to the addition of isopropylmagnesium bromide and tosylation of the resulting alcohol gave (**33**); the 1-ethoxyethyl group of (**33**) was removed and allylic oxidation utilizing MnO_2 gave aldehyde (**34**) in 85% yield. The cyanohydrin trimethylsilyl ether (**35**) was obtained after treatment of (**34**) with trimethylsilyl cyanide, KCN/dicyclohexyl-18-crown-6-complex at 0°. Subsequently, after deprotection of compound (**35**) and treatment of the cyanohydrins (**36**) with ethyl vinyl ether, the resulting protected cyanohydrins (**37**) was treated with lithium bis(trimethylsilyl)amide in refluxing benzene to obtain the cyclization product (**38**) in 57% yield. Acid and basic treatments (PPTS/MeOH, 40°C, 1 h and 1% aq. NaOH, O°C, 1 min), led to (±)-acoragermacrone (**39**).

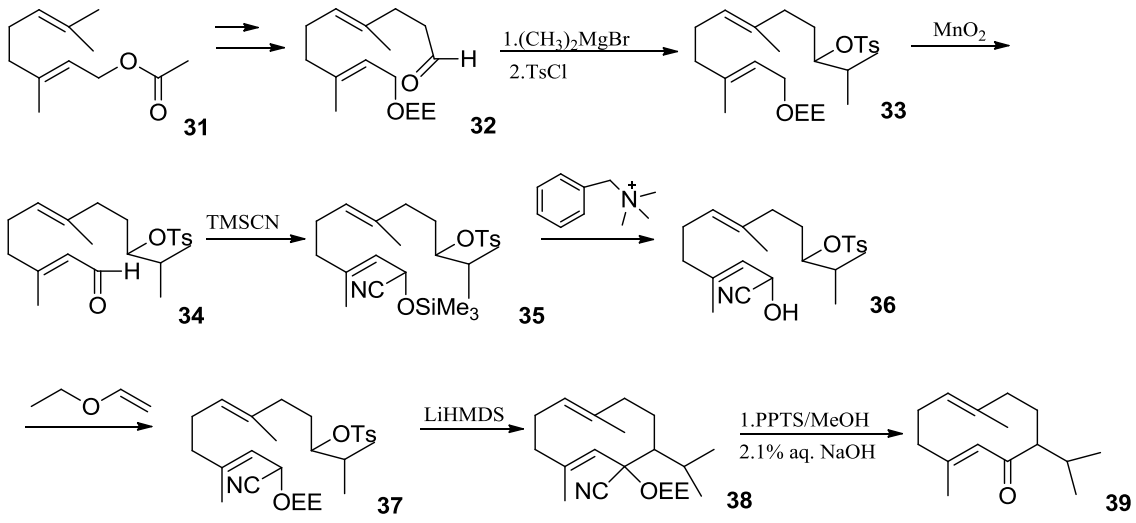

Scheme 5.5. Synthesis of (±)-acoragermacrone.

5.1.4 Baran's approach to the formation of the germacranolides' ten-membered carbocycle

An elegant and efficient procedure for the preparation of the germacrane core, starting from farnesol (**40**), was reported by Baran *et al.* in 2012.[1] The key-step reaction of the synthesis was a diastereoselective Pd-catalyzed intramolecular coupling reaction between the aldehyde and allylchloride functional groups present in intermediate (**43**). Remarkably, the reaction proceeded through the formation of an allyl anion, generated by reaction of the allyl chloride with $[PdCl_2(PPh_3)_2]$ and diethyl zinc in N,N-dimethylacetamide (DMA), which is able to react with the aldehyde to provide the 10-membered ring. As outlined in **Scheme 5.6**, farnesol was initially converted to epoxy aldehyde (**41**) using Sharpless epoxidation and Parick-Doering oxidation. Regioselective chlorination of (**42**), with concomitant transposition of the 10,11- double bond to the terminal position, provided chlorinated epoxy aldehyde (**43**) in 63% yield. Cyclisation of the latter intermediate, using the method described before, led to the germacrane ring system (**44**).

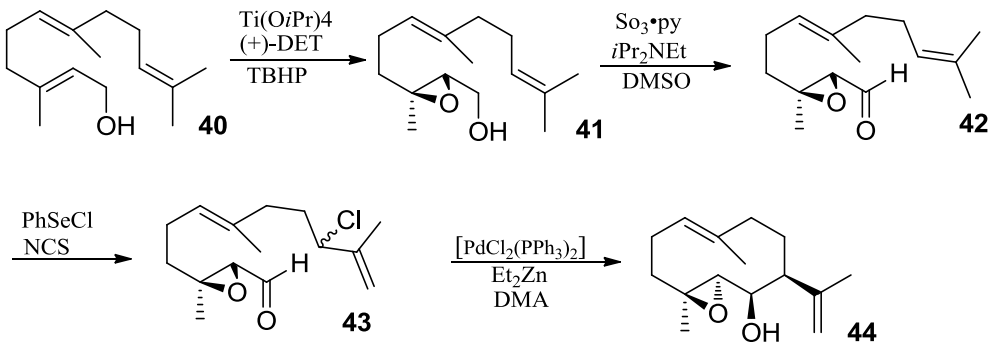

Scheme 5.6. Preparation of the ten-membered carbocycle using Baran's approach

5.2 Retrosynthetic analysis of daucovirgolide G

The retrosynthetic pathway designed for the preparation of daucovirgolide G (**45**) is outlined in **Scheme 5.7**. It was initially envisioned that the fused-bicyclic system of the final target (**45**) could be readily obtained from compound (**46)** *via* an initial stereocontrolled dihydroxylation (Sharpless dihydroxylation) and subsequent oxidation, followed by lactonization of the resulting α-hydroxy acid. An intramolecular Corey-Seebach reaction could be employed to prepare the ten-membered ring. Successive deprotection of the dithiane, stereocontrolled reduction with DIBAL-H and SN_2 reaction under Mitsunobu conditions would provide the acetate group with the correct configuration at C-8 (conversion of compound **47** to **46**). The preparation of substrate **47** for the intramolecular Corey-Seebach reaction, requires the installation of two functionalities: a dithiane and a tosylate group. The dithiane functionality, used as an acyl anion equivalent, could be introduced on **47** via sequential reduction and thioacetalization of 4**8**. The tosylate leaving group, on the other hand, could be readily installed via tosylation of allylic alcohol **48**. In turn, key intermediate **48** could be obtained via a diastero- and regio- selective addition of dienolate **49** to aldehyde **50**. Finally, aldehyde **50** could be synthesized from geranyl acetate, a commercially available monoterpene, via a high regioselective allylic hydroxylation, followed by protection of resulting allylic alcohol as TBS ether, hydrolysis of the acetyl group and oxidation to aldehyde **50**. Although this route is suitable for asymmetric synthesis, it was initially explored the preparation of racemic compound **45**.

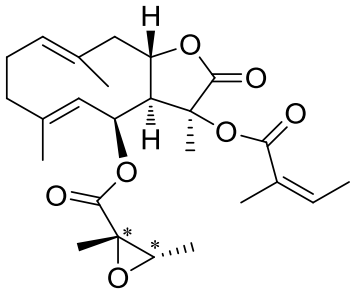

7

Daucovirgolide G

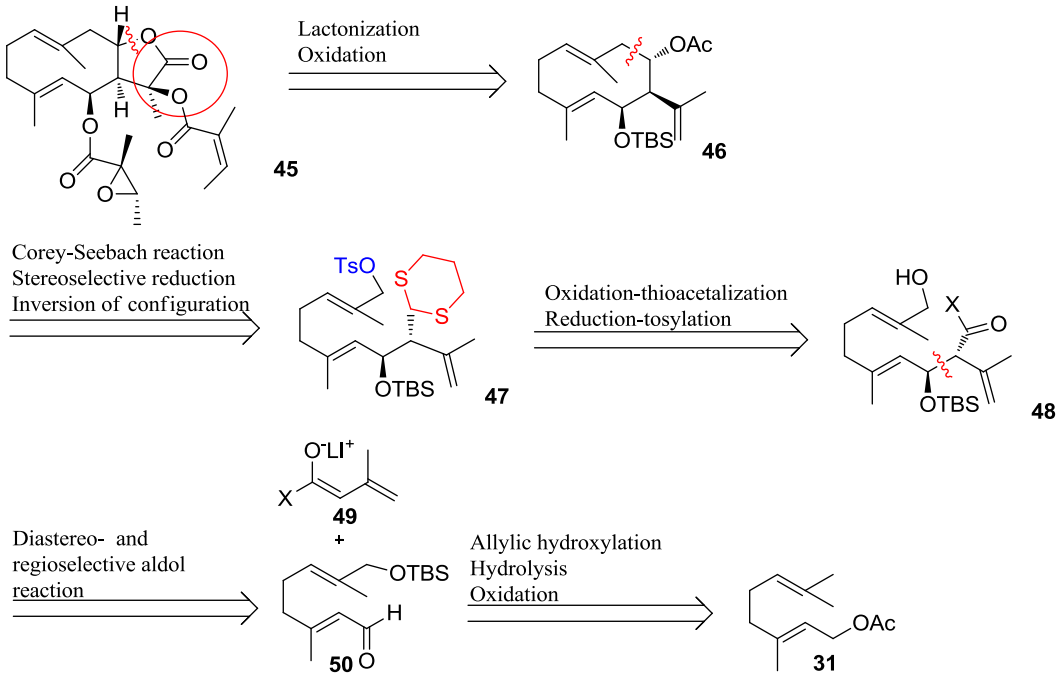

Scheme 5.7. Retrosynthetic scheme for the preparation of daucovirgolide G.

5.3 Synthesis of daucovirgolide G

5.3.1 Preparation of (2*E*,6*E*)-8-hydroxy-3,7-dimethylocta-2,6-dien-1-yl acetate

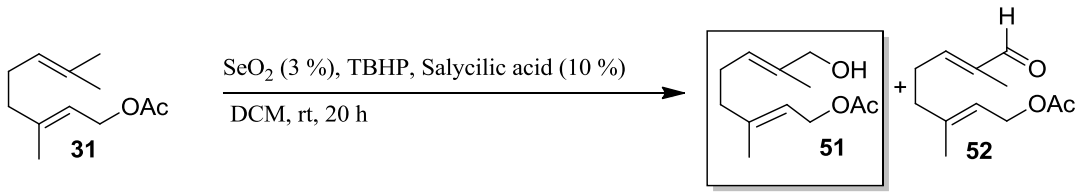

Scheme 5.8. Preparation of allylic alcohol **51** with SeO_2.

The first step of our synthetic route required the regioselective hydroxylation of geranyl acetate. This reaction was carried out following a procedure reported by Sharpless *et. al.*[8] As outlined in **Scheme 5.8**, the process involved the treatment of geranyl acetate with catalytic amounts of selenium dioxide and salicylic acid, along

with stoichiometric amounts of *tert*-butyl hydroperoxide (TBHP) as terminal oxidant. The NMR of the crude material revealed that the reaction proceeded with high regioselectivity; thus, the product was mostly contaminated only by variable amounts of aldehyde (**52**) (20-30 %), which was readily removed from the mixture by column chromatography (DCM/Ethyl acetate 8:2). Pure allylic alcohol (**51**) was obtained in 61% yield.

5.3.2 Preparation of (2*E*,6*E*)-8-((*tert*-butyldimethylsilyl) oxy)-3,7-dimethylocta-2,6-dien-1-ol (53)

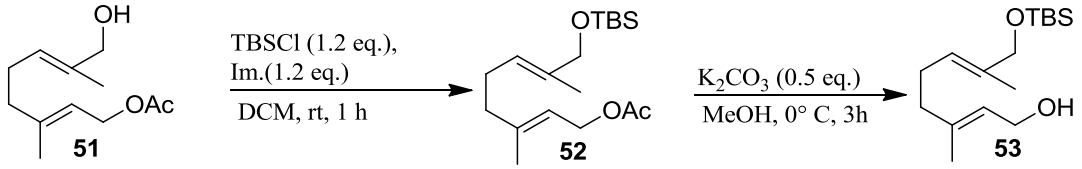

Scheme 5.9. Conversion of allylic alcohol **51** to intermediate **53** *via* sequential silylation and hydrolysis.

Protection of the free hydroxyl group presents in allylic alcohol **51** was carried out using a standard protocol for the protection of primary alcohols as silyl ethers (**Scheme 5.9**). [9] The desired protected product **52** was obtained in quantitative yield. Successive treatment of intermediate **52** with a methanolic solution of K_2CO_3 provided compound **53** in 87% yield. Remarkably, the conversion of compound **51** to **53** didn't require any purification by column chromatography.

5.3.3 Preparation of (2*E*,6*E*)-8-((*tert*-butyldimethylsilyl)oxy)-3,7-dimethylocta-2,6-dienal (50)

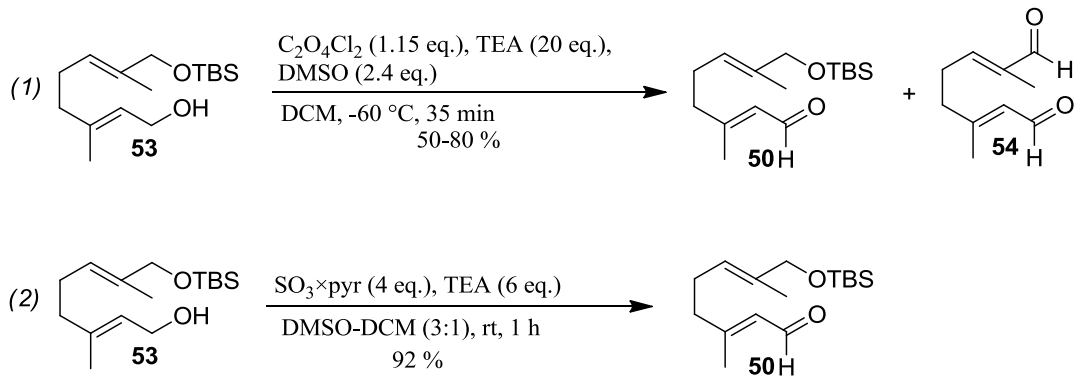

Scheme 5.10. Oxidation of protected allylic alcohol **53** to aldehyde **50**.

The oxidation of an allylic alcohol to aldehyde has been reported in the literature using MnO_2.[10] Unfortunately, the reactivity of this oxidizing system is known to be variable and could lead to non-reproducible results. As a consequence, we attempted other procedures that required the use of activating reagents of DMSO (Swern or Parick-Doering oxidation). Our preliminary investigations revealed that the reaction could be carried out for our substrate efficiently using Swern oxidation.[11] Unfortunately, the reaction gave non-reproducible results. In fact, careful analysis of the crude NMR revealed the presence of a variable amount of *bis*-aldehyde **54**. We supposed that the impurity arose from the deprotection of the acid-labile TBS group. Hence, traces of HCl would be formed by hydrolysis of oxalyl chloride, and then a sequential deprotection and oxidation would lead to by-product **54**. The low temperatures and strictly anhydrous conditions were other drawbacks that must be considered when carrying through this protocol. Subsequently, we explored Parick-Doering oxidation for the preparation of compound **50**.[12] This procedure employed SO_3·pyr complex as a mild activator of DMSO to perform the oxidation. Furthermore, the reaction could be run at room temperature under very mild conditions. To our delight, target compound **50** was obtained in excellent yield (92%). The pure product was then easily isolated from the mixture through a simple filtration over a small pad of silica gel.

5.3.4 Preparation of ethyl (2*S*,3*R*,4*E*,8*E*)-3,10-dihydroxy-5,9-dimethyl-2-(prop 1-en-2-yl)deca-4,8-dienoate (*anti*-55a)

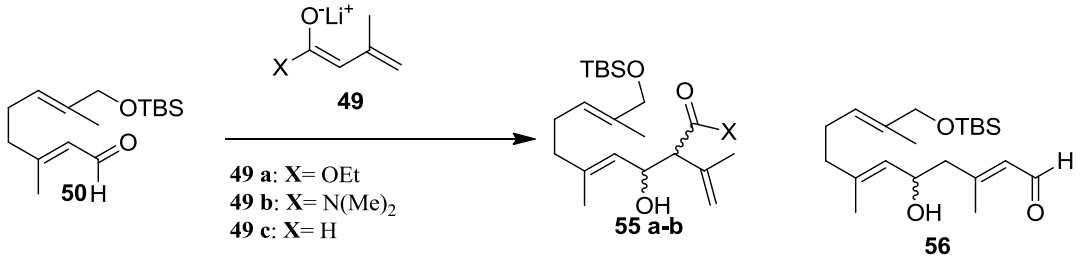

Scheme 5.11. Synthetic strategies for the preparation of β-hydroxy carbonyl compounds **55 a-b** and **56** *via* aldol condensation.

Preparation of compounds **55a** and **55b** required the introduction of a β-hydroxy carbonyl group and an *exo*-methylene in the geranyl scaffold. We envisioned that this transformation could be carried out in a single process through an aldol reaction using dienolate **49a** and **49b**. It was preferred to avoid the use of dienolate **49c**, in order to prevent the formation of product (**56**) as a result of vinylogous addition, which is known to be favorite when using soft nucleophiles (for example enolate aldehyde).

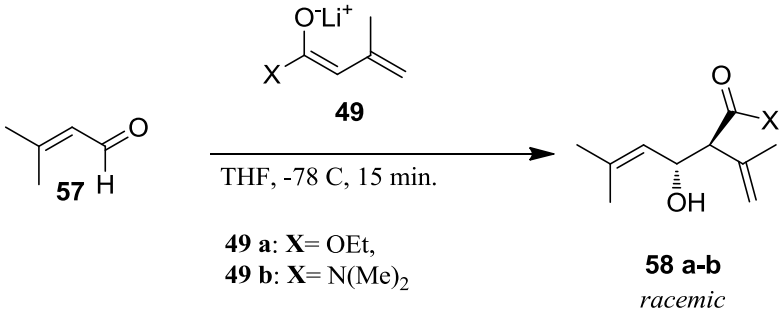

Scheme 5.12 Pilot reactions on aldehyde (**57**).

Several potential issues could derive from the aldol reaction on substrate **50**; for this reason, we initially decided to perform a series of pilot reactions on the cheap and commercially available congener aldehyde **57,** in order to find the best reagent and reaction conditions.

In fact, a competition between α *versus* γ addition on substrate **50** could potentially lead to regioselective problems. Further, with regards to the diastereoselectivity, the reaction could provide both *sin* and *anti*-products of **55 a-b**.[13]

After several trials, we discovered that the reaction could be carried out efficiently at low temperatures (-78 ˚C) using both ester **49a** and amide **49b**, with the predominant formation of the *anti*- diastereoisomer. This procedure, however, as shown by the crude NMR, was extremely selective only in the amide (**49 b**) case (more than 99% in favor of the *anti*-product). Therefore, we initially decided to progress our synthetic route using amide dienolate.

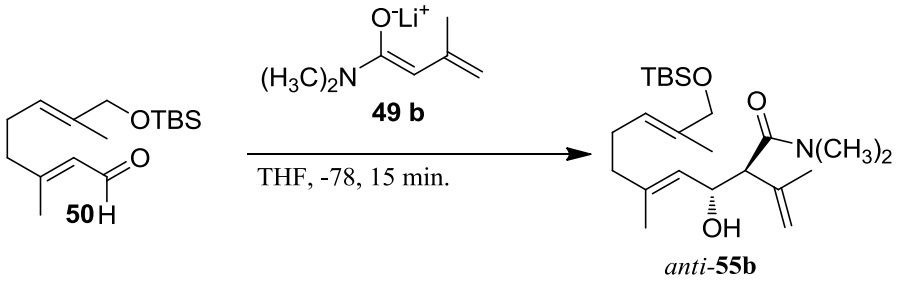

Scheme 5.13. Preparation of *anti*-β-Hydroxy-amide **55b** from aldehyde **50** and dienolate **49b**.

Once applied the optimized procedure to aldehyde **50**, however, we observed that selectivity dropped down to 3:1 in favor of the *anti*-product **55b**. Hopefully, the required *anti*-diastereoisomer was easily isolated from the mixture by column chromatography with a yield of 55-60% (the *sin*-isomer was obtained in 20% isolated yield).

Unfortunately, as discussed in the next section of this chapter, the reduction of compound **59** to alcohol **60** was unsuccessful and it was necessary to use ester dienolate **49a** to progress in our synthesis.

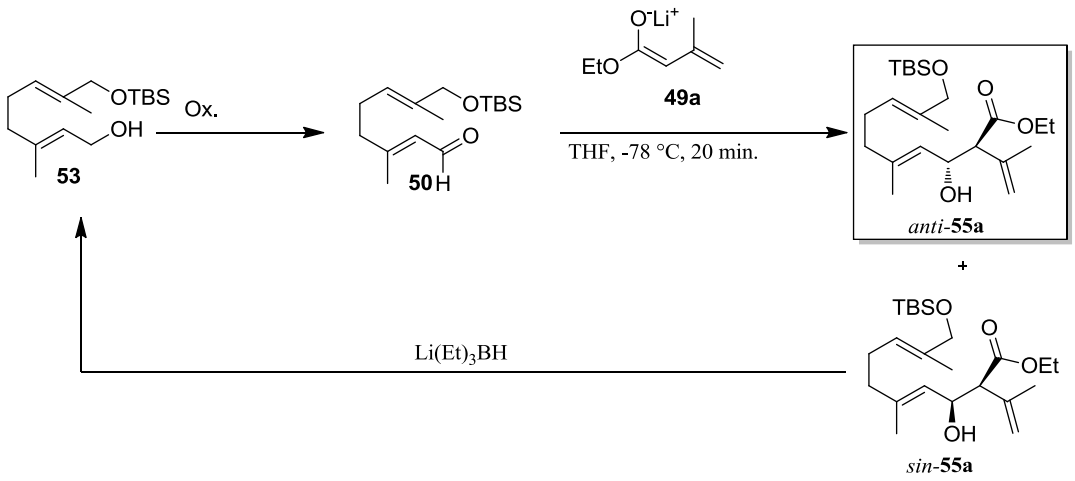

Scheme 5.14. Preparation of *anti*-β-Hydroxy-ester **55a** from aldehyde **50** and dienolate **49a.** $LiEt_3BH$ promoted retroaldol reaction for the conversion of *sin*-**55a** to **53**.

The reaction of aldehyde **50** with ester dienolate **49a** provided the *anti*-product **55a** in a good yield (52% of *anti*-product and 26% of the *sin*-product) and moderate diastereoselectivity (2:1 in favour of the *anti* diastereoisomer). We also discovered that treatment of the *sin* isomer with $LiEt_3BH$ (10 eq.), induced a retroaldol reaction with subsequent reduction of the resulting aldehyde. Hence, by reacting the *sin*-product with $LiEt_3BH$, we were able to transform the undesired diastereoisomer in compound **53**, and this was then reintroduced in our synthetic route to obtain the required *anti*-**55a** product. The yield for this process is 78%, based on recovered reagent **53**.

5.3.5 Attempted synthesis of (2R,3R,4E,8E)-3,10-bis((tert-butyldimethylsilyl)oxy)-5,9-dimethyl-2-(prop-1-en-2-yl)deca-4,8-dien-1-ol (60).

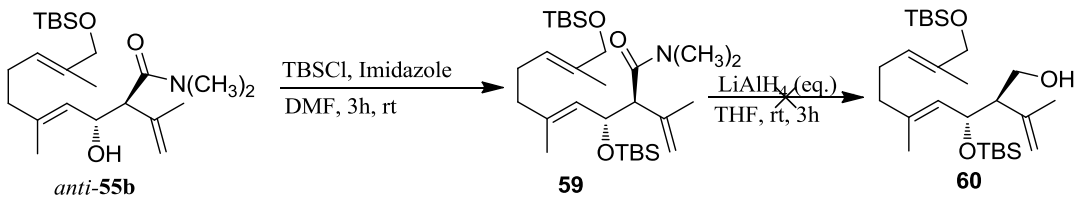

Scheme 5.15. Attempted preparation of alcohol **60** from amide **55b**

Protection of the free hydroxyl group in compound **55b** was carried out using a standard protocol for the silylation of secondary alcohols (**Scheme 5.15**). Delightfully, we obtained the desired protected material **59** in quantitative yield. Successive treatment of intermediate **59** with $LiEt_3BH$, following the procedure reported by Brown *et. el.*,[14] didn't provide the desired product **60**; thus, the starting material **59** was always recovered quantitatively. It is possible to explain this result considering that the reactivity of $LiEt_3BH$ is affected from the proximity of the sterically demanding TBS group. In order to enhance the reactivity of the reducing agent, we carried out the reaction at a higher temperature (60 ˚C). Unfortunately, also in this case, we didn't observe any conversion to the desired product and, once again, the starting material was fully recovered.

5.3.6 Preparation of (2R,3R,4E,8E)-3,10-bis((tert-butyldimethylsilyl)oxy)-5,9-dimethyl-2-(prop-1-en-2-yl)deca-4,8-dien-1-ol from *anti*-β-Hydroxy-ester and attempted oxidation to aldehyde.

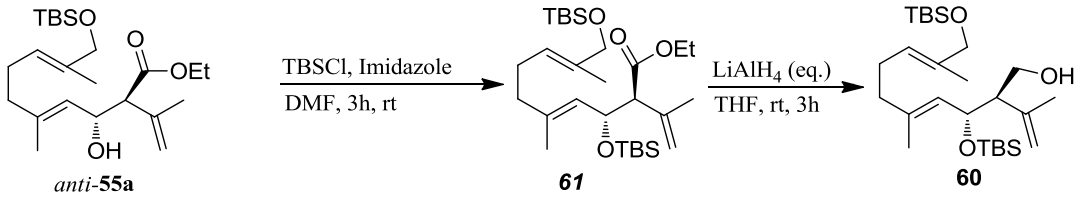

Scheme 5.16. Preparation of ester **61** and reduction to alcohol **60**.

Given the inability to achieve the reduction of amide **55b** to alcohol **60** utilizing $LiEt_3BH$, it was possible to reintroduce ester **55a** in the synthetic route. The latter was then reduced efficiently to compound **60** using $LiAlH_4$(3 eq.).

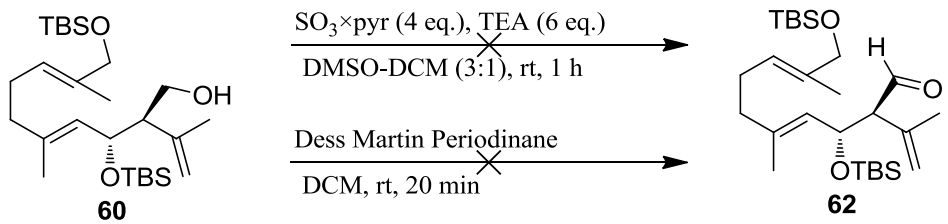

Scheme 5.17. Preparation of aldehyde **62**.

We next explored the oxidation of alcohol **60** to aldehyde **62**. Unfortunately, as shown in **Scheme 5.17**, any attempt to oxidise compound **60,** using the Parikh–Doering oxidation and the Dess Martin Periodinane, provided a complex mixture, containing only traces of the desired product. We are currently changing several reaction parameters (temperature, solvent, time of reaction) and investigating other reagents to increase the conversion to compound **62**. For example, we envisioned that others mild oxidising systems could be used to perform this reaction. Among these, we are considering the TEMPO BAIB system or Ley–Griffith oxidation. We are also considering the direct conversion of the ester to the aldehyde using DIBAL at low temperature (-78 ˚C).

5.4 Experimental section

(2*E*,6*E*) -8-Hydroxy-2,6-dimethyl-2,6-octadienyl acetate (51): to a suspension of selenium dioxide (239 mg, 2.15 mmol, 0.03 equiv) and salicylic acid (1g, 7.2 mmol, 0.1 equiv) in CH_2Cl_2 (116 mL) was added tert-butyl hydroperoxide (5.5M in nonane, 50 mL, 3.87 equiv), and the mixture was stirred for 15 min at room temperature. Then, geranyl acetate (14 g, 71 mmol, 1 equiv) was added to the suspension. After being stirred for another 20 h, the mixture was quenched with MnO_2 and a solution of NaOH 1M was added. Successively, it was extracted with DCM and washed with brine. The organic layer was dried over anhydrous Na_2SO_4 and concentrated in vacuo. The residue was chromatographed on silica gel (cyclohexane/ethyl acetate = 7/3) to give **(51)** (9.2 g, 61%) as a colorless oil.
^{1}H-NMR (400 MHz, $CDCl_3$) : δ 5.32–5.38 (m, 2H), 4.58 (d, *J* = 7.5 Hz, 2H), 3.99 (s, 2H), 2.18 (dd, *J* = 7.0, 14.0 Hz, 2H), 2.08 (dd, *J* = 7.0, 14.0 Hz, 2H), 2.06 (s, 3H), 1.71 (s, 3H), 1.67 (s, 3H); ^{13}C NMR (125 MHz, CDCl3): δ 171.2, 141.7, 135.2, 125.2, 118.6, 68.8, 61.4, 39.0, 25.6, 21.0, 16.4, 13.6. HRMS-ESI *m/z* 213.1416 $[M+H]^+$, $C_{12}H_{21}O_3$ requires 213.1412.

(2*E*,6*E*)-8-tert-Butyldimethylsiloxy-3,7-dimethyl2,6-octadienyl acetate (52): Imidazole (3.6 g, 53 mmol, 1.2 equiv) and t-butyldimethylchlorosilane (8 g, 53 mmol, 1.2 equiv) were sequentially added to a solution of alcohol **51** (9.2 g, 43.4 mmol, 1 equiv) in DCM (217 mL, 0.2M). The mixture was stirred at room

temperature for 1 h, quenched with ammonium chloride, and then extracted with diethyl ether. The organic phase was washed with brine and dried over Na_2SO_4. Solvent was removed under reduced pressure to give pure **52** (14.1 g, 43.4 mmol, 100% yield) as a colorless oil.

^{1}H NMR ($CDCl_3$, 400 MHz) δ 5.36 (t, *J* = 7.0 Hz, 1H), 5.35 (t, *J* = 7.0 Hz, 1H), 4.58 (d, *J* = 7.0 Hz, 2H), 4.00 (s, 2H), 2.15 (q, *J* = 7.4 Hz, 2H), 2.09−2.06 (m, 2H), 2.05 (s, 3H), 1.70 (s, 3H), 1.59 (s, 3H), 0.90 (s, 9H), 0.05 (s, 6H). ^{13}C NMR (CDCl3, 150 MHz) δ 171.1, 142.0, 134.9, 123.7, 118.5, 68.6, 61.4, 39.3, 26.0, 25.8, 21.1, 18.5, 16.5, 13.5, −5.2. HRMS-ESI *m/z* 327.2272 $[M+H]^+$, $C_{18}H_{35}O_3Si$ requires 327.2277.

(2*E*,6*E*) -8- ((tert-butyldimethylsilyl) oxy) -3,7-dimethylocta-2,6-dien-1-ol (53): Into a flask were added acetate **52** (14.1 g, 43.4 mmol, 1 equiv), MeOH (434 mL, 0.1 M), and K_2CO_3 (4.5 g, 32.55 mmol, 0.75 equiv). The mixture was stirred at room temperature for 4h, quenched with NH_4Cl, and extracted with diethyl ether. The combined organic phase was washed with brine and dried over Na_2SO_4. Solvent was removed under reduced pressure to obtain pure alcohol **53** (10.7 g, 37.6 mmol, 87% yield), as a colorless oil, which was used for the next step without futher purifications.

^{1}H NMR ($CDCl_3$, 400 MHz) δ 5.42 (t, *J* = 6.7 Hz, 1H), 5.36 (t, *J* = 7.0 Hz, 1H), 4.15 (d, *J* = 6.7 Hz, 2H), 4.00 (s, 2H), 2.16 (q, *J* = 7.5 Hz, 2H), 2.05 (t, *J* = 7.5 Hz, 2H), 1.68 (s, 3H), 1.59 (s, 3H), 0.90 (s, 9H), 0.06 (s, 6H). ^{13}C NMR ($CDCl_3$, 150 MHz) δ 139.5, 134.8, 124.0, 123.7, 68.7, 59.4, 39.3, 26.1, 25.9, 18.6, 16.3, 13.6, −5.1. HRMS-ESI *m/z* 285.2288 $[M+H]^+$, $C_{16}H_{33}O_2Si$ requires 285.2250

(2*E*,6*E*) -8-(tert-butyldimethylsilyloxy) - 3,7-dimethylocta-2,6- dienal (50): to a stirred solution of alcohol **53** (10.7 g, 37.6 mmol, 1 equiv) in DCM/DMSO (2:1, 513 mL, 0.07M) were added Et_3N (26.1 mL, 188 mmol, 5 equiv) and SO_3•py (23.9g, 150.4 mmol, 4 equiv) at room temperature. The mixture was stirred for 1 h and it was quenched with NH_4Cl and extracted with diethyl ether. The combined organic extracts were dried over Na_2SO_4 and concentrated under reduced pressure. The residue was chromatographed on silica gel (cyclohexane/ethyl acetate 9:1) to obtain compound **50** (9.8 g, 34.6 mmol, 92% yield), as a pale-yellow oil.

^{1}H NMR ($CDCl_3$, 400 MHz) δ 0.06 (s, 6 H), 0.92 (s, 9 H), 1.62 (d, *J* = 2 Hz, 3 H), 2.17 (s, 3 H), 2.28 (m, 4 H), 4.00 (s, 2 H), 5.38 (m, 1 H), 5.90 (br d, *J* = 8 Hz, 2H),

10.00 (1 H, d, *J* = 8 Hz, 1 H); ^{13}C NMR (101 MHz, cdcl$_3$) δ 191.18 (s), 163.48 (s), 135.80 (s), 127.46 (s), 122.12 (s), 68.16 (s), 40.29 (s), 25.91 (s, 3C), 25.15 (s), 17.54 (s), 13.45 (s), -0.03 (s), -5.31 (s, 2C). HRMS-ESI *m/z* 283.2101 [M+H] $^+$, $C_{16}H_{31}O_2Si$ requires 283.2093

Ethyl (4*E*,8*E*) -10-((tert-butyldimethylsilyl) oxy) -3-hydroxy-5,9-dimethyl-2-(prop-1-en-2-yl) deca-4,8-dienoate (55a): to a stirred solution of ethyl-3,3-dimethyl acrylate (5.8 ml, 41.8 mmol, 1.2 equiv) in THF, LDA (2M, 41.8 mmol, 1.2 equiv) was added dropwise at -78°C. After 10 minutes, compound (**50**) (9.8 g, 34.8 mmol, 1 equiv) was added dropwise. After 20 minutes the mixture was quenched with NH_4Cl and extracted with diethylether. The combined organic layers were dried (Na_2SO_4) and concentrated in vacuo. The residue was chromatographed on silica gel (cyclohexane/ethyl acetate 8:2) to obtain compound **55a** (11.1 g, 27.1 mmol, 78 % yield), as a colourless oil.

^{1}H NMR (400 MHz, $CDCl_3$) δ 5.33 (t, *J* = 6.8 Hz, 1H), 5.14 (d, *J* = 9.1 Hz, 1H), 4.90 (s, 2H), 4.75 (dt, *J* = 8.9, 4.5 Hz, 1H), 4.20 (q, *J* = 7.4 Hz, 2H), 3.99 (s, 2H), 3.08 (d, *J* = 8.8 Hz, 1H), 2.54 (d, *J* = 4.6 Hz, 1H), 2.19 – 2.00 (m, 4H), 1.72 (s, 3H), 1.71 (s, 3H), 1.59 (s, 3H), 1.27 (t, *J* = 7.2 Hz, 3H), 0.90 (s, 9H), 0.06 (s, 6H). ^{13}C NMR (101 MHz, $CDCl_3$) δ 173.23 (s), 140.48 (s), 139.84 (s), 134.74 (s), 124.49 (s), 124.04 (s), 115.21 (s), 68.69 (s), 68.10 (s), 60.85 (s), 59.63 (s), 39.27 (s), 25.95 (s, 3C), 21.51 (s), 18.42 (s), 16.79 (s), 14.10 (s), 13.41 (s), 0.03 (s),-5.27 (s, 2C). HRMS-ESI *m/z* 411.2935 [M+H] $^+$, $C_{23}H_{43}O_4Si$ requires 411.2931

Ethyl (4*E*,8*E*)-3,10-bis((tert-butyldimethylsilyl) oxy) -5,9-dimethyl-2-(prop-1-en-2-yl) deca-4,8-dienoate (61): imidazole (2.2 g, 32.5 mmol, 1.2 equiv) and t-butyldimethylchlorosilane (4.9 g, 32.5 mmol, 1.2 equiv) were sequentially added to a solution of alcohol **55a** (11.1 g, 27.1 mmol, 1 equiv) in DCM (160 mL, 0.2M). The mixture was stirred at room temperature for 1 h, quenched with ammonium chloride, and then extracted with diethyl ether. The organic phase was washed with brine and dried over Na_2SO_4. Solvent was removed under reduced pressure to give pure **61** (14.2 g, 27.1 mmol, 100% yield) as a colorless oil.

^{1}H NMR (400 MHz, CDCl3) δ 5.34 (t, *J* = 6.9 Hz, 1H), 5.02 (d, *J* = 10.5 Hz, 1H), 4.93 (s, 1H), 4.83 (s, 1H), 4.77 (t, *J* = 9.7 Hz, 1H), 4.20 – 4.13 (m, 1H), 4.12 – 4.05 (m, 1H), 3.99 (s, 2H), 3.07 (d, *J* = 9.8 Hz, 1H), 2.11 (dd, *J* = 15.4, 7.2 Hz, 2H), 2.03

– 1.97 (m, 2H), 1.70 (s, 3H), 1.67 (d, *J* = 1.1 Hz, 3H), 1.60 (s, 3H), 1.26 (t, *J* = 7.1 Hz, 3H), 0.91 (s, 9H), 0.82 (s, 9H), 0.06 (s, 6H), 0.04 – -0.01 (m, 6H). ^{13}C NMR (101 MHz, $CDCl_3$) δ 172.31 (s), 139.81 (s), 137.45 (s), 134.65 (s), 126.16 (s), 124.28 (s), 114.89 (s), 70.00 (s), 68.74 (s), 61.12 (s), 60.34 (s), 39.36 (s), 26.89 (s), 26.0 (s), 25.95 (s, 2C), 25.65 (s, 2C), 21.94 (s), 18.42 (s), 17.92 (s), 17.04 (s), 14.14 (s), 13.36 (s), 0.99 (s), -0.02 (s), -4.02 (s), -5.14 (s), -5.28 (s).

References

1. Foo, K., Usui, I., Götz, D. C., Werner, E. W., Holte, D., & Baran, P. S. (**2012**). Scalable, enantioselective synthesis of germacrenes and related sesquiterpenes inspired by terpene cyclase phase logic. *Angew. Chem. Int. Ed.*, *51*(46), 11491-11495.

2. Minnaard, A. J., Wijnberg, J. B., & de Groot, A. (**1999**). The synthesis of germacrane sesquiterpenes and related compounds. *Tetrahedron*, *55*(8), 2115-2146.

3. Corey, E. J., & Hortmann, A. G. (**1963**). Total Synthesis of Dihydrocostunolide. *J. Am. Chem. Soc.*, *85*(24), 4033-4034.

4. Chi, K. (**1987**). *Total Synthesis of (+)-dihydrocostunolide Via Tandem Cope-Claisen Rearrangement* (Doctoral dissertation, University of Washington).

5. Grieco, P. A., & Nishizawa, M. (**1977**). Total synthesis of (+)-costunolide. *J. Org. Chem.*, *42*(10), 1717-1720.

6. Shibuya, H., Ohashi, K., Kawashima, K., Hori, K., Murakami, N., & Kitagawa, I. (**1986**). Synthesis of (±)-costunolide, an antitumor germacranolide, from (*E*,*E*)-farnesol by use of a low-valent chromium reagent. *Chem. Lett.*, 15(1), 85-86.

7. Takahashi, T., Nemoto, H., Tsuji, J., & Miura, I. (**1983**). Simple total syntheses of (±)-acoragermacrone and (±)-mukulol by intramolecular alkylation of protected cyanohydrin. *Tetrahedron Lett.*, *24*(33), 3485-3488.

8. Sharpless, K. B., & Lauer, R. F. (**1972**). Selenium dioxide oxidation of olefins. Evidence for the intermediacy of allylseleninic acids. *J. Am. Chem. Soc.*, *94*(20), 7154-7155.

9. Wuts, P. G., & Greene, T. W. (**2006**). *Greene's protective groups in organic synthesis*. John Wiley & Sons.

10. Tojo, G., & Fernández, M. I. (**2006**). *Oxidation of alcohols to aldehydes and ketones: a guide to current common practice*. Springer Science & Business Media.

11. Mancuso, A. J., Huang, S. L., & Swern, D. (**1978**). Oxidation of long-chain and related alcohols to carbonyls by dimethyl sulfoxide" activated" by oxalyl chloride. *J. Org. Chem.*, *43*(12), 2480-2482.

12. Tidwell, T. T. (**1990**). Oxidation of alcohols by activated dimethyl sulfoxide and related reactions: an update. *Synthesis*, *1990*(10), 857-870.

13. Evans, D. A., Nelson, J. V., & Taber, T. R. (**1982**). Stereoselective aldol condensations. *Topics in stereochemistry*, 1-115.

14. Krishnamurthy, S., & Brown, H. C. (**1983**). Selective reductions. 31. Lithium triethylborohydride as an exceptionally powerful nucleophile. A new and remarkably rapid methodology for the hydrogenolysis of alkyl halides under mild conditions. *J. Org. Chem.*, *48*(18), 3085-3091.

CHAPTER 6

CONCLUSIONS

Natural products contribute greatly to the discovery of lead compounds for the development of new therapeutically active compounds, representing over one-third of all FDA-approved new molecular entities (NMEs). It is well known that natural sources have been largely studied, in order to search new therapeutic agents, and in particular plants have provided the starting material to develop promising drugs for the treatment of a broad spectrum of diseases. In this context, the main part of the research activity described in my PhD thesis has resulted in the isolation and structural elucidation of new natural products, deriving from Apiaceae plants belonging to Mediterranean and Iranian flora, to evaluate and enhance their pharmacological potential. In particular, the analysis of the polyacetylenic fraction obtained from *Echinophora platyloba* has shown a new interesting modulation of TRPA1 channels, which are involved in the mediation of neuropathic and inflammatory pain. Polyacetylenes have already shown anti-inflammatory effects, mainly related to inhibition of NF-kB or to the modulation of prostaglandin catabolism, but the results obtained from the study reported in my thesis, suggest that modulation of TRPA1 could be another anti-inflammatory mechanism of polyacetylenes worthy of additional studies.

As regards the phytochemical investigation of *Daucus virgatus*, the plant has been a treasure trove of new molecules with different skeletons, mainly belonging to germacranolide-type, a class of natural products never found before in *Daucus* species. The bio-guided fractionation of *D. virgatus* apolar extract has resulted in the isolation of eight new angeloylated germacranolides, showing a promising *Plasmodium* transmission-blocking activity; among all the isolated compounds, daucovirgolide G has displayed the highest antimalarial activity and, remarkable, it has been also lacking in general toxicity against both normal and tumor cell lines. Given the small amounts of daucovirgolide G present in the plant, I spent the last part of my PhD period at University College of Dublin, to start a project aiming to the total synthesis of this antimalarial metabolite. The synthesis is still in progress and it will result in the preparation of the target compound, along with analogues, in order to better understand the unknown mechanism of action at molecular level and to

perform further *in vivo* biological studies. In addition, the total synthesis of daucovirgolide G could support the stereostructure determined for the natural compound, and clarify the relationship between the stereochemistry of the germacranolide core and that of the epoxyangeloyl group present in the side chain. This project paves the way for a prolific collaboration leading to bridge the gap between the natural procuts research and drug discovery. Lastly, the complete phytochemical investigation of *D. virgatus* afforded additional secondary metabolites evaluated for their antiproliferative activity, against three human cell lines, A375 (melanoma), MCF-7 (breast adenocarcinoma), and HACAT (keratinocyte). All the three tested new sesquiterpenoids isolated from the plant showed a significantly higher antiproliferative activity against tumor cell lines compared to that against non-tumor keratinocytes, that is worthy of further investigation. In conclusion, it is important to underline that the research in the natural products field can be considered as a great opportunity to discover new candidates for drug discovery, but also a source of new challenges for organic chemists; indeed, the structural diversity associated to secondary metabolites coming from natural sources, represents an appealing opportunity to devise new synthetic methodologies, which constitute the driving force to develop synthetic routes for the total synthesis of natural products.

CHAPTER 7

SPECTRAL DATA

Spectral data for CHAPTER 3

^{1}H spectrum (500 MHz) of echinophorin D (**1**) in $CDCl_3$

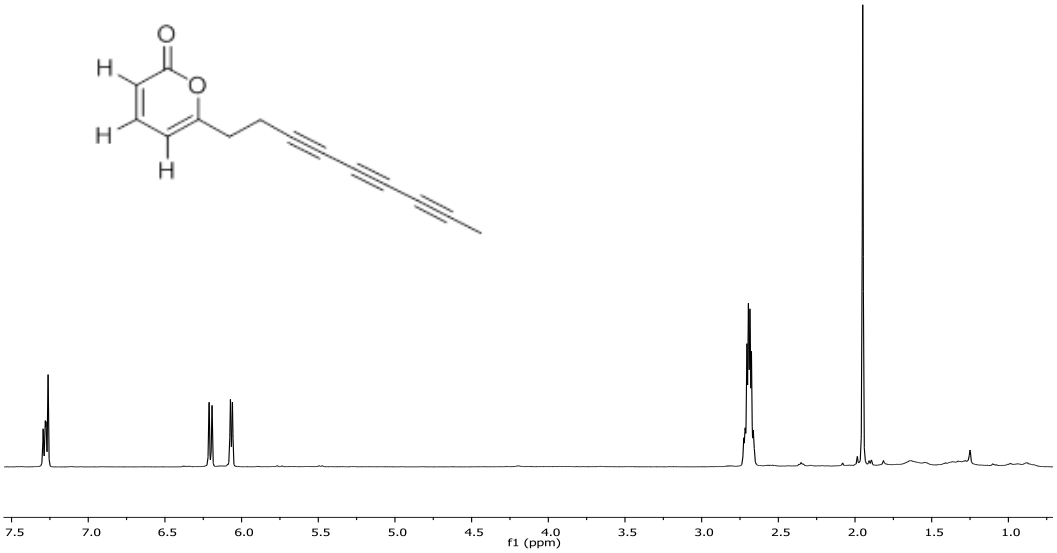

COSY spectrum (500 MHz) of echinophorin D (**1**) in $CDCl_3$

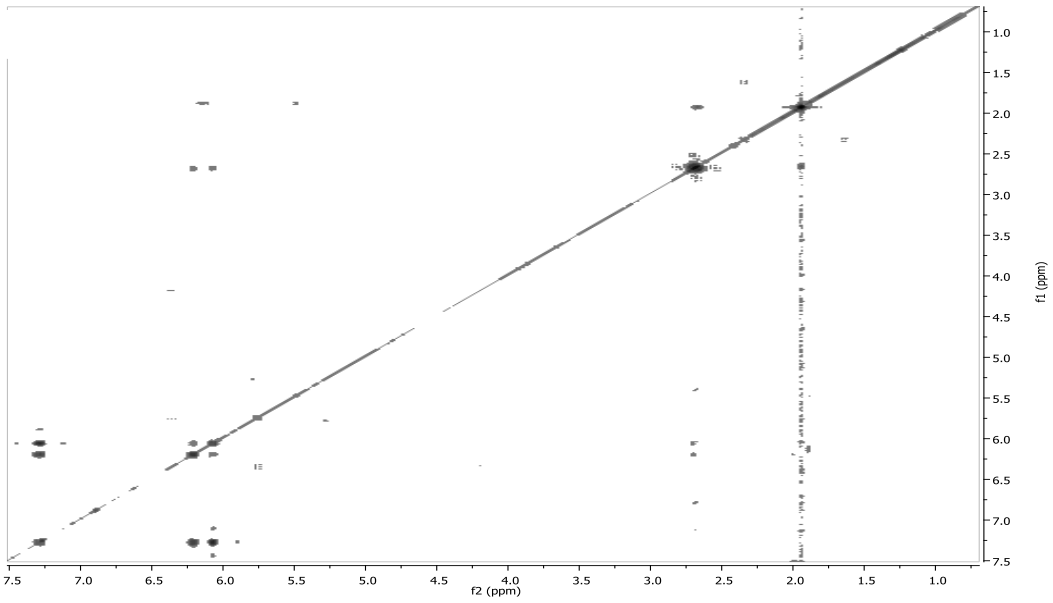

HMBC spectrum (500 MHz) of echinophorin D (**1**) in $CDCl_3$

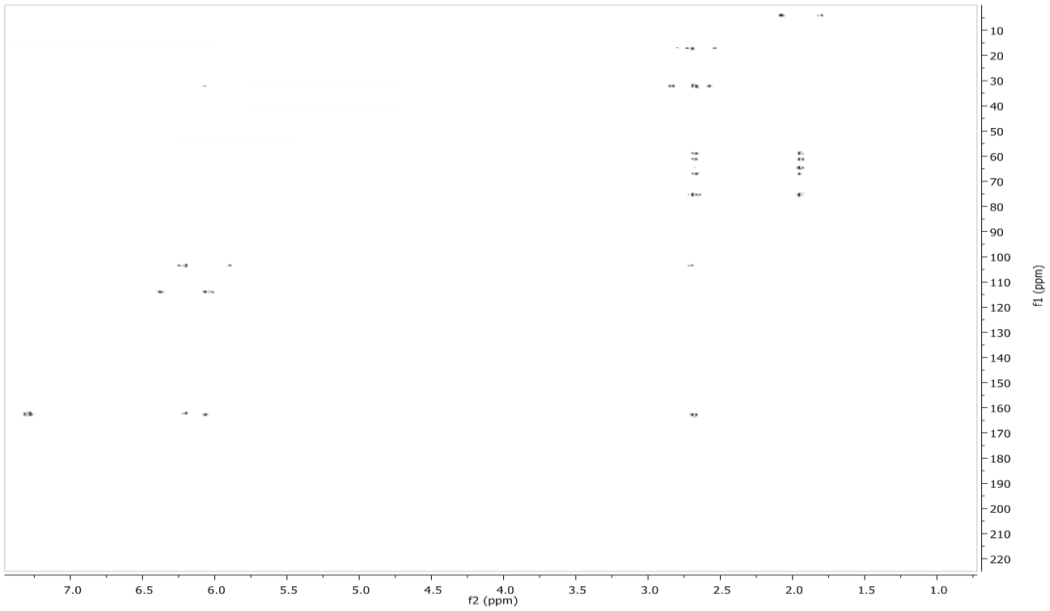

HSQC spectrum (500 MHz) of echinophorin D (**1**) in $CDCl_3$

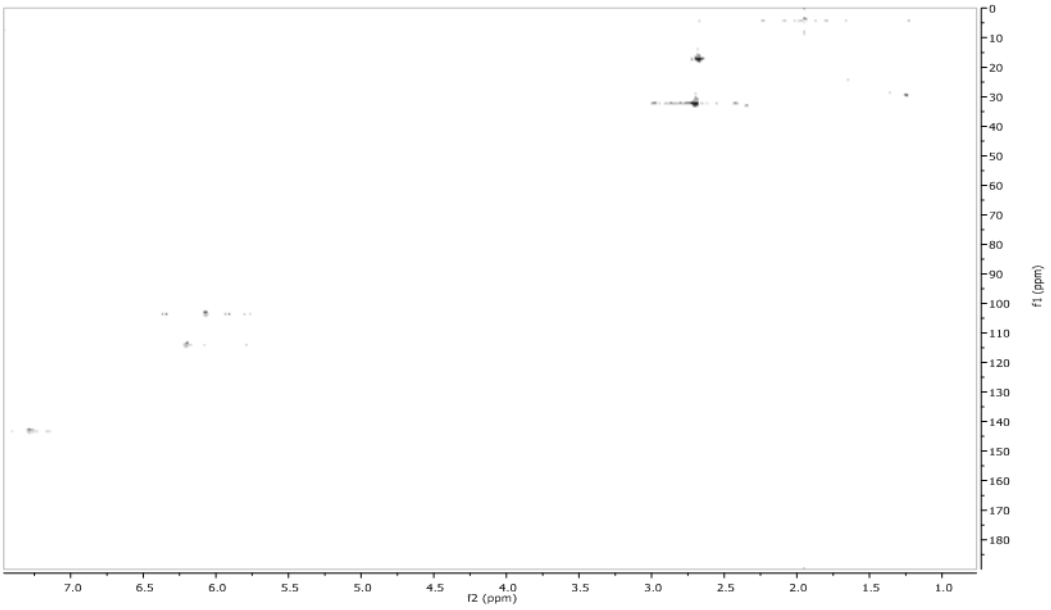

Spectral data for CHAPTER 4

^{1}H spectrum (500 MHz) of daucovirgolide A (**1**) in $CDCl_3$

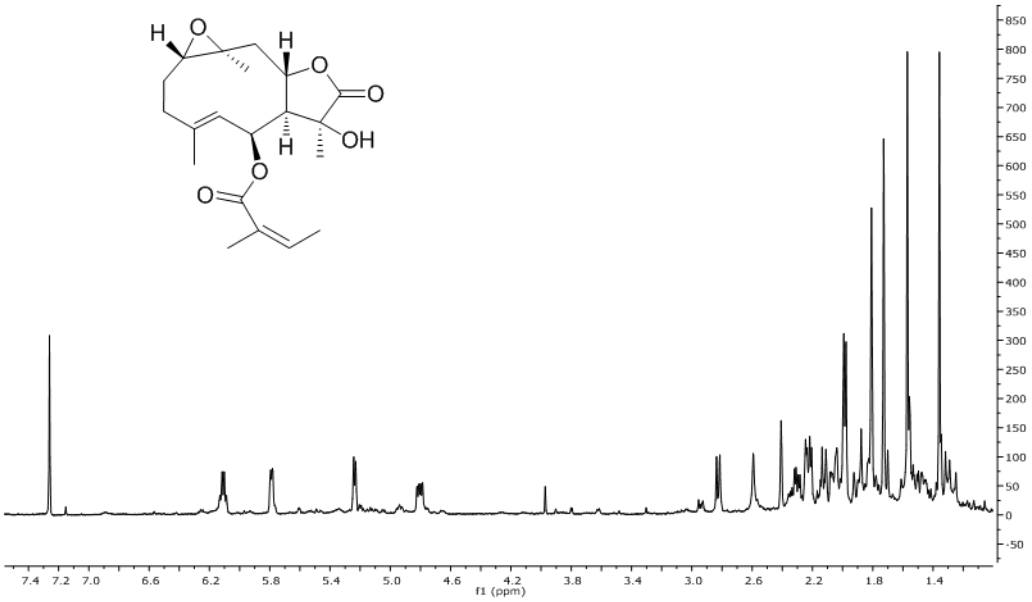

COSY spectrum (500 MHz) of daucovirgolide A (**1**) in $CDCl_3$

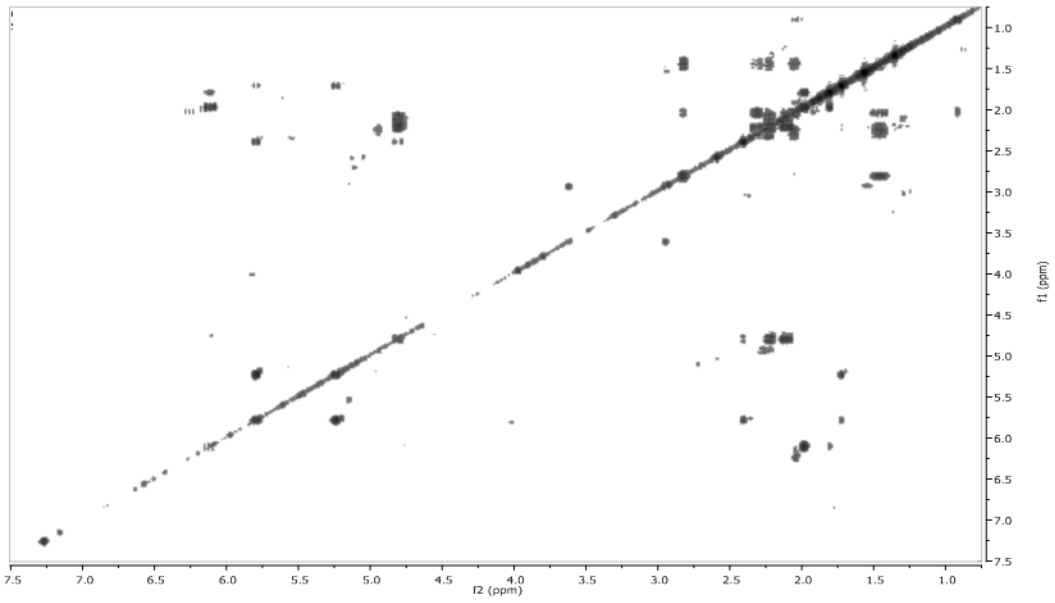

HMBC spectrum (500 MHz) of daucovirgolide A (**1**) in $CDCl_3$

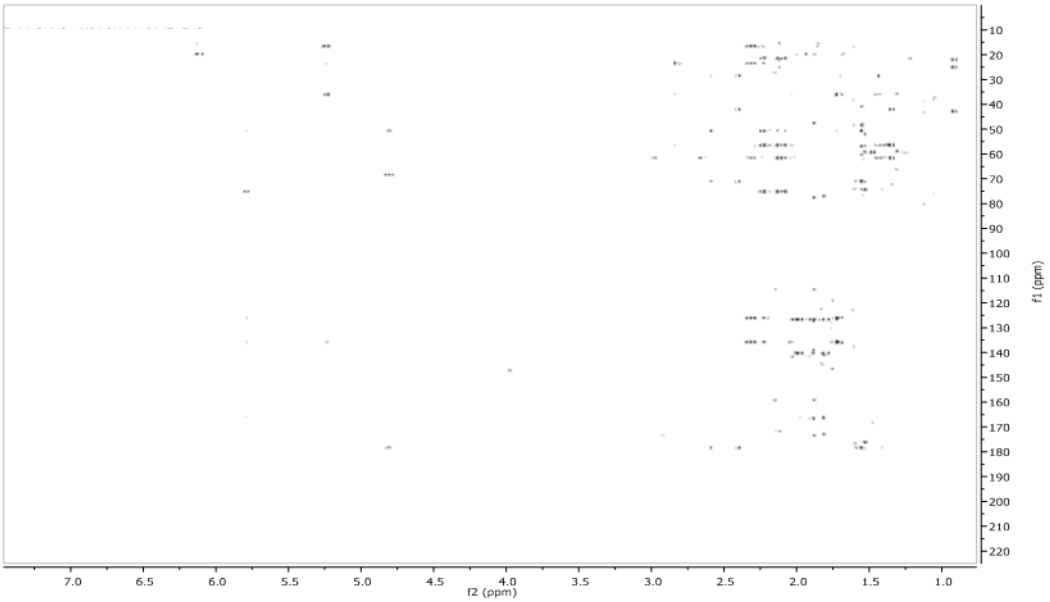

HSQC spectrum (500 MHz) of daucovirgolide A (**1**) in $CDCl_3$

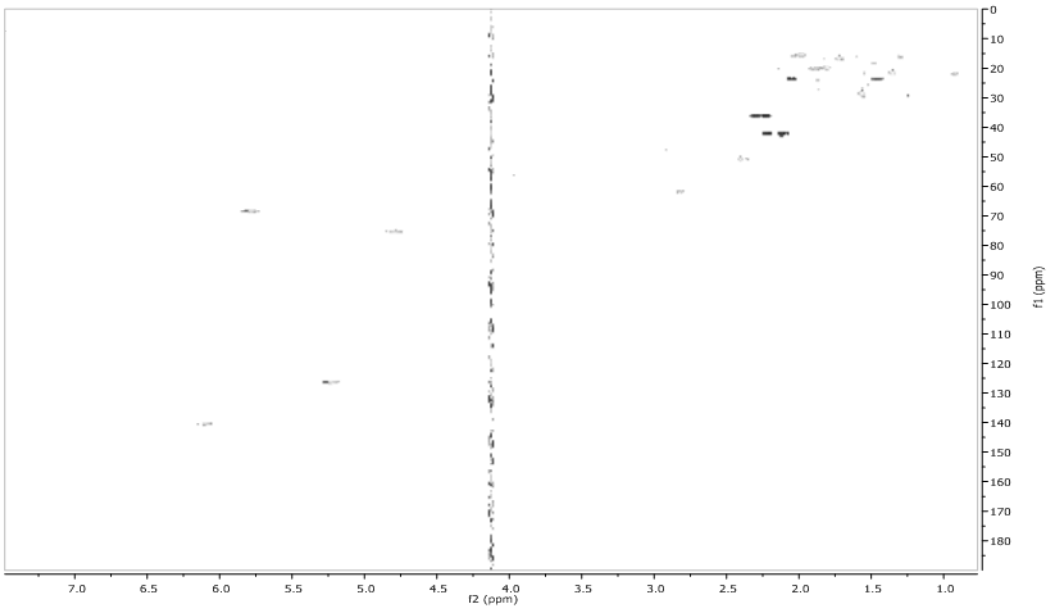

^{1}H spectrum (500 MHz) of daucovirgolide B (**2**) in $CDCl_3$

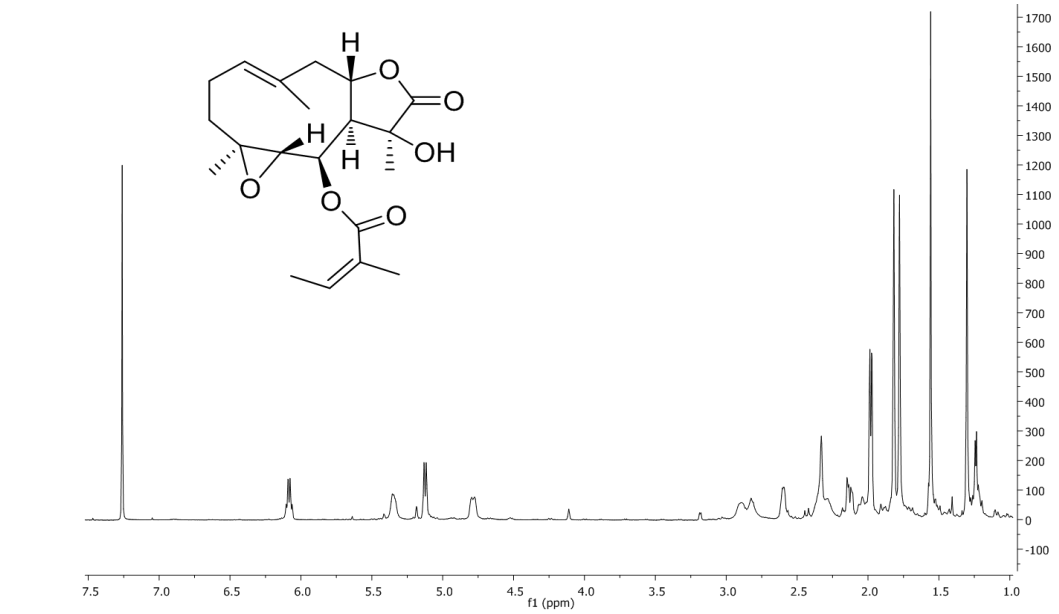

COSY spectrum (500 MHz) of daucovirgolide B (**2**) in $CDCl_3$

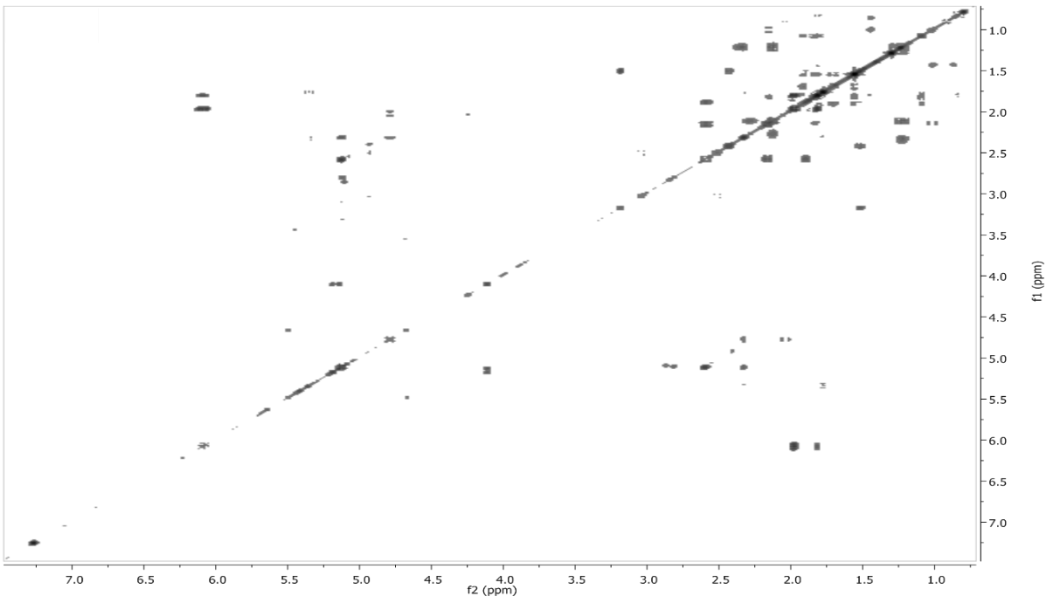

HMBC spectrum (500 MHz) of daucovirgolide B (**2**) in $CDCl_3$

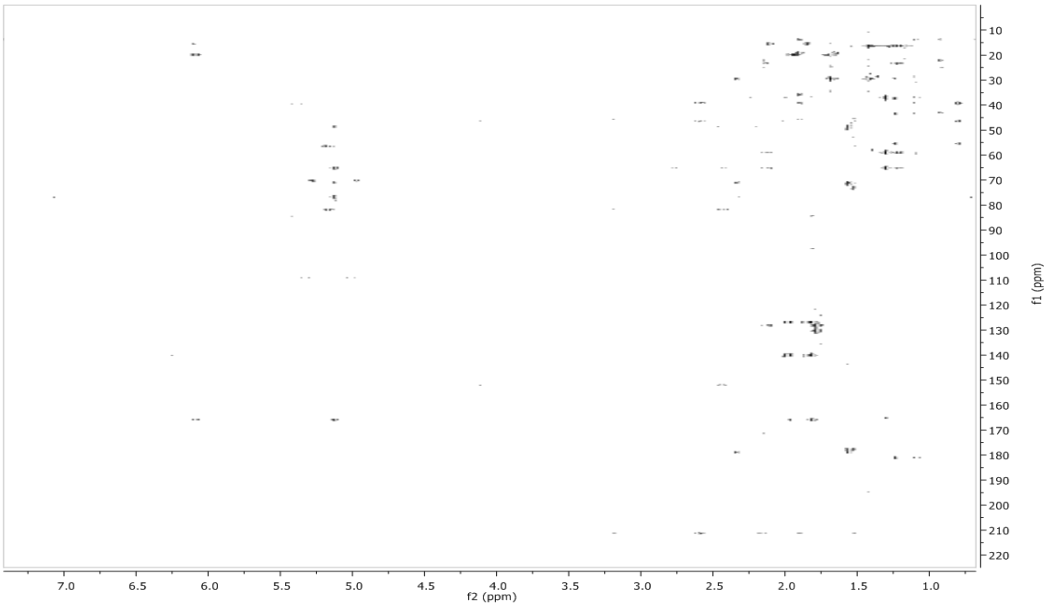

HSQC spectrum (500 MHz) of daucovirgolide B (**2**) in $CDCl_3$

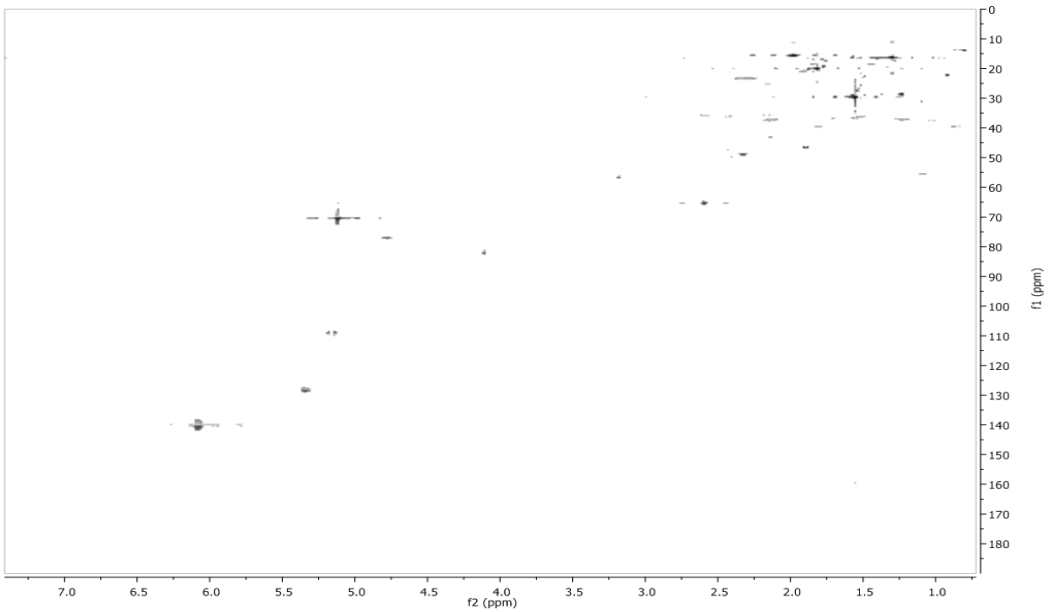

^{1}H spectrum (500 MHz) of daucovirgolide C (**3**) in $CDCl_3$

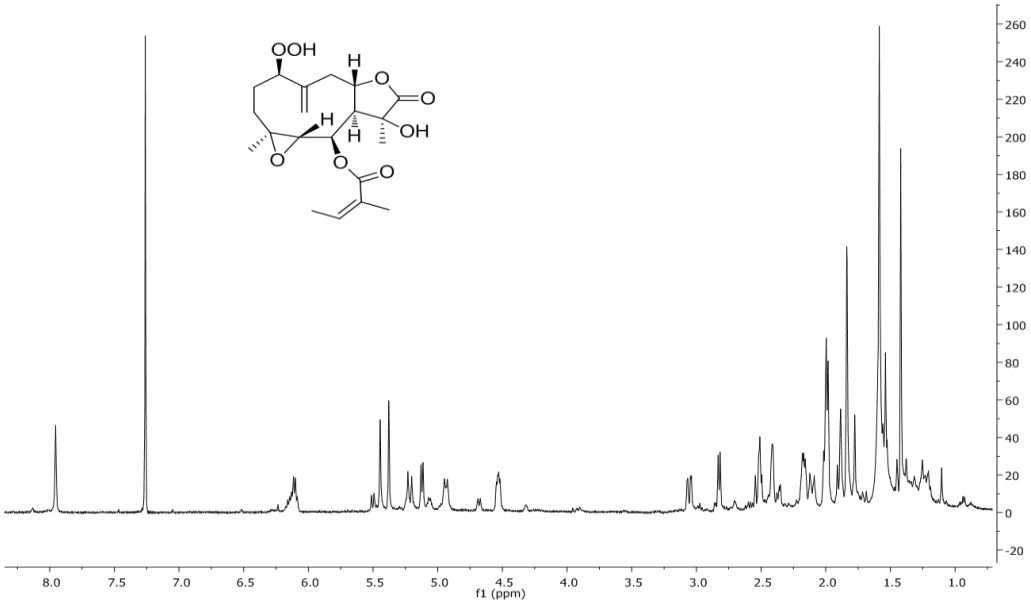

COSY spectrum (500 MHz) of daucovirgolide C (**3**) in $CDCl_3$

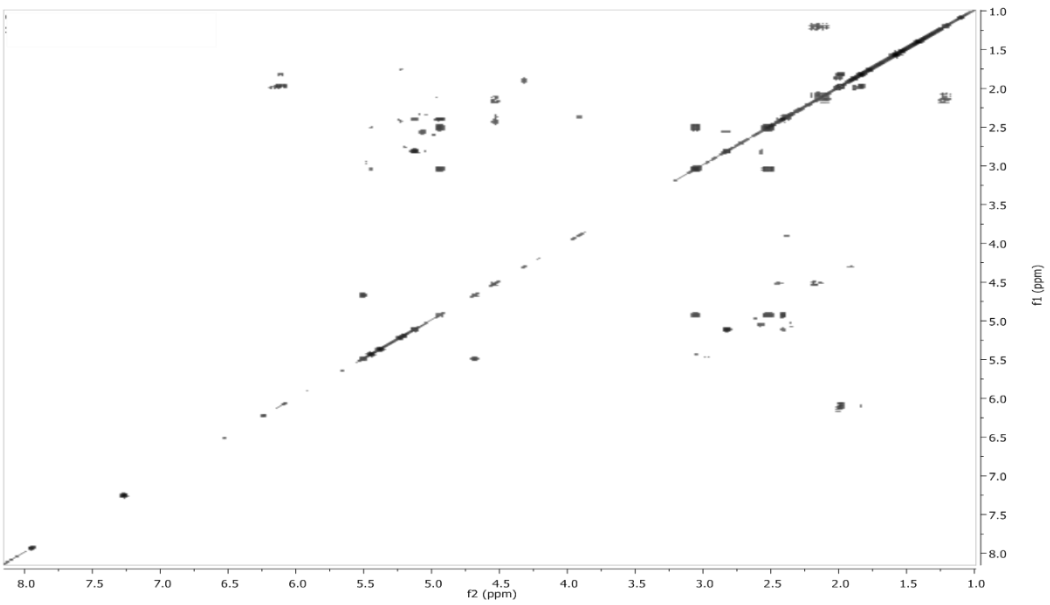

HMBC spectrum (500 MHz) of daucovirgolide C (**3**) in $CDCl_3$

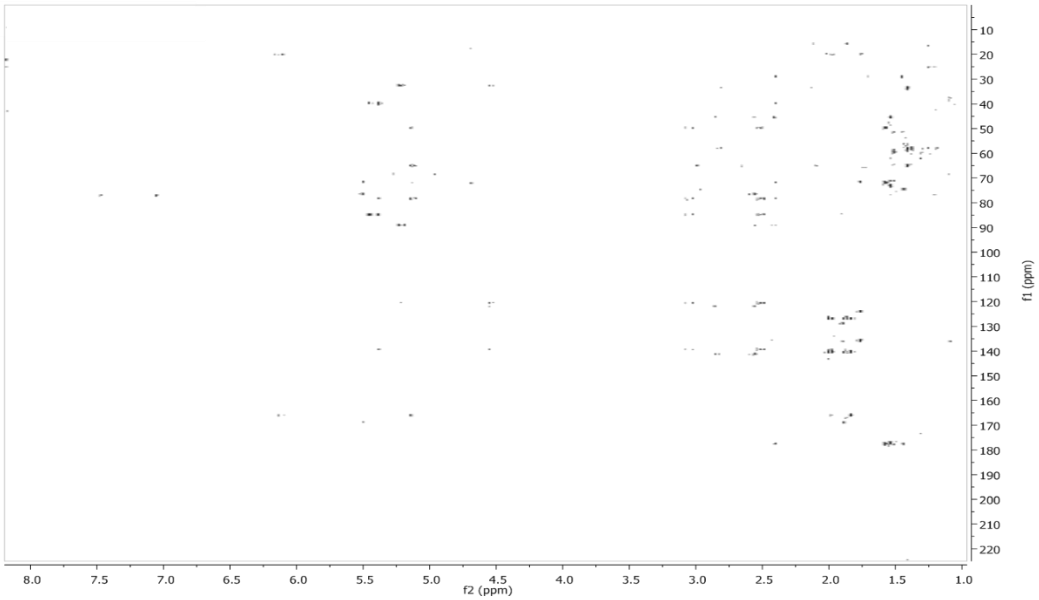

HSQC spectrum (500 MHz) of daucovirgolide C (**3**) in $CDCl_3$

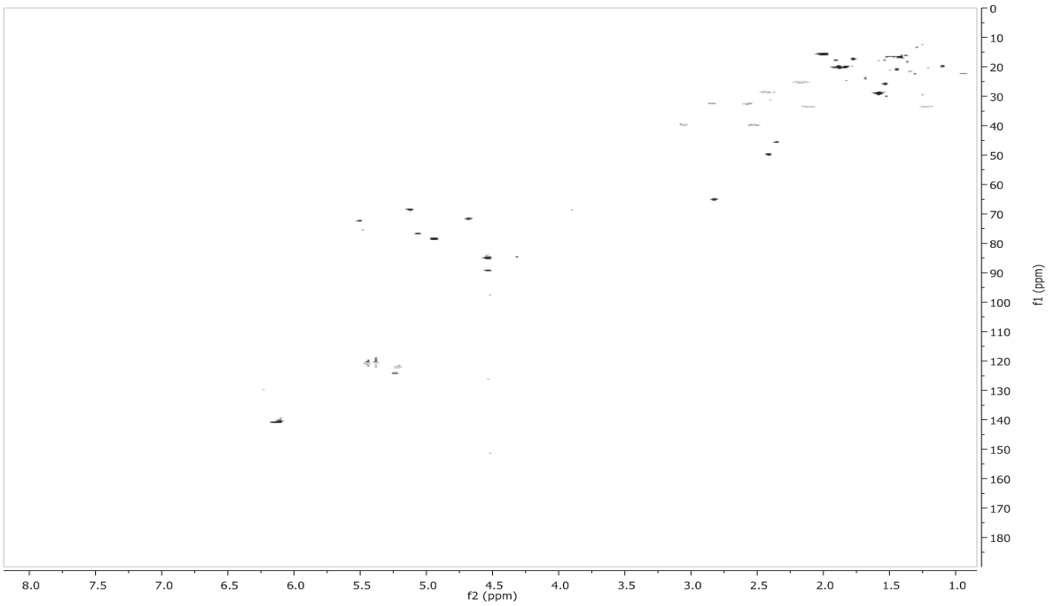

ROESY spectrum (500 MHz) of daucovirgolide C (**3**) in $CDCl_3$

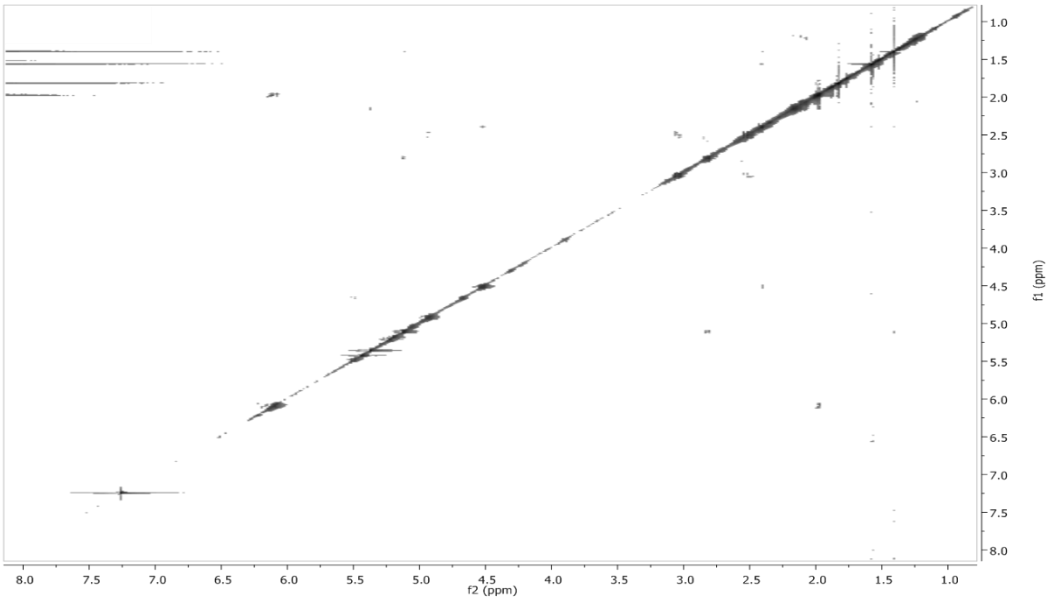

^1H spectrum (500 MHz) of daucovirgolide D (**4**) in $CDCl_3$

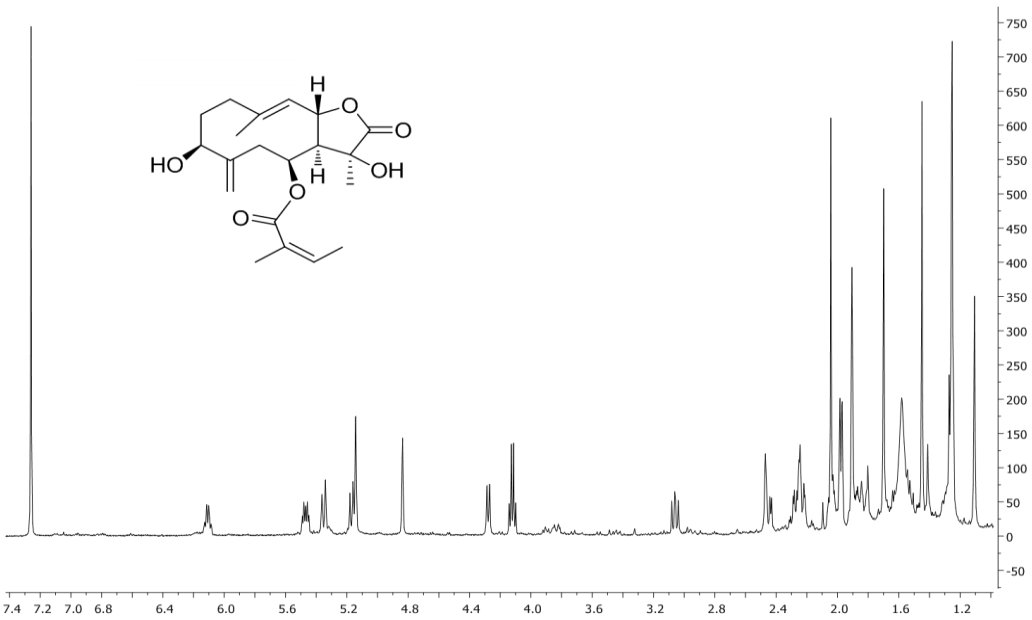

COSY spectrum (500 MHz) of daucovirgolide D (**4**) in $CDCl_3$

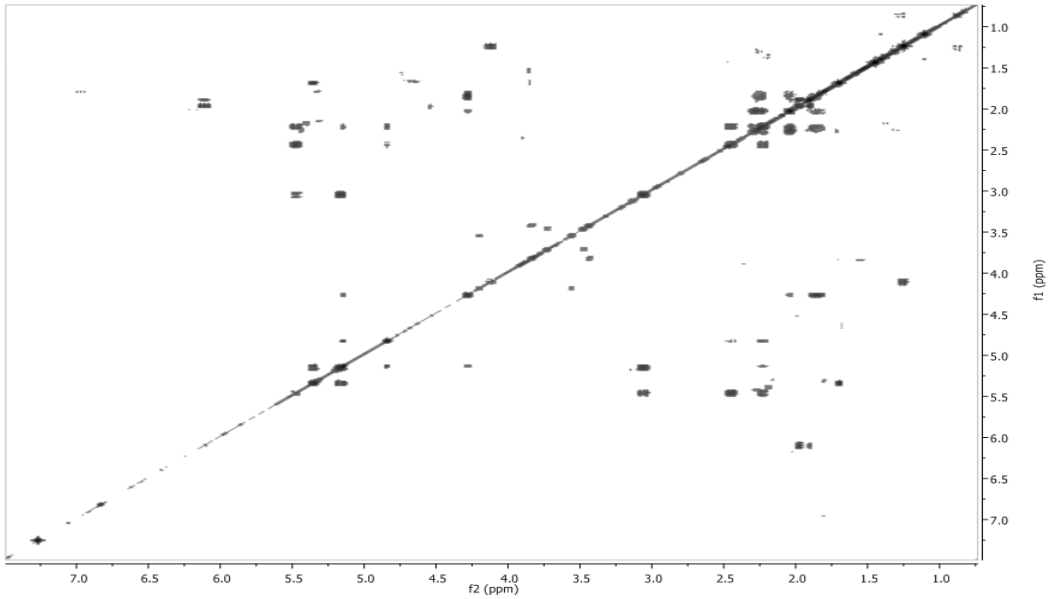

HMBC spectrum (500 MHz) of daucovirgolide D (**4**) in $CDCl_3$

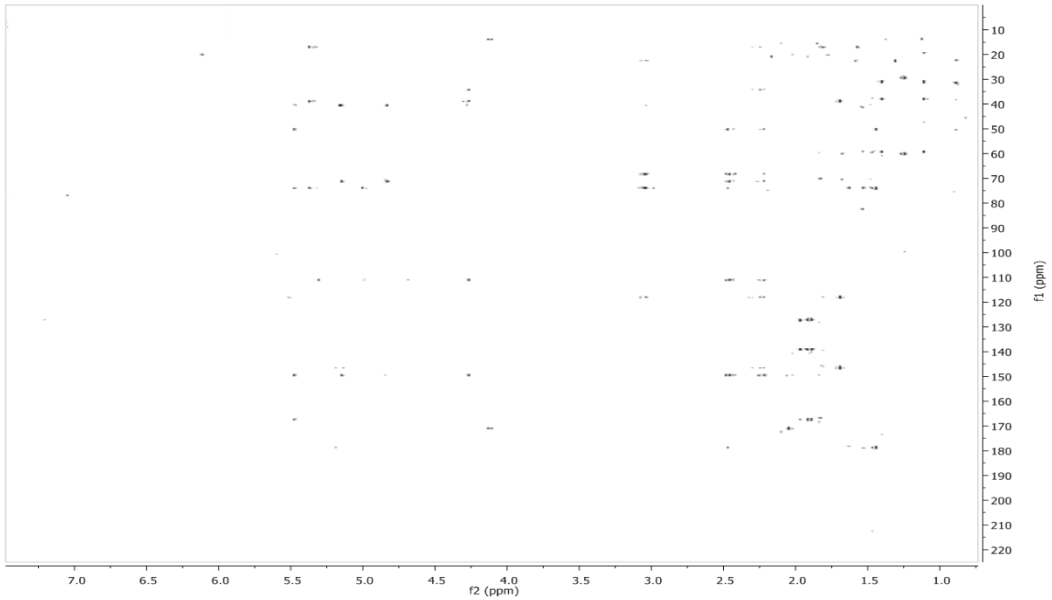

HSQC spectrum (500 MHz) of daucovirgolide D (**4**) in $CDCl_3$

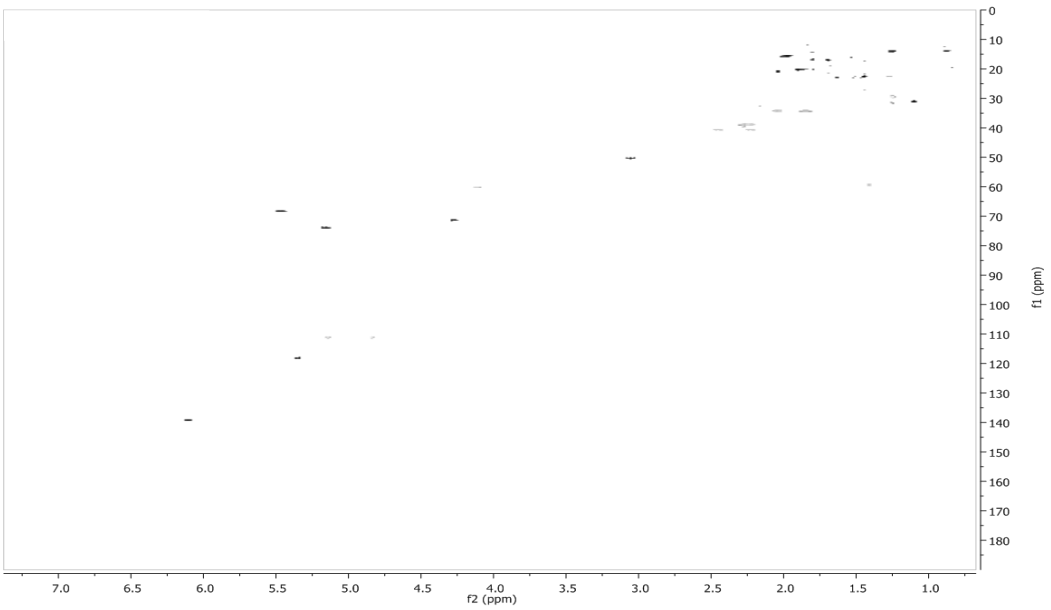

^1H spectrum (500 MHz) of daucovirgolide E (**5**) in $CDCl_3$

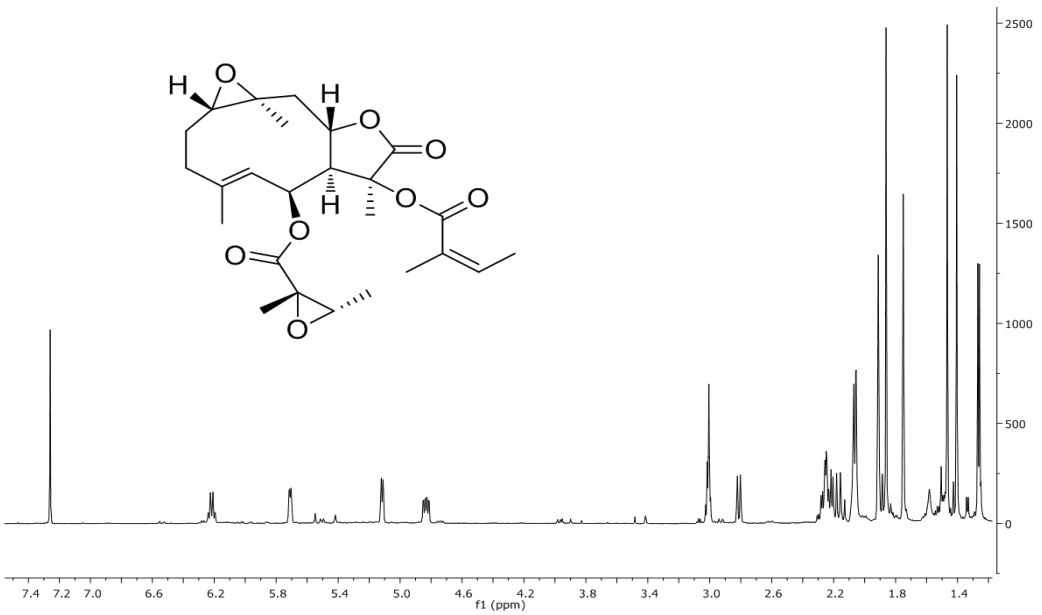

COSY spectrum (500 MHz) of daucovirgolide E (**5**) in $CDCl_3$

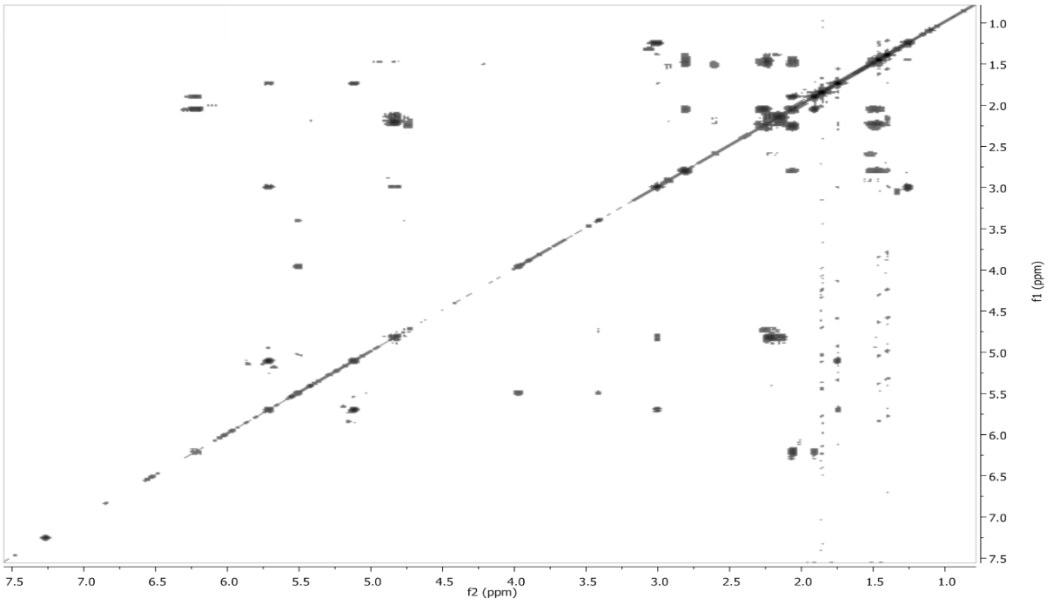

HMBC spectrum (500 MHz) of daucovirgolide E (**5**) in $CDCl_3$

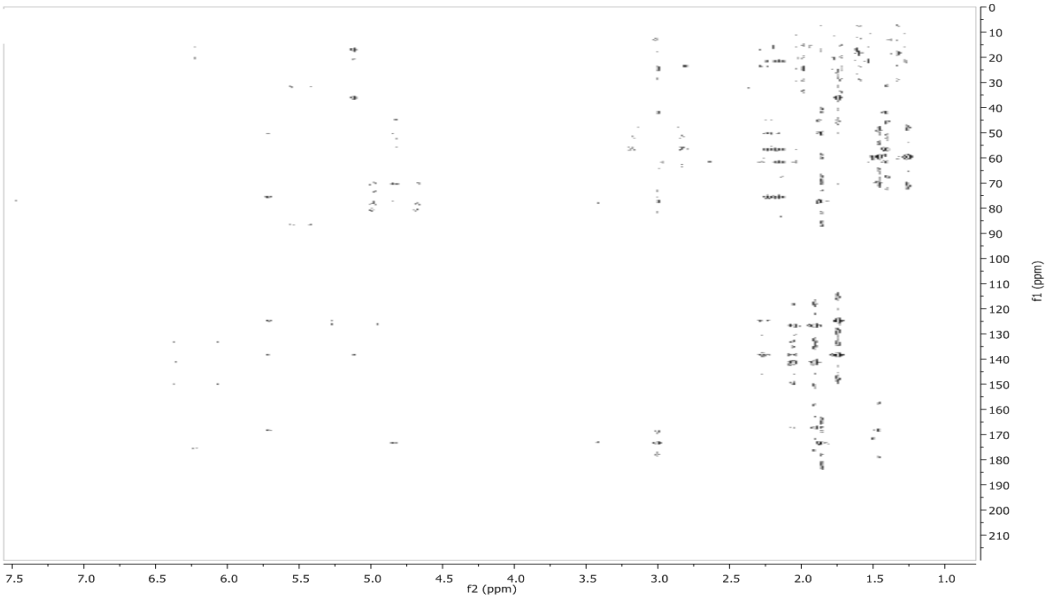

HSQC spectrum (500 MHz) of daucovirgolide E (**5**) in $CDCl_3$

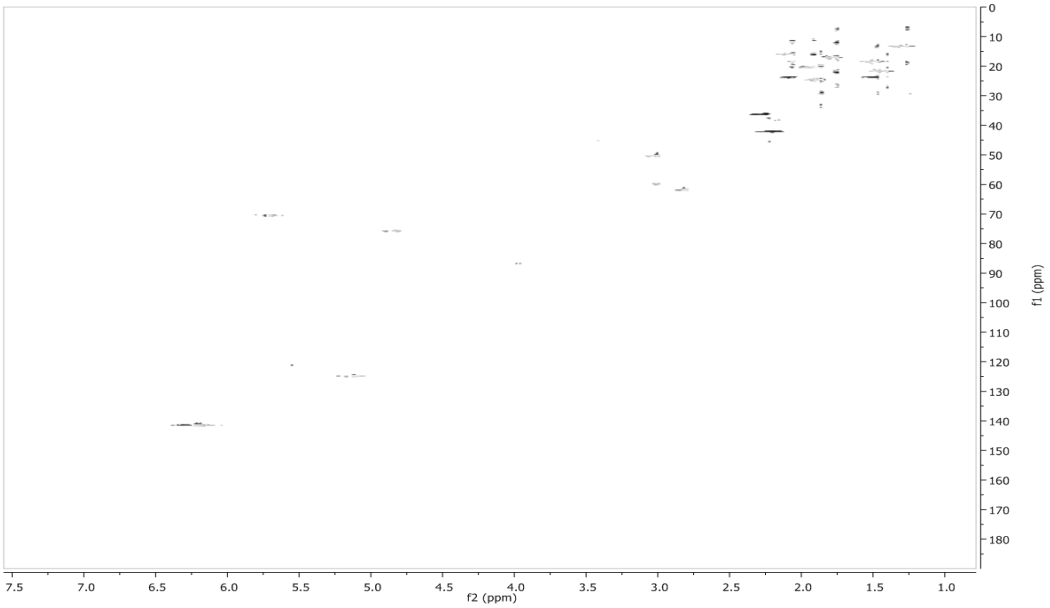

ROESY spectrum (500 MHz) of daucovirgolide E (**5**) in $CDCl_3$

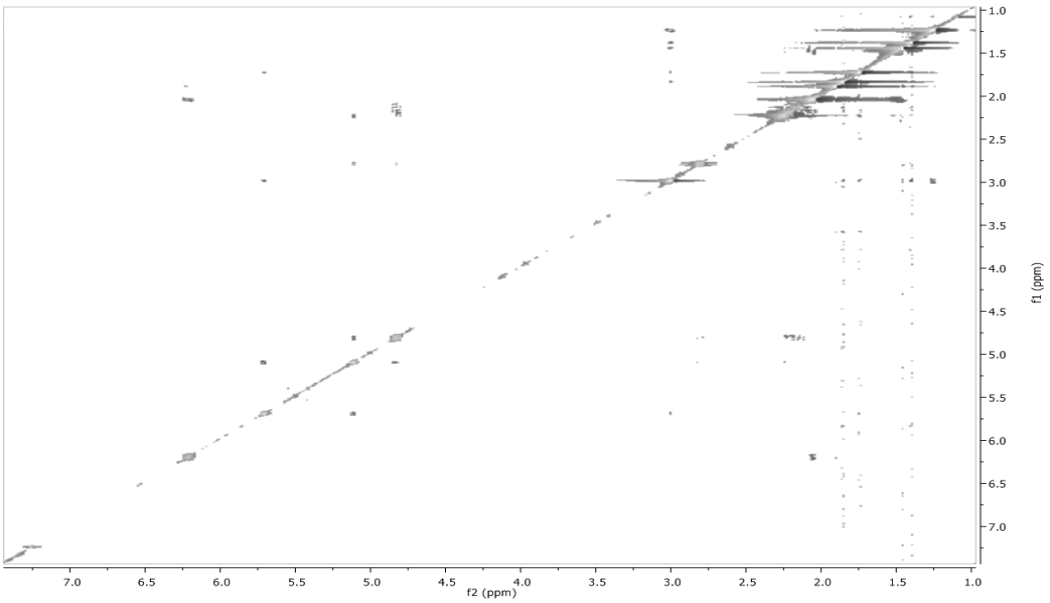

^{1}H spectrum (500 MHz) of daucovirgolide F (**6**) in $CDCl_3$

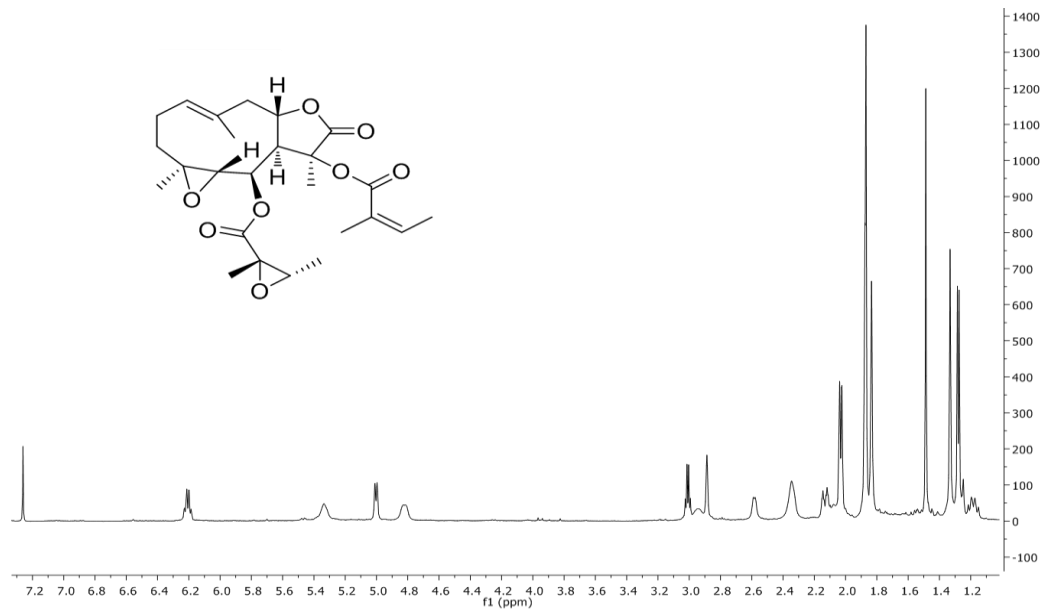

COSY spectrum (500 MHz) of daucovirgolide F (**6**) in $CDCl_3$

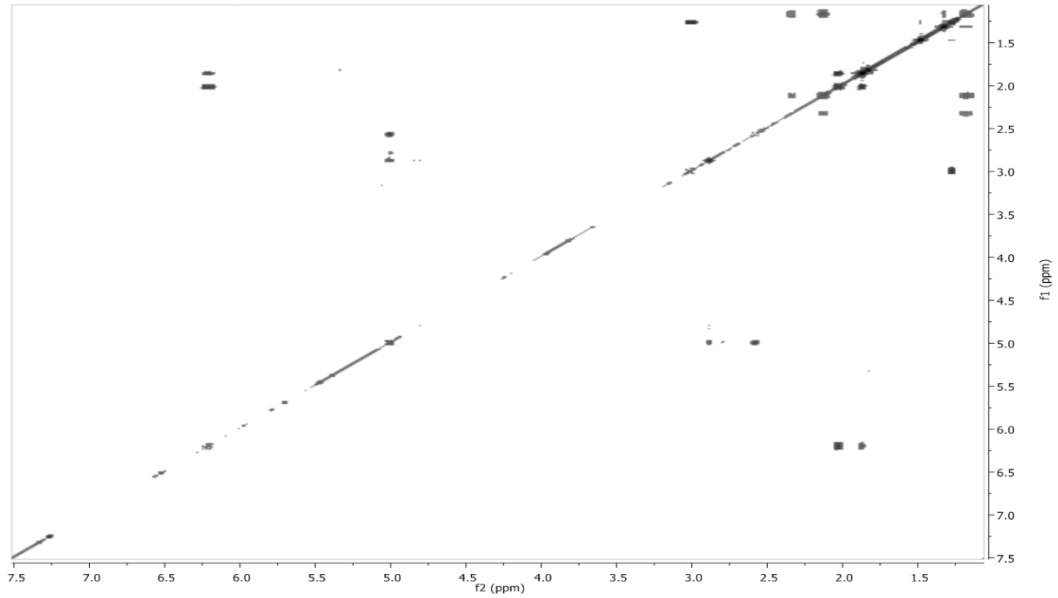

HMBC spectrum (500 MHz) of daucovirgolide F (**6**) in $CDCl_3$

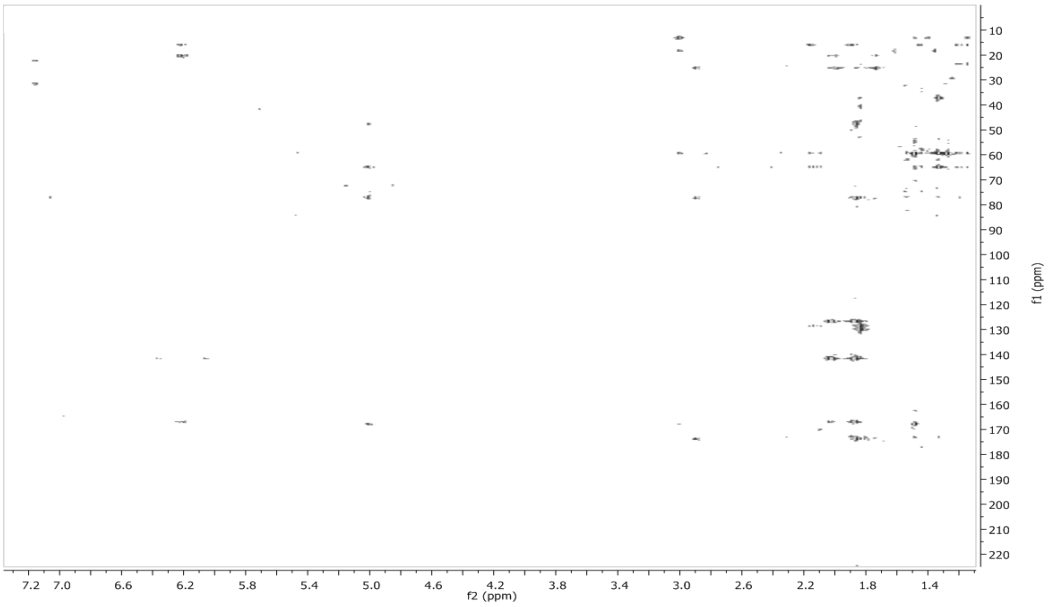

HSQC spectrum (500 MHz) of daucovirgolide F (**6**) in $CDCl_3$

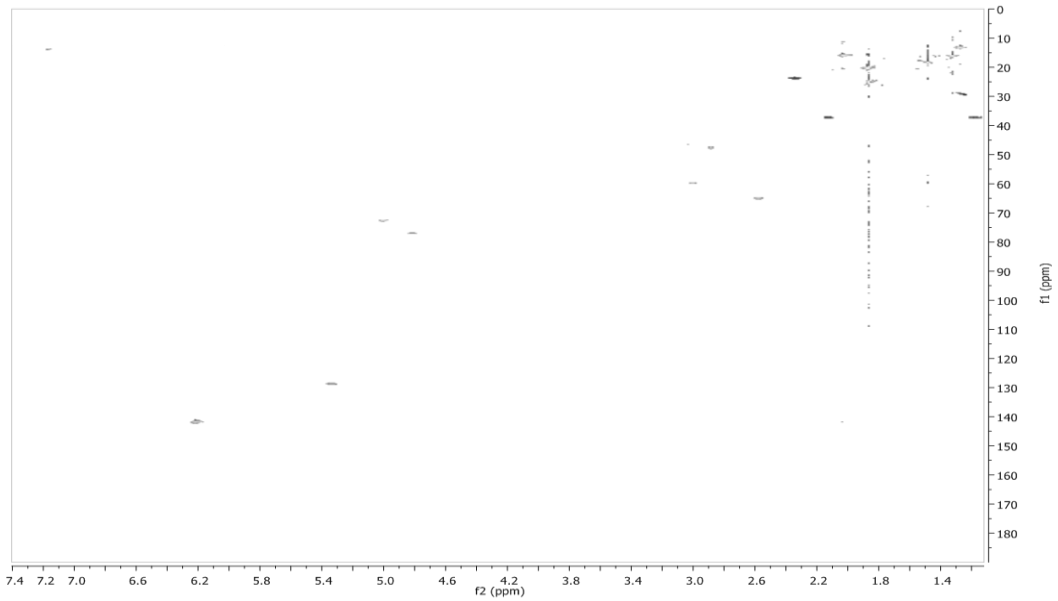

ROESY spectrum (500 MHz) of daucovirgolide F (**6**) in $CDCl_3$

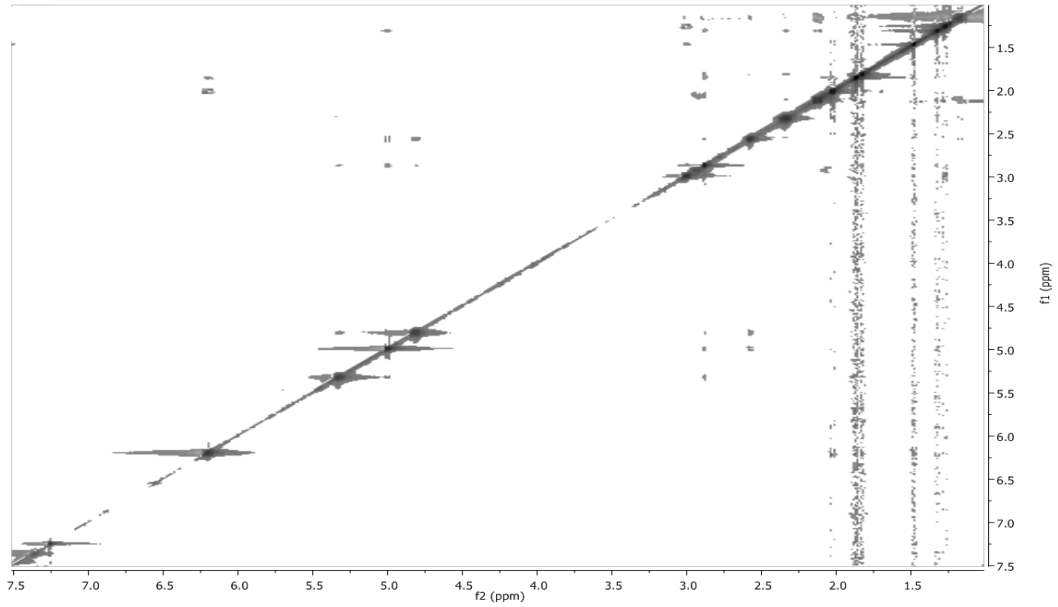

^1H spectrum (500 MHz) of daucovirgolide G (**7**) in $CDCl_3$

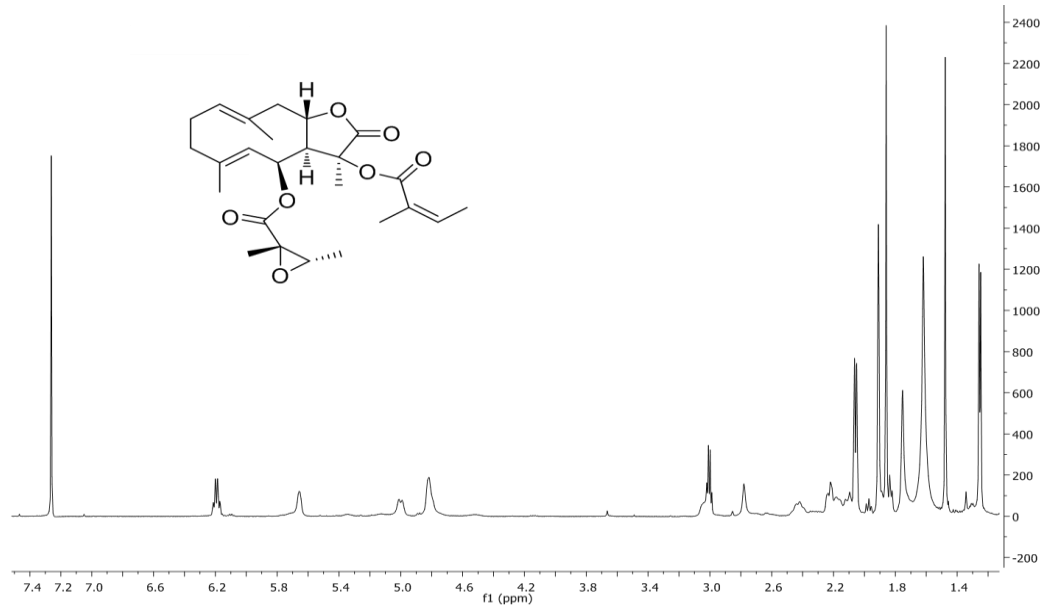

COSY spectrum (500 MHz) of daucovirgolide G (**7**) in $CDCl_3$

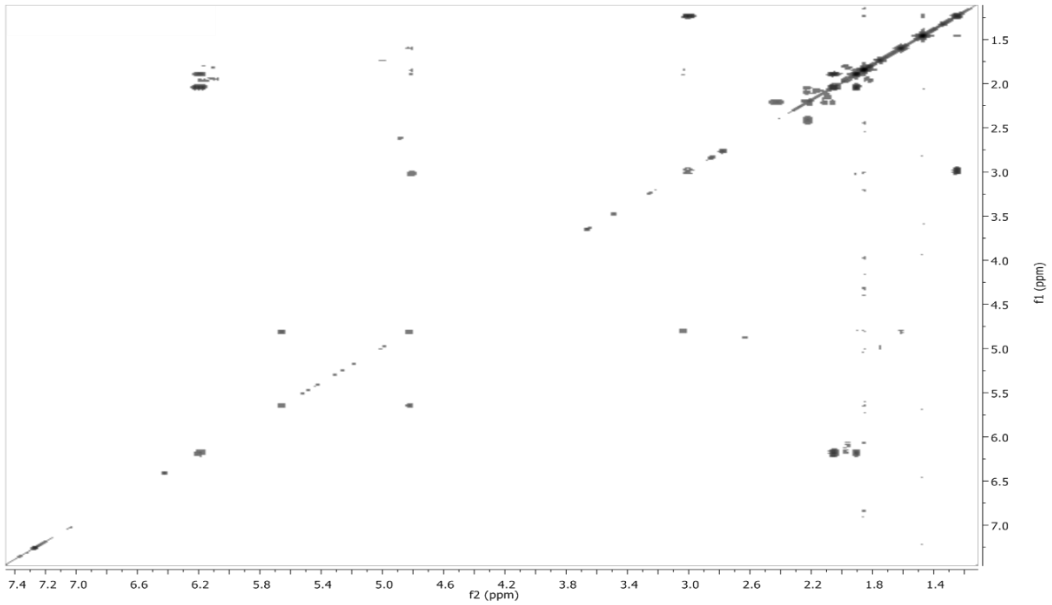

HSQC spectrum (500 MHz) of daucovirgolide G (**7**) in $CDCl_3$

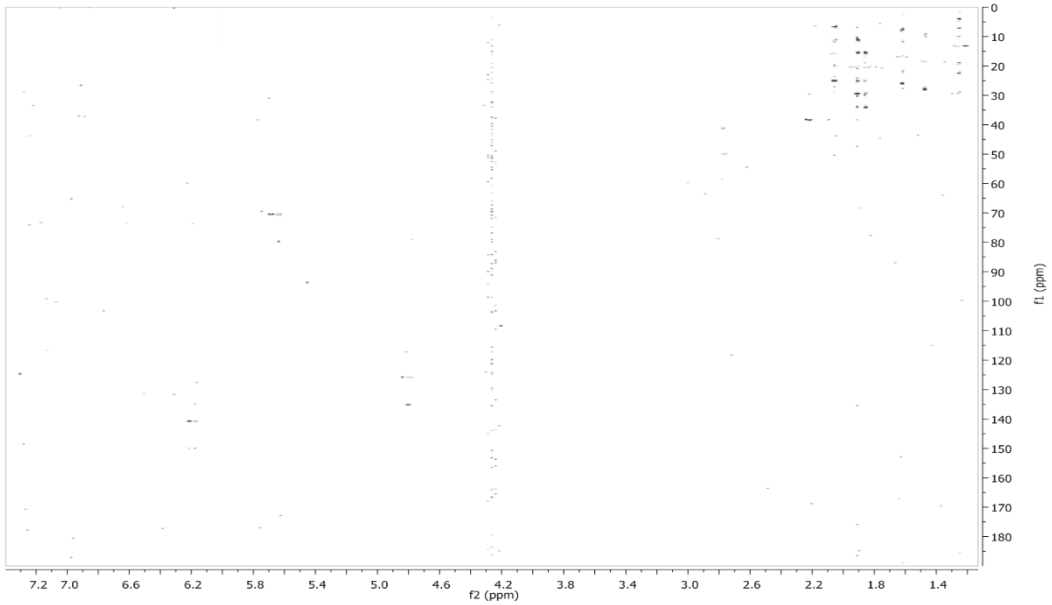

^{1}H spectrum (500 MHz) of daucovirgolide H (**8**) in $CDCl_3$

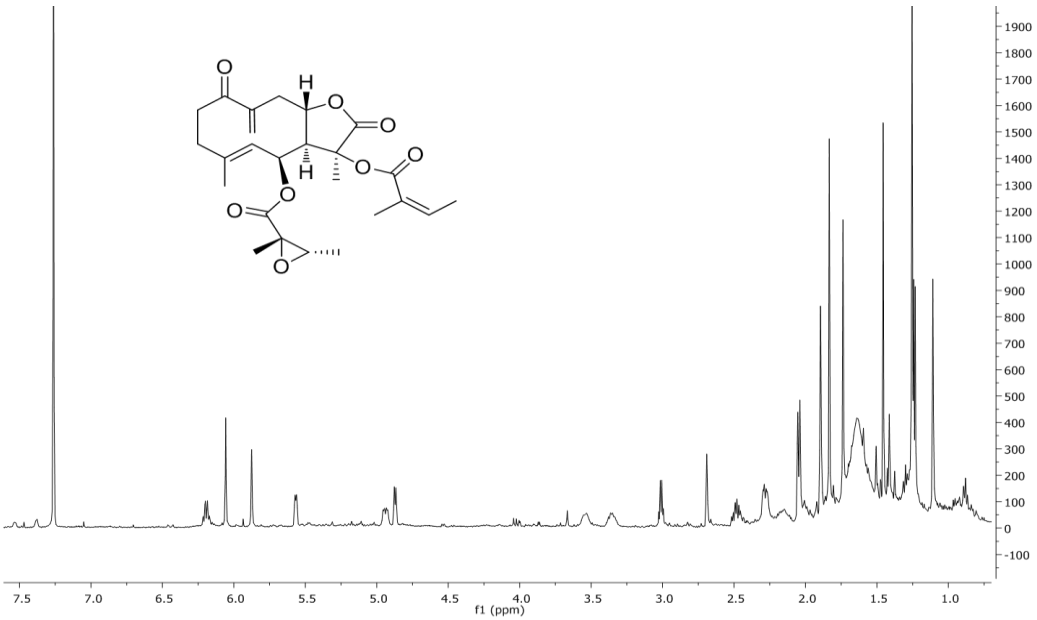

COSY spectrum (500 MHz) of daucovirgolide H (**8**) in $CDCl_3$

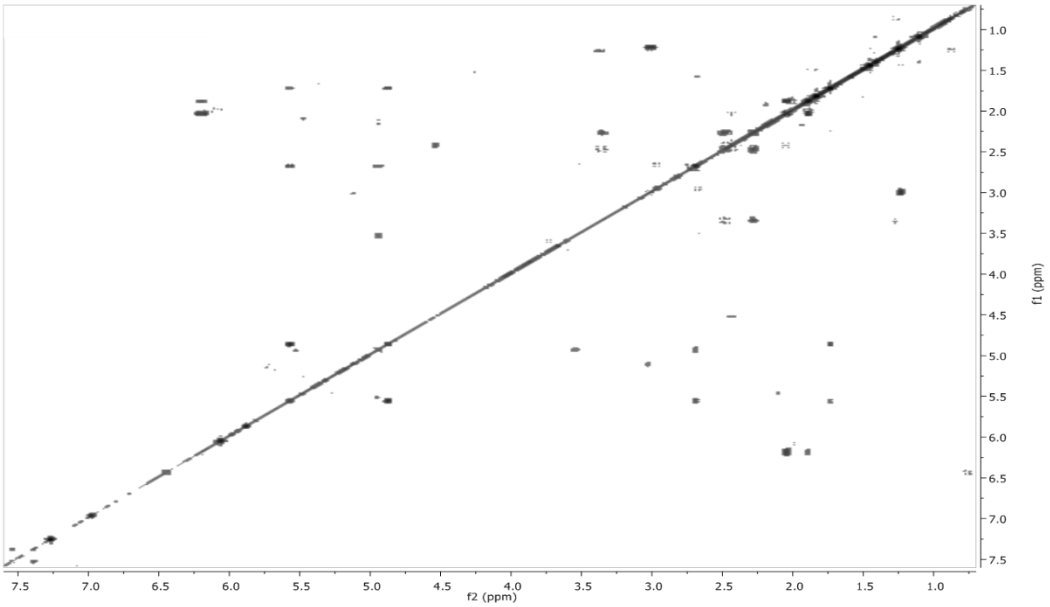

HMBC spectrum (500 MHz) of daucovirgolide H (**8**) in $CDCl_3$

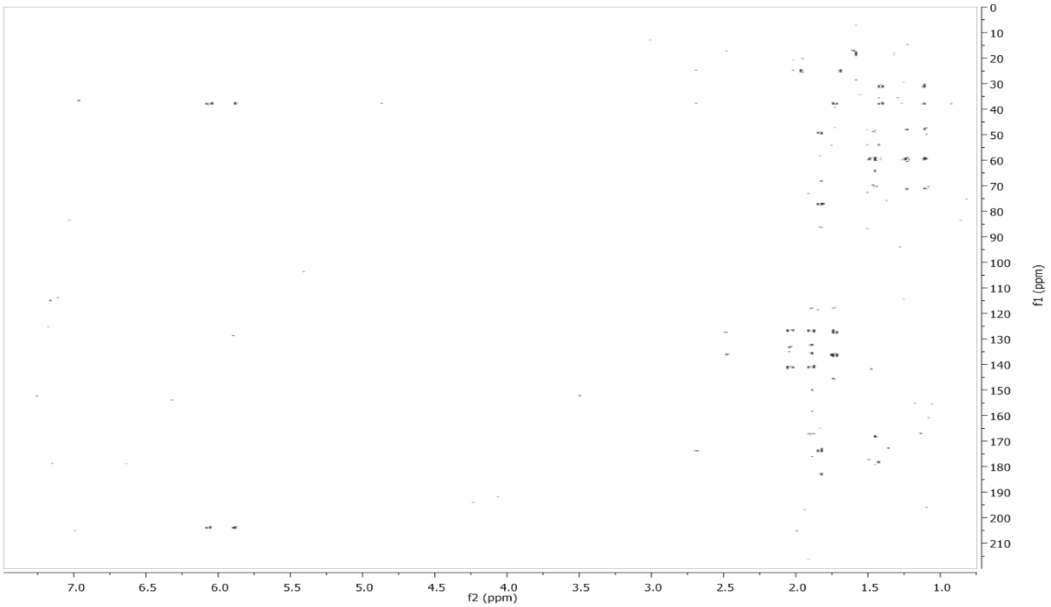

^1H spectrum (500 MHz) of vaginatin B (**14**) in $CDCl_3$

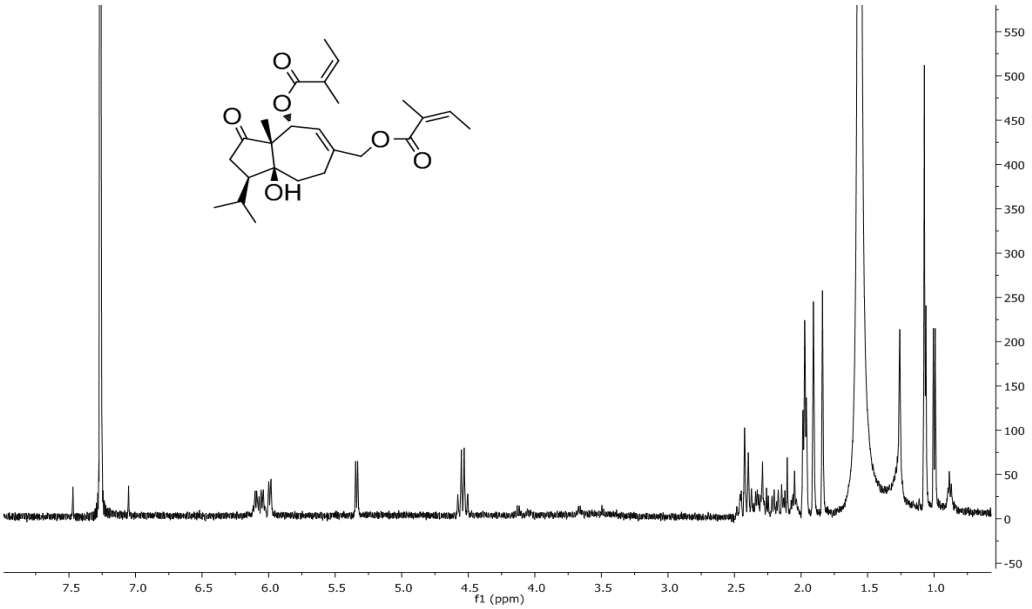

COSY spectrum (500 MHz) of Vaginatin B (**14**) in $CDCl_3$

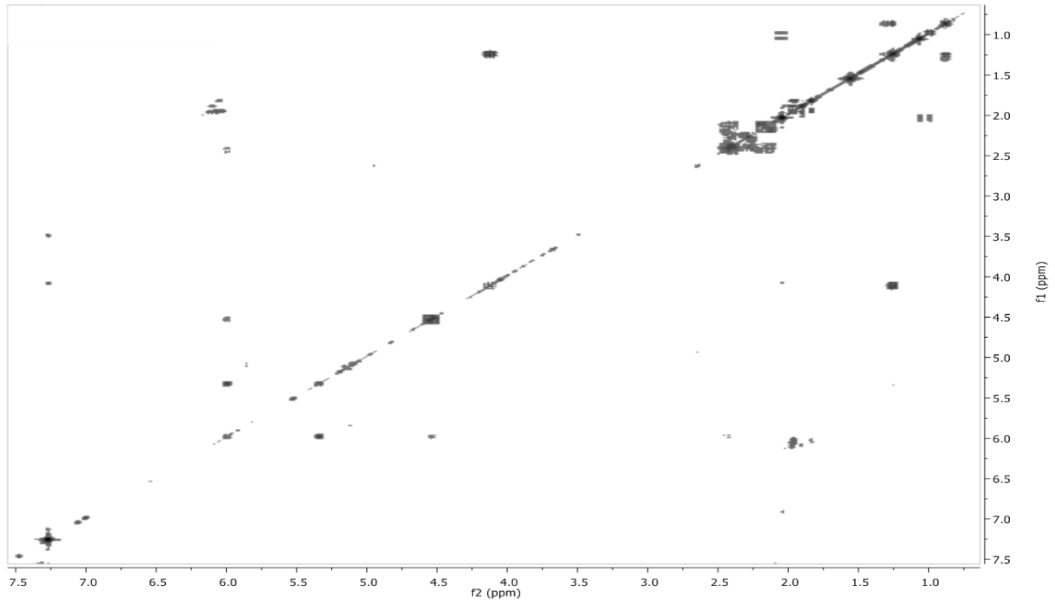

^1H spectrum (500 MHz) of compound (**15**) in $CDCl_3$

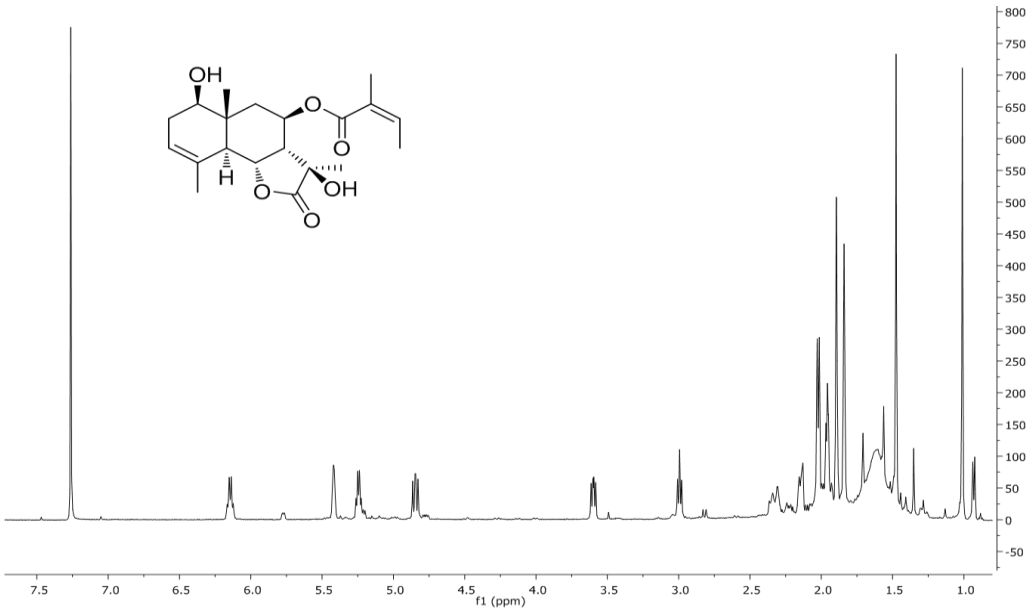

COSY spectrum (500 MHz) of compound (**15**) in $CDCl_3$

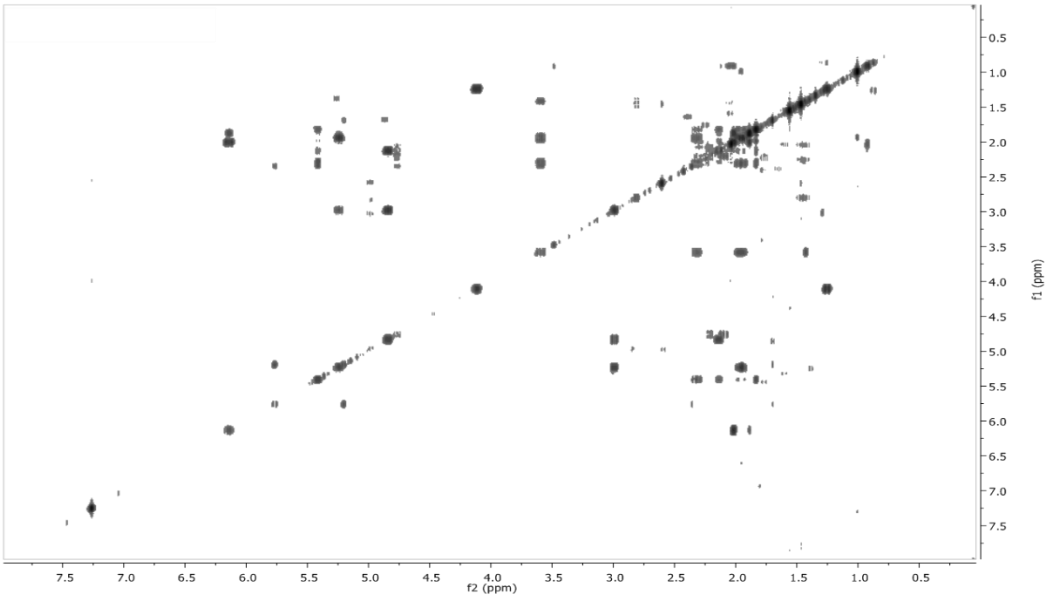

HMBC spectrum (500 MHz) of compound (**15**) in $CDCl_3$

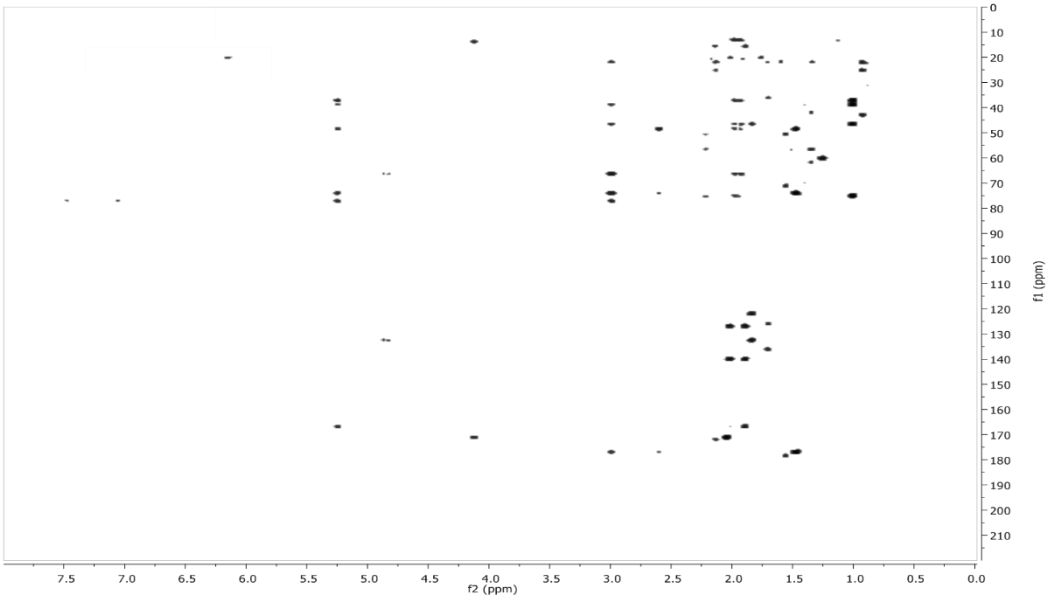

HSQC spectrum (500 MHz) of compound (**15**) in CDCl3

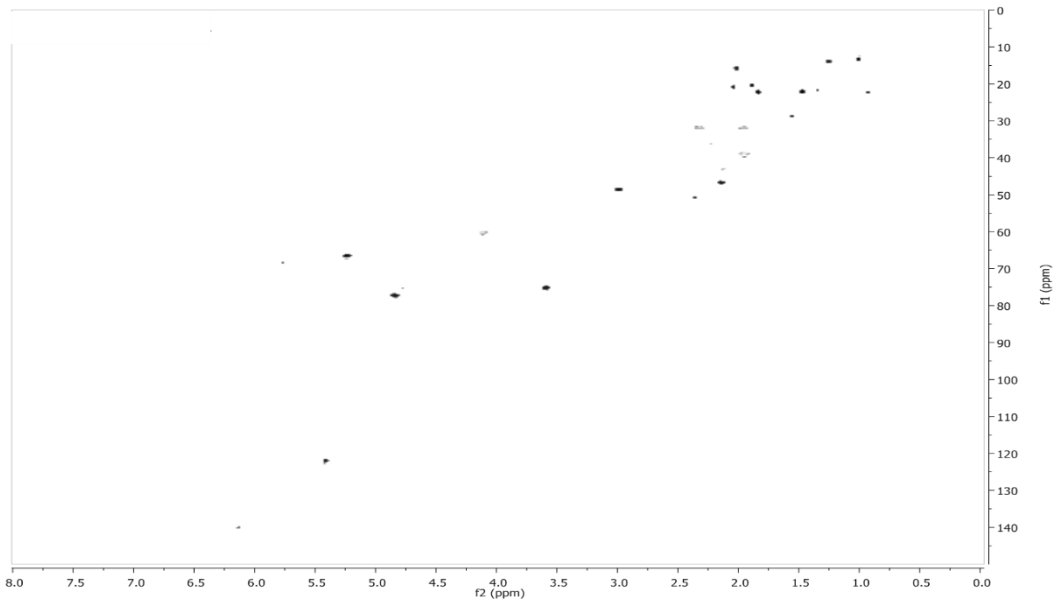

ROESY spectrum (500 MHz) of compound (**15**) in $CDCl_3$

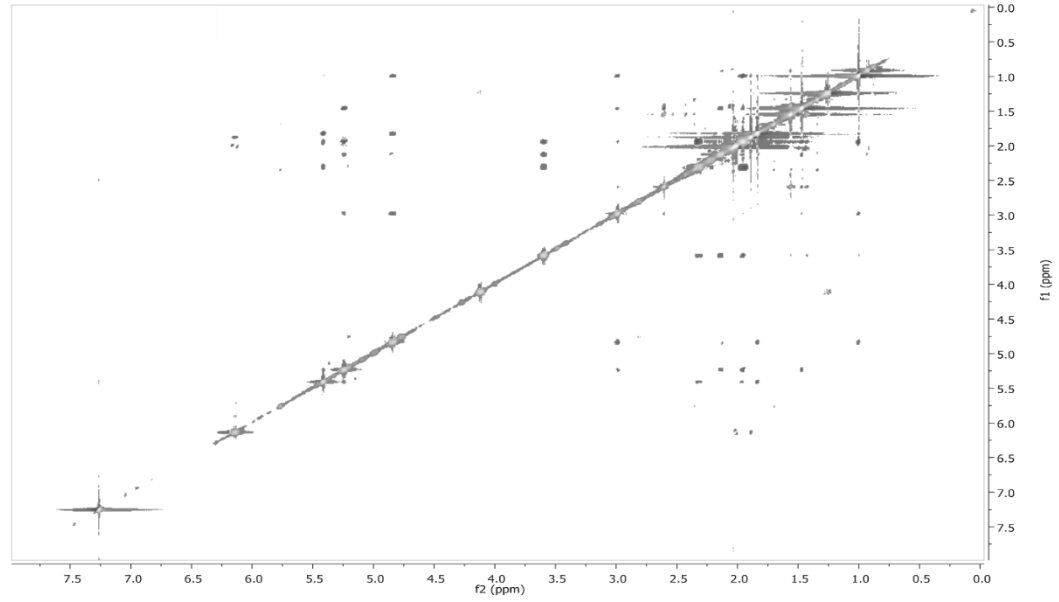

^{1}H spectrum (500 MHz) of elemavirgolide (**16**) in $CDCl_3$

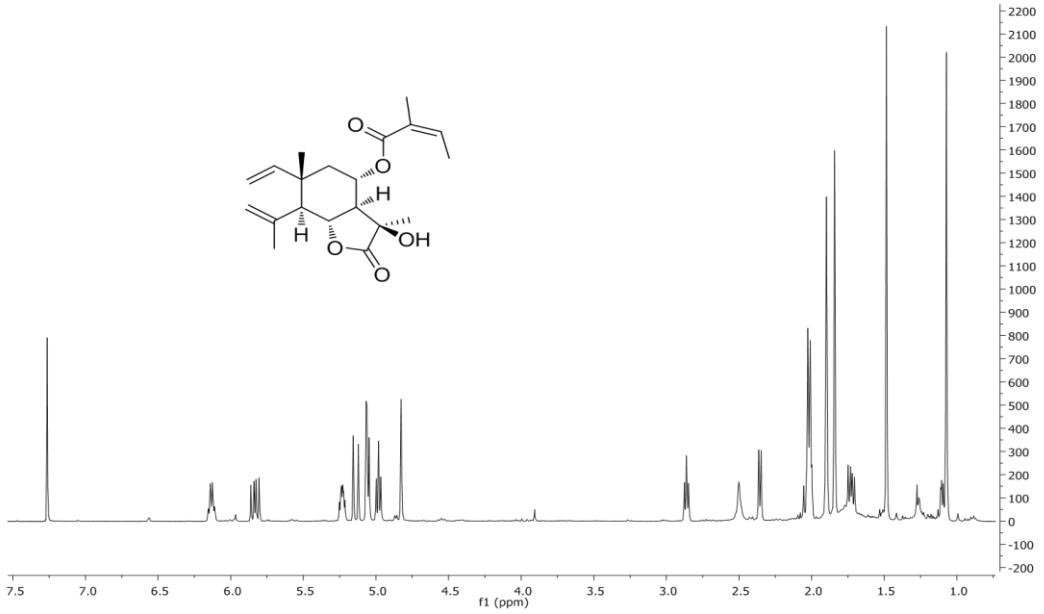

COSY spectrum (500 MHz) of elemavirgolide (**16**) in $CDCl_3$

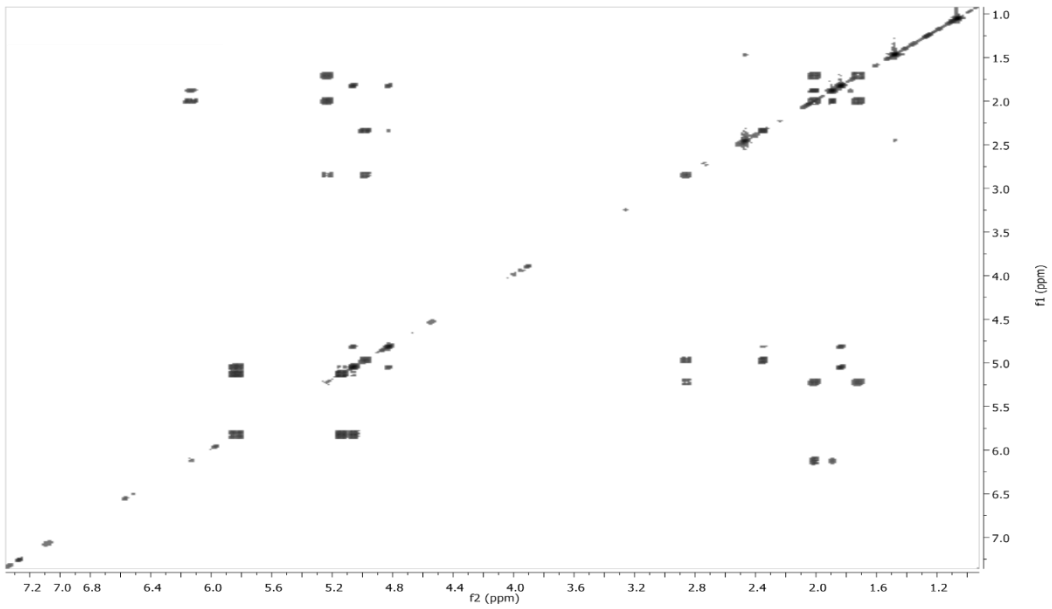

HMBC spectrum (500 MHz) of elemavirgolide (**16**) in $CDCl_3$

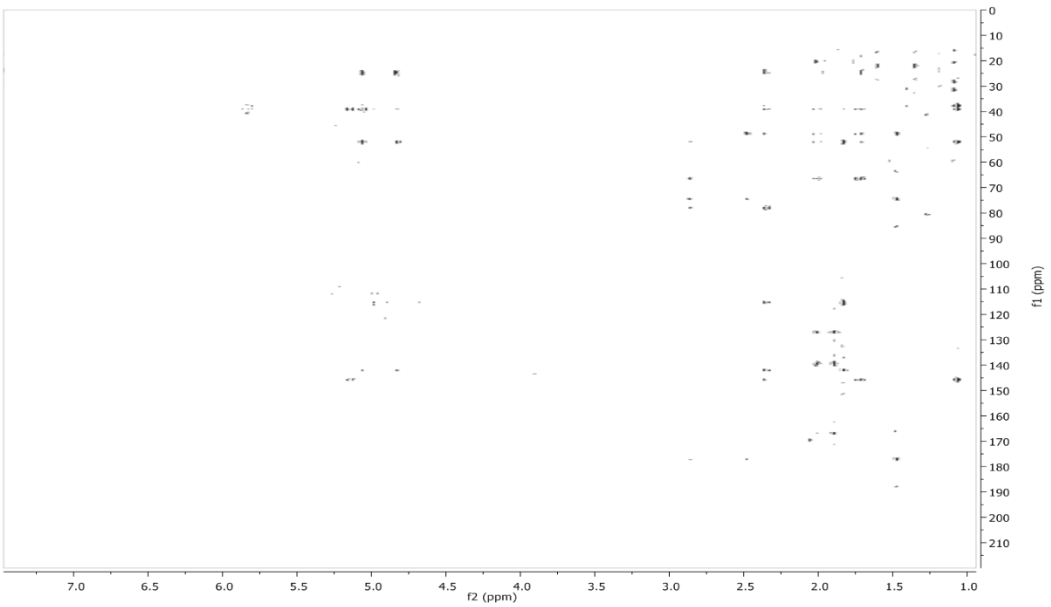

HSQC spectrum (500 MHz) of elemavirgolide (**16**) in $CDCl_3$

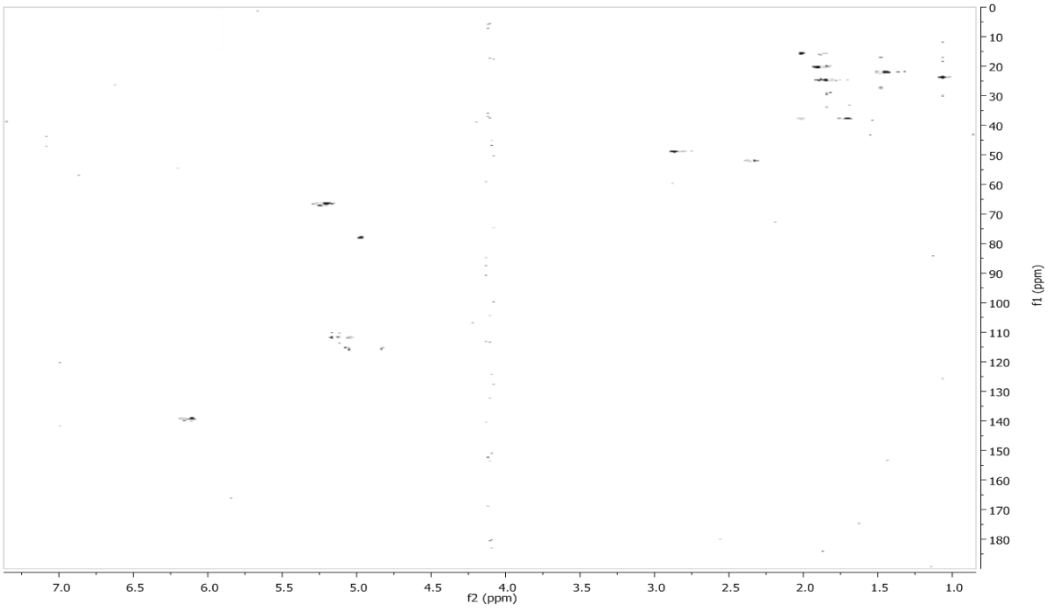

Spectral data for CHAPTER 5

^{1}H spectrum (500 MHz) of compound (**50**) in $CDCl_3$

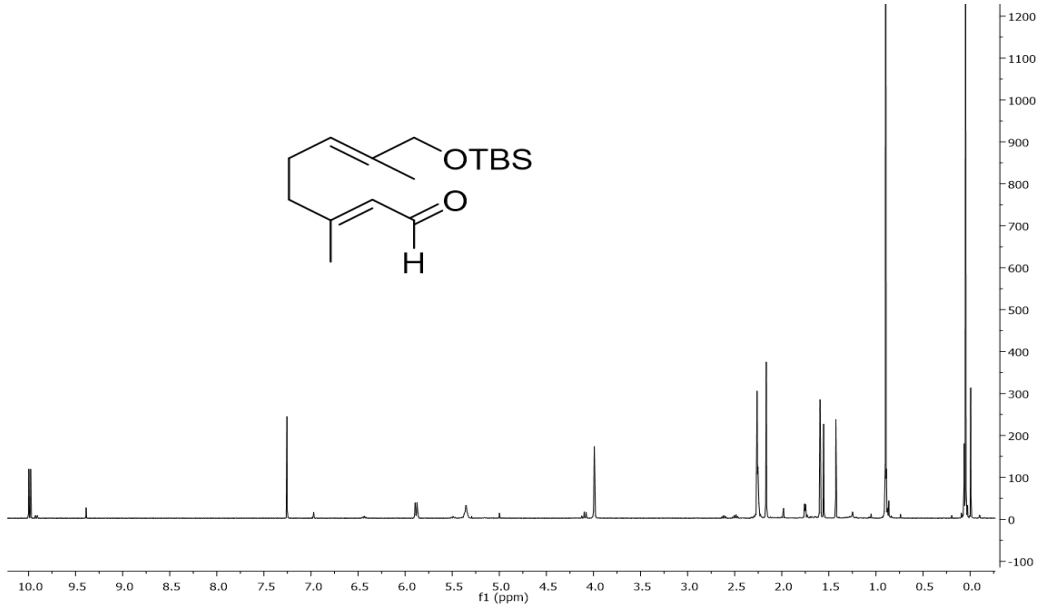

^{13}C spectrum (500 MHz) of compound (**50**) in $CDCl_3$

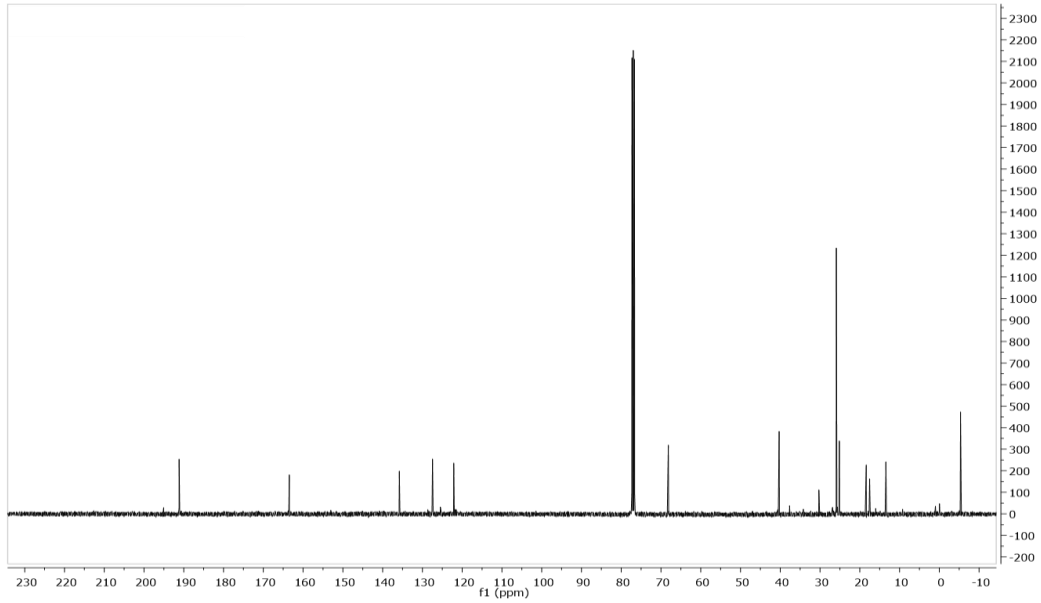

^{1}H spectrum (500 MHz) of compound (**55a**) in $CDCl_3$

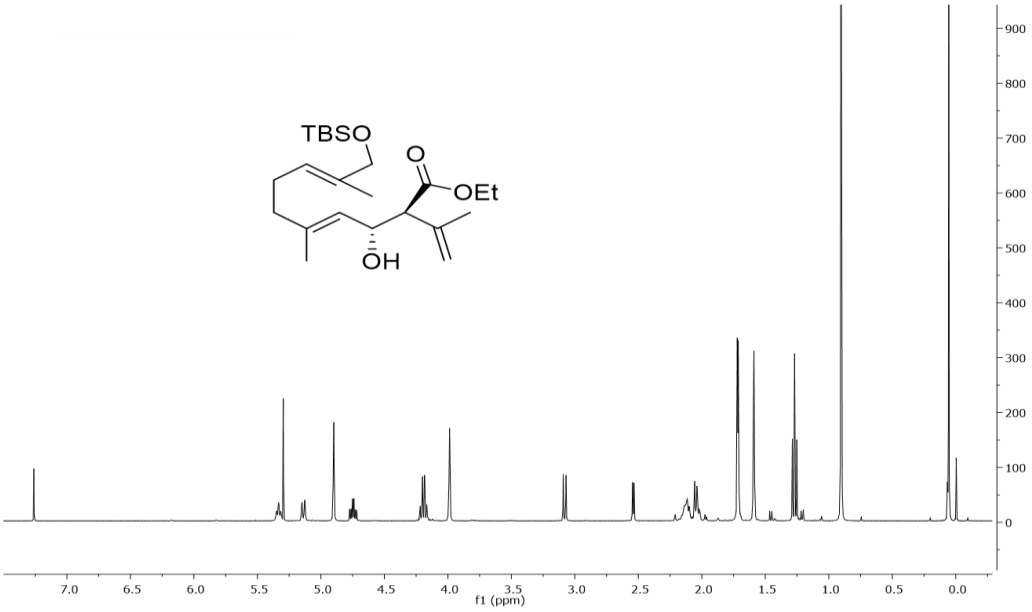

^{13}C spectrum (500 MHz) of compound (**55a**) in $CDCl_3$

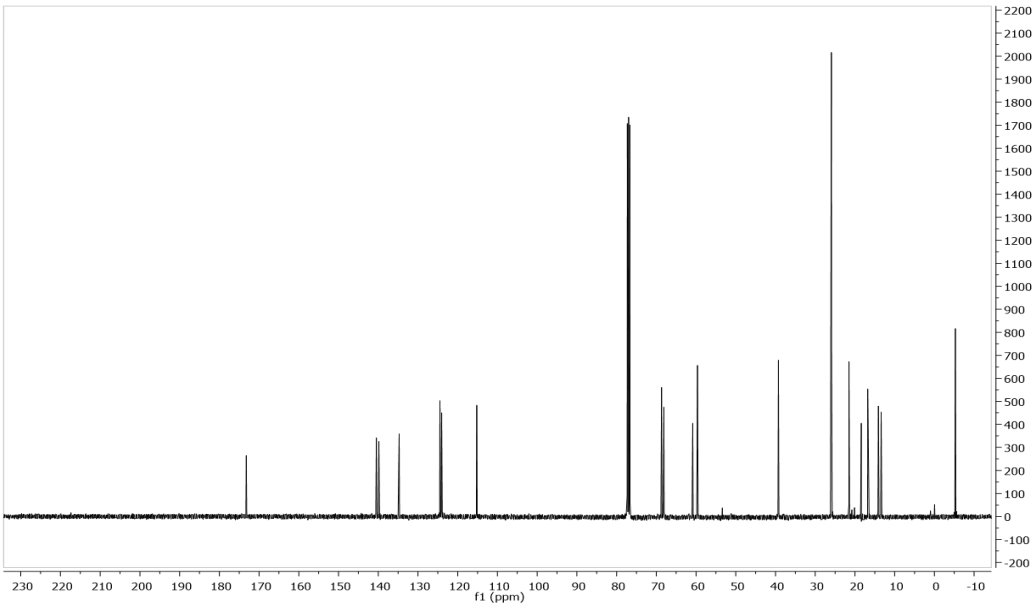

^{1}H spectrum (500 MHz) of compound (**61**) in $CDCl_3$

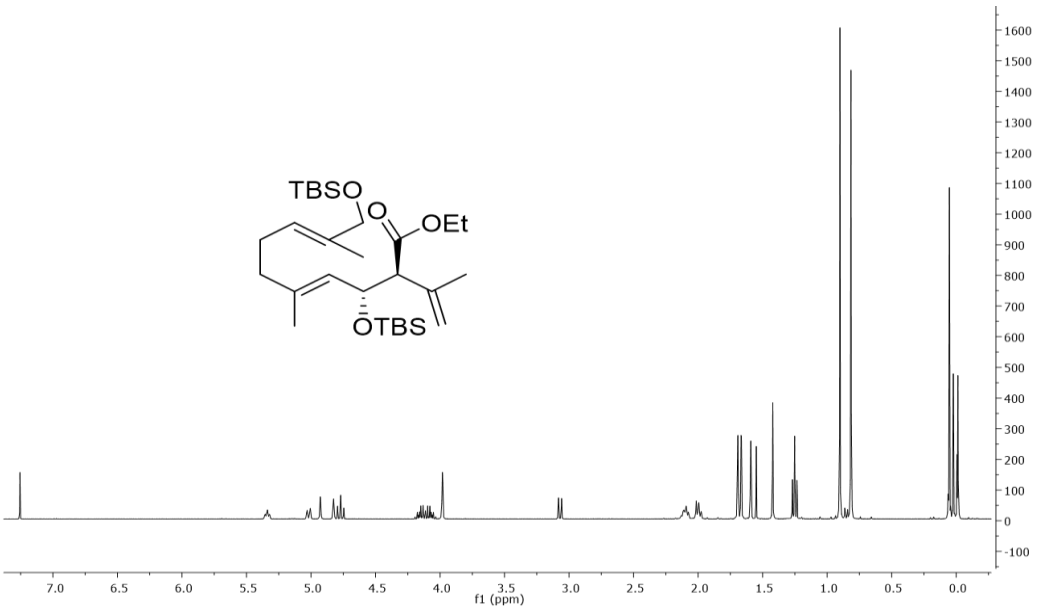

^{13}C spectrum (500 MHz) of compound (**61**) in $CDCl_3$

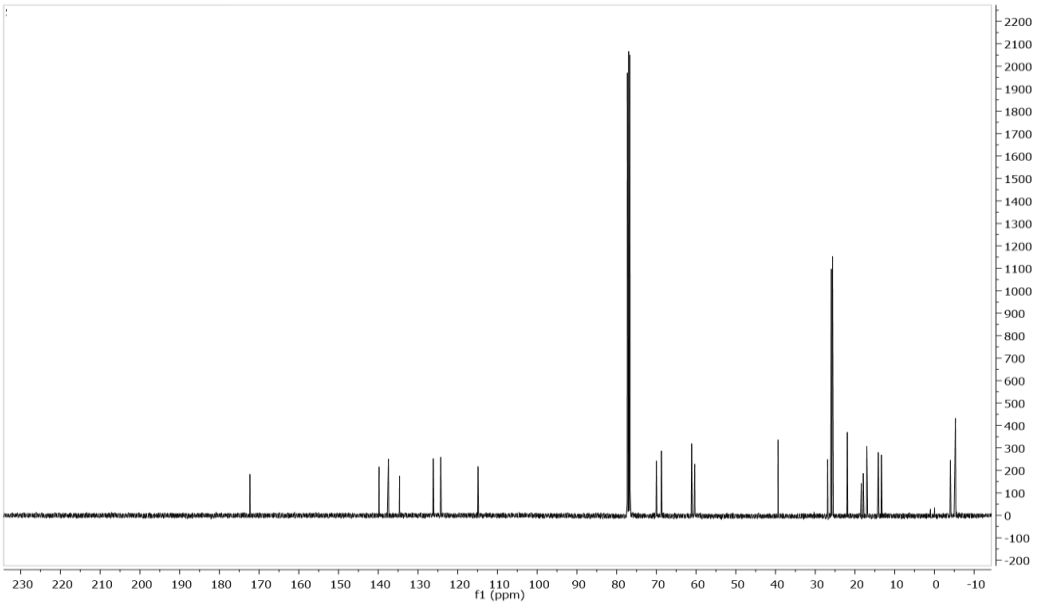

^{1}H spectrum (500 MHz) of compound (**60**) in $CDCl_3$